

Alma Mater Studiorum – Università di Bologna

DOTTORATO DI RICERCA IN

Meccanica e Scienze Avanzate dell'Ingegneria:
Disegno e Metodi dell'Ingegneria Industriale
e Scienze Aerospaziali

Ciclo XXV

Settore Concorsuale di afferenza: 09/A1 – Ingegneria Aeronautica, Aerospaziale e Navale

Settore Scientifico disciplinare: ING-IND/03 – Meccanica del Volo

NONLINEAR CONTROL OF
MAGNETICALLY ACTUATED SPACECRAFT

Presentata da: Emanuele Luigi de Angelis

Coordinatore Dottorato

Prof. Vincenzo Parenti Castelli

Relatore

Prof. Fabrizio Giulietti

Esame finale anno 2013

Ποταμείς τούς αὐτοὺς ἐμβαίνομεν τε καὶ οὐκ ἐμβαίνομεν,
εἶμεν τε καὶ οὐκ εἶμεν.

*Man cannot step into the same river twice,
because neither the man nor the river is the same.*

—Herakleitos of Ephesus, Ionia, Greece

*Living systems are never in equilibrium. They are inherently unstable.
They may seem stable, but they're not. Everything is moving and changing.
In a sense, everything is on the edge of collapse.*

—Michael Crichton, from “Jurassic Park”

Preface and Acknowledgments

This thesis is submitted in partial fulfillment of the requirements for the Doctor of Philosophy in 'Advanced Mechanics and Sciences of Engineering: Design and Methods of Industrial Engineering'. The work has been carried out during the period from October 2009 to March 2013 under the supervision of Prof. Fabrizio Giulietti.

I would like to thank Prof. Fabrizio Giulietti for his guidance during the research work and for all the time spent with patience and perseverance while dealing with all the non-linearities encountered on the working path.

I also greatly acknowledge Prof. Giulio Avanzini of the Università del Salento and Prof. Anton de Ruiter of the Ryerson University for their precious support, valuable advice, and inspiring discussions during this work.

I would like to express my deepest thanks to my family and to all the people who, in different ways, made me feel encouraged and serene, even in the most difficult periods.

Emanuele Luigi de Angelis
March 2013, Forlì, Italy

Summary

The topic of this thesis is the feedback stabilization of the attitude of magnetically actuated spacecraft. The use of magnetic coils as attitude effectors is an attractive solution for the generation of control torques on small satellites flying inclined low Earth orbits, since magnetic control systems are characterized by reduced weight and cost, higher reliability, and require less power with respect to other kinds of actuators. At the same time, the possibility of smooth modulation of control torques reduces coupling of the attitude control system with flexible modes, thus preserving pointing precision with respect to the case when pulse-modulated thrusters are used.

As a matter of fact, the principle based on the interaction between the Earth's magnetic field and the magnetic field generated by the set of coils introduces an inherent nonlinearity, because control torques can be delivered only in a plane that is orthogonal to the direction of the geomagnetic field vector. In other words, the system is underactuated, because the rotational degrees of freedom of the spacecraft, modeled as a rigid body, exceed the number of independent control actions. The solution of the control issue for underactuated spacecraft is also interesting in the case of actuator failure, e.g. after the loss of a reaction-wheel in a three-axes stabilized spacecraft with no redundancy. The application of well known control strategies is no longer possible in this case for both regulation and tracking, so that new methods have been suggested for tackling this particular problem, that shows to be challenging both from a practical and theoretical point of view.

It is a statement of fact that the underactuated rigid spacecraft model cannot be stabilized by means of a continuous time-invariant state feedback. The main contribution of this thesis is to propose continuous time-varying controllers that globally stabilize the attitude of a spacecraft, when magneto-torquers alone are used and when a momentum-wheel

supports magnetic control in order to overcome the inherent underactuation. A kinematic maneuver planning scheme, stability analyses, and detailed simulation results are also provided, with new theoretical developments and particular attention toward application considerations.

Sommario

L'argomento di questa tesi è la stabilizzazione in retroazione dell'assetto di un satellite attraverso attuazione magnetica. L'uso di bobine percorse da corrente quale sistema per il controllo d'assetto rappresenta un'interessante soluzione per la generazione di coppie su piccoli satelliti in orbite terrestri basse ed inclinate, poiché i relativi sistemi di attuazione sono caratterizzati da ridotto peso e costo, maggiore affidabilità, e richiedono minor potenza rispetto ad altre tecnologie. Allo stesso tempo, la possibilità di una modulazione continua delle coppie di controllo riduce la possibilità di accoppiamento con i modi flessibili, in questo modo preservando la precisione di puntamento rispetto al caso in cui, per esempio, vengano usati thrusters a modulazione pulsata.

Tuttavia, il principio basato sull'interazione tra il campo magnetico terrestre ed il campo generato dal set di bobine implica una inerente non linearità, poiché le coppie di controllo generate possono giacere esclusivamente su di un piano ortogonale alla direzione locale del campo terrestre. In altre parole, il sistema risulta sottoattuato, essendo i gradi di libertà rotazionali del satellite, modellato come un corpo rigido, in numero superiore alle azioni di controllo indipendenti disponibili. La soluzione al problema della stabilizzazione di un satellite sottoattuato risulta inoltre interessante anche nel caso di guasto di un attuatore, rappresentato, ad esempio, dalla perdita di una ruota di reazione in un satellite controllato a tre assi senza ridondanza di sistemi. In questo caso, l'applicazione delle strategie di controllo classiche non è più possibile né per la regolazione né per il puntamento, cosicché nuovi metodi sono stati suggeriti per fronteggiare questo particolare problema, che si rivela affascinante sia dal punto di vista pratico che teorico.

E' un dato di fatto che il modello di un corpo rigido sottoattuato non possa essere stabilizzato attraverso una legge di retroazione dello stato continua e tempo-invariante. Il

maggiore contributo di questa tesi consiste dunque nel proporre dei controllori continui e tempo-varianti che stabilizzino l'assetto di un satellite nei casi in cui venga utilizzata la sola attuazione magnetica oppure una ruota di momento affianchi l'utilizzo di bobine, superando così l'inerente sottoattuazione. Uno schema cinematico di pianificazione di manovra, analisi di stabilità e dettagliate simulazioni sono inoltre presentati, con nuovi sviluppi matematici e particolare attenzione dedicata a considerazioni applicative.

Contents

List of Figures	xi
List of Tables	xiii
1 Introduction	1
1.1 Satellite Attitude Control	1
1.2 Outline of the Thesis	3
2 Spacecraft Dynamics	5
2.1 Angular Momentum Balance	5
2.2 Kinematics	7
2.2.1 Unit Quaternions	7
2.2.2 Euler Angles	8
2.3 Disturbances	9
3 Kinematic Planning for Single-Axis Pointing in the Presence of Path Constraints	11
3.1 Introduction	11
3.2 Problem Statement	12
3.2.1 Underactuation Direction and Feasible Rotation Axis	14
3.2.2 Constraint on Bright Light Source Direction	15
3.3 Maneuver Planning	16
3.3.1 Outline of the Maneuver Strategies	16
3.3.2 Method 1	17

3.3.3	Choice of δ for Method 1	19
3.3.4	Method 2	21
3.4	Conclusions	24
4	Acquisition of a Desired Pure Spin Condition	27
4.1	Introduction	27
4.2	Acquisition of a Desired Pure Spin Condition	28
4.2.1	Choice of the Control Gain	31
4.3	Results and Discussion	34
4.4	Conclusions	37
5	Spin-Axis Pointing	39
5.1	Introduction	39
5.2	Acquisition of a Pure Spin Condition in the Inertial Frame	40
5.2.1	Effects Due to Uncertainties on the Geomagnetic Field	44
5.3	Results and Discussion	45
5.4	Conclusions	50
6	Attitude Control Using Magnetic and Mechanical Actuation	51
6.1	Introduction	51
6.2	Attitude Stabilization in the Orbit Frame	52
6.2.1	Control Laws	52
6.2.2	Momentum Management	54
6.2.3	Control of the Pitch Angle	55
6.3	Results and Discussion	56
6.4	Conclusions	59
7	Conclusions	63
A	Proofs of Global Exponential Stability	65
	Bibliography	69

List of Figures

2.1	Spacecraft sketch.	6
3.1	Geometry of the problem.	13
3.2	Geometric parameters as functions of δ	21
3.3	The two-steps maneuver (Method 1).	23
3.4	The two-steps maneuver (Method 2).	25
4.1	Position of $\hat{\mathbf{e}}_i$, $\hat{\mathbf{b}}$ and $\boldsymbol{\varepsilon}$	33
4.2	Time histories of relevant variables for a sample maneuver	35
4.3	Performance analysis in terms of spin acquisition average time	36
5.1	Convergence time and electrical energy consumption of the test cases, as functions of $k_\varepsilon = k_\zeta = k$	47
5.2	Pointing error time history.	48
5.3	Angular rates time history ($\boldsymbol{\omega}_d = (0, 0.110, 0)^T$ rad/s).	48
5.4	Convergence time and electrical energy consumption of the test cases, as functions of $\log_{10}(k_\varepsilon/k_\zeta)$	49
6.1	Spacecraft and wheel angular momenta.	58
6.2	Spacecraft attitude error.	59
6.3	Spacecraft and wheel angular momenta (external disturbances).	60
6.4	Spacecraft attitude error (external disturbances).	60

List of Tables

3.1	Maneuver case analysis: crossing verification.	20
3.2	Maneuver case analysis: crossing avoidance (Method 1).	22
3.3	Maneuver case analysis: crossing avoidance (Method 2).	24
4.1	Spacecraft and orbit data, with initial conditions for a sample maneuver (pure spin stabilization).	34
5.1	Spacecraft and orbit data, with initial conditions for a sample maneuver (spin-axis stabilization).	46
6.1	Spacecraft and orbit data, with initial conditions for a sample maneuver (attitude stabilization).	57

List of Symbols

\mathbf{b}	Geomagnetic field vector expressed in \mathbb{F}_B
C_D	Spacecraft drag coefficient
$\hat{\mathbf{e}}_1, \hat{\mathbf{e}}_2, \hat{\mathbf{e}}_3$	Spacecraft principal axes of inertia
\mathbb{F}_B	Body-fixed frame
\mathbb{F}_I	Inertial frame
\mathbb{F}_O	Local-vertical/local-horizontal orbit frame
\mathbf{h}_w	$= (0, h_w, 0)^T$ Angular momentum of the wheel relative to \mathbb{F}_B
i	Orbit inclination
\mathbb{I}_3	3×3 identity matrix
g_w	Torque on the momentum-wheel
\mathbf{J}	$= \text{diag}(J_1, J_2, J_3)$ Spacecraft inertia matrix
J_w	Moment of inertia of the momentum-wheel
$k, k_\varepsilon, k_h, k_\zeta, \lambda$	Control gains
$\bar{l}_1, \bar{l}_2, \bar{l}_3$	Rectangular parallelepiped spacecraft dimensions
\mathbf{M}	$= (M_1, M_2, M_3)^T$ External torque acting on the spacecraft
\mathbf{m}	$= (m_1, m_2, m_3)^T$ Magnetic dipole moment vector
n	Orbit rate
$\hat{\mathbf{o}}_1, \hat{\mathbf{o}}_2, \hat{\mathbf{o}}_3$	Orbital axes
r_c	Orbit radius
t_F	Convergence time to the desired condition
T_{orb}	Orbit period
\mathbb{T}_{BI}	Coordinate transformation matrix between \mathbb{F}_I and \mathbb{F}_B
\mathbb{T}_{BO}	Coordinate transformation matrix between \mathbb{F}_O and \mathbb{F}_B
V	Orbital speed
$\mathbf{0}_{p \times q}$	$p \times q$ zero matrix

Greek symbols

$\boldsymbol{\varepsilon}$	$= (\varepsilon_1, \varepsilon_2, \varepsilon_3)^T$ Error between body-fixed desired and actual angular momentum vectors
Ω	Wheel speed with respect to the spacecraft
$\boldsymbol{\omega}$	$= (\omega_1, \omega_2, \omega_3)^T$ Absolute angular velocity vector
$\boldsymbol{\omega}^r$	$= (\omega_1^r, \omega_2^r, \omega_3^r)^T$ Relative angular velocity vector
ρ	Air density at the considered orbit altitude
$\hat{\boldsymbol{\sigma}}$	Body-fixed unit vector prescribed for single-axis pointing
$\hat{\boldsymbol{\tau}}$	Unit vector along the target direction
$\boldsymbol{\zeta}$	$= (\zeta_1, \zeta_2, \zeta_3)^T$ Error between inertially-fixed desired and actual angular momentum vectors

Subscripts and superscripts

\perp	Vector component perpendicular to Earth magnetic field
0	Initial condition at time t_0
d	Desired value
max	Maximum
min	Minimum
\mathcal{O}	Vector components in the orbit frame $\mathbb{F}_{\mathcal{O}}$
$*$	Nominal value

Acronyms

ACS	Attitude Control System
CCD	Charge Coupled Device
GEASV	Generalized Exponential Asymptotic Stability in Variation
IGRF	International Geomagnetic Reference Field
LEO	Low Earth Orbit
LVLH	Local-Vertical/Local-Horizontal

1.1 Satellite Attitude Control

The use of magnetic actuators on satellites flying Low Earth Orbits (LEO) poses several problems in the selection of suitable control strategies because of the fact that the interaction between the local geomagnetic field and the coils generates torques that lie on a plane that is orthogonal to the geomagnetic field itself. This makes the system inherently underactuated, with the inability to provide three independent control torques at each time instant. As a consequence, the application of well known control strategies is no longer possible in this case for both regulation and tracking of desired attitude profiles.

The interest in magnetic actuators is due to different reasons [1], such as: (i) the absence of catastrophic failure modes; (ii) a virtually unlimited operational life, because of their simple and reliable architecture and the need for renewable electrical power only to operate them; (iii) the possibility of smoothly modulating the control torque, which does not induce unwanted coupling with flexible modes (thus harming pointing precision), as it occurs with thrusters; (iv) significant savings in overall system weight and complexity with respect to any other class of actuators, as there are no moving parts or plumbing [2]. These features motivate the strong interest in magnetic actuators since they were first proposed almost 50 years ago [3], although a different type of actuator usually accompanies the magnetics to provide full three-axes control. In many cases, an Attitude Control System (ACS) based on a combination of reaction or momentum-bias-wheels is adopted for accurate pointing, whereas magnetic coils are installed for angular momentum dumping tasks (detumbling

and wheel desaturation) [4, 5]. Only more recently, fully magnetic attitude control was considered as a viable option, especially interesting for low-cost microsatellites or for control system reconfiguration after failure. In this framework, attitude stabilization is possible because, on average, the system proves to be controllable if the orbit possesses an adequate inclination with respect to the geomagnetic equator [6, 7]. This mechanism is based on the fact that the magnetic field vector periodically rotates over inclined orbits as the spacecraft flies around the Earth, making the problem intrinsically time-varying.

Different approaches have been investigated in the past for tackling the problem of control in underactuated conditions [8, 9], which represents an attractive solution also as a strategy for failure mitigation systems (e.g. after loss of a reaction wheel in a three-axes stabilized spacecraft with no redundancy) [10, 11, 12], possibly at the cost of reduced closed-loop performance in terms of pointing accuracy and/or maneuver time. It is a fact that actuator failure is generally handled with a certain degree of redundancy during the design phase. The disadvantage of this philosophy resides within (more) complicated mechanical systems and increased weight. The alternative is thus represented by the application of more complicated controllers that manage to reach attitude stabilization with less than three control torques.

The techniques developed up to the present days for the control of magnetically actuated spacecraft are based on both linear and nonlinear approaches. The former have been mainly studied in the perspective of LQ control, whereas the latter have been usually analyzed by means of Lyapunov methods and exploiting the periodicity of the Earth magnetic field along inclined orbits. Nonlinear techniques prove to be particularly useful upon egress of the spacecraft from the launch vehicle, when high rotation rates are present and the procedure of attitude acquisition is still ongoing. In this case, one of the most common control laws is the b-dot algorithm, according to which the commanded dipole is dependent on the time derivative of the geomagnetic field vector expressed in a body frame, actually related to the angular rates of the spacecraft [13]. This control law is easily implemented for detumbling purpose, since magnetometers provide measurements that are sufficiently accurate to be derived, and proves to be equivalent to a dissipative time-dependent control that aims at reducing the kinetic energy of the spacecraft.

In a recent work [14] that paved the way to some theoretical aspects of the present thesis, a rigorous proof of global asymptotic stability was derived for detumbling performed by magnetic actuators, where the angular velocity components are driven to zero asymptotically by means of a static linear feedback. The task was simpler than that considered by Lovera and Astolfi, but the proposed solution was based on a novel lemma of general validity derived from a corollary to Barbalat's Lemma [15]. The new Lemma is applicable, under some conditions, to all those non-autonomous systems that feature a time-invariant

1.2 Outline of the Thesis

candidate Lyapunov function. The cited command law represents an alternative version of the b-dot controller. The proof demonstrates that, in the presence of a time-varying magnetic field, the kinetic energy of the spacecraft is strictly decreasing, which means that it approaches zero monotonically. This is a stronger property than what Stickler and Alfriend demonstrated, proving that the time derivative of the kinetic energy is $\dot{\mathcal{T}} \leq 0$, but showing only empirically that the residual motion about the direction of the geomagnetic field is almost cancelled by their command law with the rotation of the magnetic field over time with respect to the orbital frame.

The same approach is partly used in the present thesis, where the angular momentum vector of the satellite is required to reach desired conditions among which complete detumbling represents a particular case. As a further contribution, the novel Lemma is rewritten in Appendix A with additional requirements that allow for a final statement of global exponential stability for the considered system, thus enforcing the previous result about asymptotic convergence. The novel framework also allows for a physical interpretation of the mechanism at the basis of the asymptotic convergence obtained by means of the proposed controllers. The critical parameter to keep under control shows to be the angular distance between the direction of the magnetic field and the nominal control vector. This angle should not be allowed to be zero, in order to maintain a non-zero control power. In particular, by means of this interpretation, it is also possible to derive a simple, yet effective way of sizing the feedback control law gain in Ch. 4, that performs a pure spin acquisition maneuver in a relatively short duration.

In what follows, the proofs of stability for the controllers proposed in Chs. 4–6 are derived in terms of robustness of the global exponential stability of a nominal system (obtained through the result in Appendix A) with respect to vanishing perturbation terms. In particular, a stronger notion of stability is introduced in Ch. 4 [16, 17], where a magnetic controller is proposed that drives a rigid spacecraft to a pure spin condition around a principal axis of inertia. In this case, after proving the generalized exponential asymptotic stability in variation (GEASV) for the nominal system, such result is extended to the perturbed system [18].

Numerical simulations finally confirm closed-loop stability and a reasonable response of spacecraft attitude parameters to the considered control actions.

1.2 Outline of the Thesis

The work is divided into three main parts. The first part, Chapter 2, copes with the mathematical model of a low Earth orbit micro-satellite, with the description of the main

disturbance torques. In the second part, Chapter 3, a kinematic maneuver planning scheme is provided for a single-axis pointing scenario, where a sensor boresight is required to stay out of a cone defined about the direction of bright sources of light, while the rotation eigenaxis is constrained on a plane perpendicular to the torqueless direction. In the third part, global stability analysis results are given for the problem of attitude control. In particular, time-varying controllers are proposed in order to acquire a pure spin condition about a principal axis of inertia (Chapter 4), to aim the spin axis in a prescribed direction in the inertial frame (Chapter 5), and to drive the spacecraft to three-axes stabilization with the support of a momentum wheel spinning about the pitch axis (Chapter 6). A section of concluding remarks ends this thesis.

2.1 Angular Momentum Balance

A sketch of the spacecraft, featuring one momentum-wheel and three mutually orthogonal magnetic coils is represented in Fig. 2.1. The spacecraft is assumed to be rigid. Consequently, the evolution of angular speed components can be derived from angular momentum balance projected onto a frame of principal axes of inertia, $\mathbb{F}_B = \{P; \hat{\mathbf{e}}_1, \hat{\mathbf{e}}_2, \hat{\mathbf{e}}_3\}$, centered in the spacecraft center of mass P :

$$\mathbf{J}\dot{\boldsymbol{\omega}} + \dot{\mathbf{h}}_w + \boldsymbol{\omega} \times (\mathbf{J}\boldsymbol{\omega} + \mathbf{h}_w) = \mathbf{M}^{(c)} + \mathbf{M}^{(d)} \quad (2.1)$$

where $\boldsymbol{\omega} = (\omega_1, \omega_2, \omega_3)^T$ is the absolute angular velocity vector of the spacecraft, $\mathbf{J} = \text{diag}(J_1, J_2, J_3)$ is the spacecraft inertia matrix including the moment of inertia of the wheel, and \mathbf{h}_w is the angular momentum of the wheel relative to \mathbb{F}_B . In general, it is $\mathbf{h}_w = J_w \Omega \hat{\mathbf{a}}$, where J_w is the moment of inertia of the wheel about its spin axis $\hat{\mathbf{a}}$, and Ω is the wheel spin rate with respect to the spacecraft. Letting $h_w = J_w \Omega$, it is

$$\dot{h}_w = g_w - J_w \dot{\boldsymbol{\omega}}^T \hat{\mathbf{a}} \quad (2.2)$$

where g_w is the torque applied to the wheel about its spin axis by its electric motor. Assuming that $\hat{\mathbf{a}} = \hat{\mathbf{e}}_2$ (that is, the wheel spins around an axis parallel to the spacecraft pitch axis), it is $\mathbf{h}_w = (0, h_w, 0)^T$ and Eq. (2.2) reduces to the scalar equation

$$\dot{h}_w = g_w - J_w \dot{\omega}_2 \quad (2.3)$$

In the case when the system is frictionless, g_w represents the control input. Alternatively, it is possible to take \dot{h}_w directly to be the control input for the pitch control law design. This is often done in practice, and removes any argument over whether or not friction needs to be accounted for.

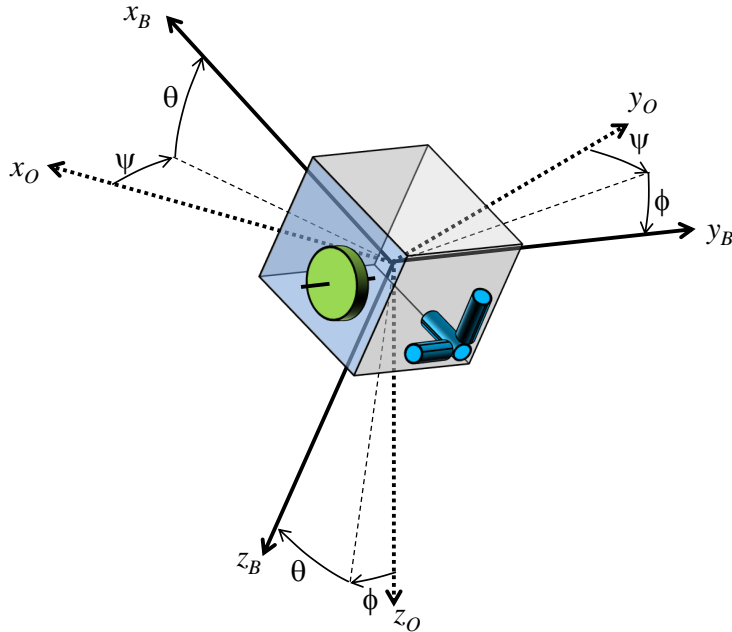


Figure 2.1: Spacecraft sketch.

No external disturbance $\mathbf{M}^{(d)}$ is considered in the stability analyses, so that the external torque acting on the spacecraft coincides with the magnetic control torque, namely $\mathbf{M}^{(c)} = \mathbf{m} \times \mathbf{b}$, where \mathbf{m} is the magnetic dipole moment vector generated by the coils and \mathbf{b} is the local geomagnetic field vector expressed in terms of body-frame components.

Earth magnetic field can be approximated by a tilted magnetic dipole of moment $M_\oplus = 7.8379 \times 10^6 \text{ T km}^3$, with a tilt angle $\gamma_m = 11.44 \text{ deg}$ with respect to the polar axis. Consider now a local-vertical/local-horizontal (LVLH) orbit frame, \mathbb{F}_O , where the z_O -axis lies along the local vertical pointing downwards, the y_O -axis is normal to the orbit plane, in a direction opposite to the orbital angular speed $\boldsymbol{\omega}^{orb}$, and the transverse axis x_O completes a right-handed triad, in the direction of the orbital velocity. For a circular low Earth orbit of radius r_c and period T_{orb} , the components of the geomagnetic vector can be expressed in \mathbb{F}_O as [19]

$$\mathbf{b}_O = \frac{M_\oplus}{r_c^3} \begin{bmatrix} \sin \xi_m \cos(n t - \eta_m) \\ -\cos \xi_m \\ 2 \sin \xi_m \sin(n t - \eta_m) \end{bmatrix} \quad (2.4)$$

2.2 Kinematics

where

$$\begin{aligned}\cos \xi_m &= \cos i \cos \gamma_m + \sin i \sin \gamma_m \cos \beta'_m \\ \sin \eta_m \sin \xi_m &= -\sin \gamma_m \sin \beta'_m \\ \cos \eta_m \sin \xi_m &= \sin i \cos \gamma_m - \cos i \sin \gamma_m \cos \beta'_m \\ \beta'_m &= \beta_m + \omega_e t - \Omega_{an}\end{aligned}$$

and i is orbit inclination, $n = 2\pi/T_{orb}$ the orbit rate, ω_e is the Earth angular rate, Ω_{an} is the ascending node of the spacecraft orbit, and β_m is the initial value of the angle between the vernal equinox and the line of intersection of the equatorial plane with the geomagnetic equator. The angle ξ_m represents the inclination of spacecraft orbit relative to the geomagnetic equatorial plane, and η_m is the angle between the ascending node relative to the Earth's equator and the ascending node relative to the geomagnetic equator. The tilted dipole model is used in Chs. 4 and 5. Conversely, the International Geomagnetic Reference Field (IGRF) model is implemented for simulations in Ch. 6, in order to test the relative proposed controller in a more realistic environment [13].

The components of the Earth magnetic field in \mathbb{F}_B are $\mathbf{b} = \mathbb{T}_{BO} \mathbf{b}_O$, where \mathbb{T}_{BO} is the coordinate transformation matrix between \mathbb{F}_O and \mathbb{F}_B , parameterizable in different ways. In the next Section, the unit quaternions and the Euler angles representations will be discussed. The preference for a certain parameterization is clearly problem-dependent.

2.2 Kinematics

2.2.1 Unit Quaternions

The unit quaternions, also called Euler parameters, are attractive due to their non-singular parameterization and linear kinematic differential equations if the angular velocities are known.

Consider the unit quaternion $\mathbf{Q} = (\mathbf{q}^T, \bar{q})^T$, that represents satellite's attitude with respect to the orbit frame. The coordinate transformation matrix between \mathbb{F}_O and \mathbb{F}_B is given by

$$\mathbb{T}_{BO} = (\bar{q}^2 - \mathbf{q}^T \mathbf{q}) \mathbb{I}_3 + 2\mathbf{q}\mathbf{q}^T - 2\bar{q} \tilde{\mathbf{Q}}, \quad (2.5)$$

where \mathbb{I}_3 is the 3×3 identity matrix and $\tilde{\mathbf{Q}}$ is the skew symmetric matrix equivalent to the cross product, such that $\tilde{\mathbf{Q}} \mathbf{v} = \mathbf{q} \times \mathbf{v}$, for any $\mathbf{v} \in \mathbb{R}^3$.

The unit quaternion evolves as a function of the angular speed of the spacecraft relative to \mathbb{F}_O , given by $\boldsymbol{\omega}^r = \boldsymbol{\omega} - \mathbb{T}_{BO} \boldsymbol{\omega}_O^{orb}$, where $\boldsymbol{\omega}_O^{orb} = (0, -n, 0)^T$ is the angular speed of \mathbb{F}_O

with respect to an inertial frame [20]. The kinematics of \mathbf{Q} is given by

$$\begin{aligned}\dot{\mathbf{q}} &= \frac{1}{2}(\bar{q}\boldsymbol{\omega}^r - \boldsymbol{\omega}^r \times \mathbf{q}) \\ \dot{\bar{q}} &= -\frac{1}{2}\boldsymbol{\omega}^{rT}\mathbf{q}\end{aligned}\tag{2.6}$$

2.2.2 Euler Angles

According to Euler's rotation theorem, any rotation may be described using three angles. In the case discussed in Ch. 6, the attitude of the spacecraft with respect to \mathbb{F}_O will be conveniently described by means of an unusual 3-1-2 Euler sequence, where the ‘‘yaw’’ angle ψ around the local vertical z_O is given by the angular distance between the y_O axis and the projection of y_B on the orbit plane, whereas the ‘‘roll’’ angle ϕ is represented by the elevation of y_B with respect to the orbit plane. The sequence of elementary rotations is completed by a ‘‘pitch’’ rotation θ around the unit vector $\hat{\mathbf{e}}_2$, parallel to y_B , as represented in Fig. 2.1.

The Euler angles also evolve as functions of the angular speed of the spacecraft relative to \mathbb{F}_O . The kinematics of roll, pitch, and yaw angles is given by

$$\omega_1^r = \dot{\phi} \cos \theta - \dot{\psi} \cos \phi \sin \theta \tag{2.7}$$

$$\omega_2^r = \dot{\theta} + \dot{\psi} \sin \phi \tag{2.8}$$

$$\omega_3^r = \dot{\phi} \sin \theta + \dot{\psi} \cos \phi \cos \theta \tag{2.9}$$

while the relations with the absolute angular velocity vector of the spacecraft, $\boldsymbol{\omega}$, is

$$\omega_1 = \dot{\phi} \cos \theta - \dot{\psi} \cos \phi \sin \theta - n (\cos \theta \sin \psi + \sin \phi \sin \theta \cos \psi) \tag{2.10}$$

$$\omega_2 = \dot{\theta} + \dot{\psi} \sin \phi - n \cos \phi \cos \psi \tag{2.11}$$

$$\omega_3 = \dot{\phi} \sin \theta + \dot{\psi} \cos \phi \cos \theta - n (\sin \theta \sin \psi - \sin \phi \cos \theta \cos \psi) \tag{2.12}$$

As usual, the use of Euler angles requires some attention, as long as singular configurations always occur when attitude is represented by means of elementary rotations. In the present case, when the second rotation ϕ is equal to ± 90 deg, the pitch axis coincides with the local vertical, and the first and third rotations are performed around the same axis. On the other hand, this situation is unlikely to be encountered in practice. As a matter of fact, after a spacecraft is injected into its orbit, an initial detumbling maneuver is performed in order to dump the angular momentum accumulated during payload ejection. During this phase, the spacecraft is generally driven toward a pure spin condition by means of a b-dot-like control law (see Ch. 4), such that the spin axis gets sufficiently close to the normal to the orbit plane [13]. As a consequence, small values for the angles ψ and ϕ are

2.3 Disturbances

expected. This means that $\phi = \pm 90$ deg is an unlikely situation and the applicability of the control law developed in Ch. 6 is not at stake.

2.3 Disturbances

In order to assess robustness of the control laws proposed in Ch. 6, the three most relevant sources of external disturbance torque in low Earth orbit are included in the model used for simulations discussed in the relative section of Results, namely gravity gradient, aerodynamic, and residual magnetic torques [13].

The gravity gradient torque affects a non-symmetric body in the Earth's gravity field. For a circular orbit, gravity gradient torque is given by

$$\mathbf{M}^{(gg)} = 3n^2 [\hat{\mathbf{o}}_3 \times (\mathbf{J}\hat{\mathbf{o}}_3)]$$

where $\hat{\mathbf{o}}_3$ is the unit vector parallel to the local vertical.

For low orbit satellites the air density is high enough to influence the attitude dynamics. The interaction of the upper atmosphere molecules with satellite's surface introduces an aerodynamic torque. Assuming that the incident air particles lose their entire energy on collision, the force $d\mathbf{f}_a$ on a surface element dA , with outward normal $\hat{\mathbf{N}}$, is described by

$$d\mathbf{f}_a = -\frac{1}{2}\rho V^2 C_D (\hat{\mathbf{N}} \cdot \hat{\mathbf{V}}) \hat{\mathbf{V}} dA \quad (2.13)$$

where $\hat{\mathbf{V}}$ is the unit vector in the direction of the translational velocity, \mathbf{V} , of the surface element relative to the incident stream, $\rho \approx 3.614 \cdot 10^{-14}$ kg/m³ is the density of the rarefied air at the considered orbit altitude (see Tab. 6.1), and C_D is a drag coefficient. The aerodynamic torque $\mathbf{M}^{(a)}$ acting on the spacecraft due to the force $d\mathbf{f}_a$ is

$$\mathbf{M}^{(a)} = \int \mathbf{r}_s \times d\mathbf{f}_a \quad (2.14)$$

where \mathbf{r}_s is the vector from the spacecraft's center of mass to the surface element dA and the integral is over the spacecraft surface for which $\hat{\mathbf{N}} \cdot \hat{\mathbf{V}} > 0$. Suppose the surface area is decomposed into simple geometric shapes, for example the six faces of a parallelepiped satellite. The overall torque can thus be evaluated by the vector sum of the individual torques calculated by the cross product of the vector distance from the spacecraft center of mass to the center of pressure of the geometric shapes and the force acting on the component.

Several internal effects can also generate disturbance torques. The residual magnetic torque $\mathbf{M}^{(rm)}$ is produced by the overall dipole moment \mathbf{m}_r generated by on-board electrical systems and circuits. When magnetic torquerods are active, this residual dipole moment

is negligible, but when they are switched off, it produces a significant contribution to the disturbance torque,

$$\mathbf{M}^{(rm)} = \mathbf{m}_r \times \mathbf{b}.$$

Kinematic Planning for Single-Axis Pointing in the Presence of Path Constraints

3.1 Introduction

In Ref. [21] a planning scheme for attitude slew maneuvers that point a given body-fixed axis along a prescribed inertial direction in the presence of constraints on admissible rotation axes is proposed. The present work aims at extending the approach discussed in [21] to cases where the same axis is required to stay away (with adequate tolerance) from forbidden directions. This requirement is typical of those situations in which the boresight of an instrument needs to be kept sufficiently far from bright objects such as Sun, Moon, and Earth albedo, while pointing maneuvers are performed, in order to avoid that the sensor is exposed to a level of radiation that may damage it [22]. This is the case, for example, of star sensors mounting Charge Coupled Devices (CCD) [23] and cryogenically cooled infrared telescopes [24]. In other cases payloads should not be aligned with the direction of the velocity vector along the orbit in order to avoid hazardous debris [25].

The task of maneuvering a spacecraft while avoiding hazardous directions becomes more difficult when full actuation is not possible and the availability of only two independent control torque components does not allow for arbitrary slews. When actuator failure is dealt with, the underactuated direction, $\hat{\mathbf{b}}$, is fixed in the body frame. Conversely, if $\hat{\mathbf{b}}$ is prescribed in the orbit frame, namely when magnetic control is considered, the underactuated direction is then parallel to the magnetic field. In both cases, the available torques lie on a plane perpendicular to $\hat{\mathbf{b}}$. In Ref. [21] it was shown that, regardless of the orientation

of $\hat{\mathbf{b}}$, there always exists a single feasible eigenaxis rotation that allows for pointing any given body-fixed axis exactly along an arbitrary line-of-sight, where the rotation axis is feasible if it lies on the plane perpendicular to $\hat{\mathbf{b}}$. The maneuver planning scheme was thus based on the identification of a feasible eigenaxis and the corresponding rotation angle by means of a computationally inexpensive strategy based on simple goniometric calculations.

Accurate pointing of a certain body-fixed axis may be required for aiming a directional antenna toward a ground station for communication purposes or a thruster nozzle for orbit maneuvers, where the accuracy must lie within a fraction of a degree [26]. These cases do not usually pose constraints on the angular path that can be followed for attaining the desired single-axis pointing. Conversely, celestial observation is often based on the use of delicate sensor payloads [27]. As an example, Earth pointing may be required in the case of Earth observation. It is the case of ALMASat-EO, a micro-satellite under development at the University of Bologna, mounting an innovative multispectral camera and testing a novel micropropulsion system for orbit control [28]. In these cases, constraints on admissible attitudes can become an issue. In Ref. [29], a simple maneuver strategy based on a kinematic result was presented, with the aim to avoid the Sun during maneuvers between pairs of target radiation sources, with the identification of the shortest angular path.

In this Chapter a result is given for a single-axis pointing scenario, where the sensor boresight is required to stay out of a cone defined about the direction of the bright sources of light, while the rotation eigenaxis is constrained on a plane perpendicular to the torqueless direction. This allows for taking into account those cases in which the spacecraft is underactuated. When the maneuver is planned according to the scheme presented in [21], the feasible rotation may drive the sensor inside the forbidden region. In the present work, the condition for such an unwanted situation is determined in the next Section and an alternative maneuver planning scheme, based on two rotations, is derived for accomplishing the required single-axis pointing in the following one. The shortest path in terms of angular displacement is also calculated, with a numerical test case that shows the effectiveness of the algorithm. A section of concluding remarks ends this Chapter.

3.2 Problem Statement

As stated in the Introduction, the desired maneuver is represented by the rotation of a body-fixed axis $\hat{\boldsymbol{\sigma}}$ (which is aligned to the boresight of the sensor) toward a prescribed target direction $\hat{\boldsymbol{\tau}}$ (Fig. 3.1). The minimum amplitude rotation that allows the desired maneuver can be determined by means of an inverse cosine function, $\alpha_m = \cos^{-1}(\hat{\boldsymbol{\sigma}} \cdot \hat{\boldsymbol{\tau}})$,

3.2 Problem Statement

with $0 \leq \alpha_m \leq \pi$. The rotation takes place on a plane Π that contains both $\hat{\sigma}$ and $\hat{\tau}$, around the nominal axis defined by $\hat{e}_m = (\hat{\sigma} \times \hat{\tau}) / (\|\hat{\sigma} \times \hat{\tau}\|)$. The target direction can be expressed as

$$\hat{\tau} = \hat{\sigma} \cos \alpha_m + (\hat{e}_m \times \hat{\sigma}) \sin \alpha_m \quad (3.1)$$

whereas the unit vector \hat{e}_M defining the bisector of the angle α_m is

$$\hat{e}_M = \frac{\hat{\sigma} + \hat{\tau}}{\|\hat{\sigma} + \hat{\tau}\|} = \frac{(1 + \cos \alpha_m)\hat{\sigma} + \sin \alpha_m(\hat{e}_m \times \hat{\sigma})}{\sqrt{2(1 + \cos \alpha_m)}}$$

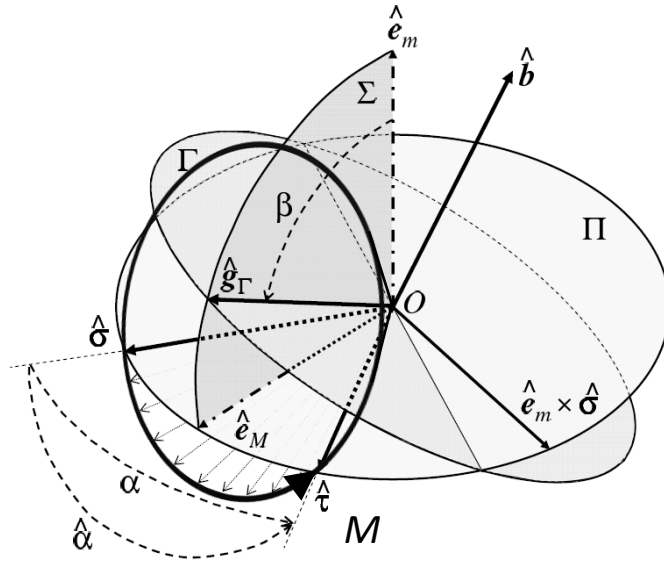


Figure 3.1: Geometry of the problem.

The rotation that takes $\hat{\sigma}$ onto $\hat{\tau}$ can be accomplished by rotating the body-fixed frame \mathbb{F}_B about any axis \hat{g} on the plane Σ , perpendicular to Π , that contains both \hat{e}_m and \hat{e}_M . If β is the angle between \hat{e}_m and \hat{g} , then \hat{g} can be expressed by the linear combination

$$\hat{g} = \hat{e}_m \cos \beta + \hat{e}_M \sin \beta \quad (3.2)$$

where $-\pi/2 < \beta \leq \pi/2$. In other words,

$$\hat{g} = \left[\sin \beta \cos \frac{\alpha_m}{2} \right] \hat{\sigma} + \left[\sin \beta \sin \frac{\alpha_m}{2} \right] (\hat{e}_m \times \hat{\sigma}) + [\cos \beta] \hat{e}_m \quad (3.3)$$

where a positive sign is assumed for the goniometric relations

$$\cos \frac{\alpha_m}{2} = \sqrt{\frac{1 + \cos \alpha_m}{2}}, \quad \sin \frac{\alpha_m}{2} = \sqrt{\frac{1 - \cos \alpha_m}{2}},$$

3. Kinematic Planning for Single-Axis Pointing in the Presence of Path Constraints

given the bounds on α_m . The three unit vectors $\hat{\sigma}$, $(\hat{e}_m \times \hat{\sigma})$, and \hat{e}_m form a right-handed triad so that, without loss of generality, they can be considered as the initial position of the body-frame, $\mathbb{F}_B^{(1)} \equiv (O, \hat{\mathbf{i}}_1, \hat{\mathbf{j}}_1, \hat{\mathbf{k}}_1)$ [21]. In this framework, all the vector components will be referred to this frame, starting from $\hat{\mathbf{g}} = (g_1, g_2, g_3)^T$, whose components are expressed by the terms in the square brackets in Eq. (3.3). At the same time, with this choice of axes, it is $\hat{\sigma} = (1, 0, 0)^T$, $\hat{\tau} = (\cos \alpha_m, \sin \alpha_m, 0)^T$, and $\hat{e}_m = (0, 0, 1)^T$.

The coordinate transformation matrix, \mathbb{T}_{21} , from $\mathbb{F}_B^{(1)}$ to $\mathbb{F}_B^{(2)} \equiv (O, \hat{\mathbf{i}}_2, \hat{\mathbf{j}}_2, \hat{\mathbf{k}}_2)$ is expressed in terms of eigenaxis rotation $\hat{\alpha}$ about the generic unit vector $\hat{\mathbf{g}} \in \Sigma$ as [20]

$$\mathbb{T}_{21} = \begin{bmatrix} c\hat{\alpha} + g_1^2(1 - c\hat{\alpha}) & g_1g_2(1 - c\hat{\alpha}) + g_3s\hat{\alpha} & g_1g_3(1 - c\hat{\alpha}) - g_2s\hat{\alpha} \\ g_1g_2(1 - c\hat{\alpha}) - g_3s\hat{\alpha} & c\hat{\alpha} + g_2^2(1 - c\hat{\alpha}) & g_2g_3(1 - c\hat{\alpha}) + g_1s\hat{\alpha} \\ g_1g_3(1 - c\hat{\alpha}) + g_2s\hat{\alpha} & g_2g_3(1 - c\hat{\alpha}) - g_1s\hat{\alpha} & c\hat{\alpha} + g_3^2(1 - c\hat{\alpha}) \end{bmatrix} \quad (3.4)$$

where $c\hat{\alpha} = \cos \hat{\alpha}$ and $s\hat{\alpha} = \sin \hat{\alpha}$. Given the choice of axes discussed above, the final position of $\hat{\mathbf{i}}_1 \equiv \hat{\sigma}$ is $\hat{\mathbf{i}}_2 \equiv \hat{\tau}$, represented in $\mathbb{F}_B^{(2)}$ by the vector $\hat{\tau}_2 = (1, 0, 0)^T$. The rotation angle $\hat{\alpha} \geq \alpha_m$ around $\hat{\mathbf{g}}$ that takes $\hat{\sigma}$ onto $\hat{\tau}$ is obtained from [21]

$$\cos \hat{\alpha} = 1 - \frac{2 \sin^2 \alpha_m}{\sin^2 \alpha_m \sin^2 \beta + 2(1 + \cos \alpha_m) \cos^2 \beta}. \quad (3.5)$$

The procedure described above can be generalized to any body-axes choice. Letting $\hat{\sigma}_B = (\sigma_1, \sigma_2, \sigma_3)^T$ and $\hat{e}_{m_B} = (e_1, e_2, e_3)^T$ be, respectively, the components of $\hat{\sigma}$ and \hat{e}_m expressed in a generic body frame $\mathbb{F}_B = (O; \hat{\mathbf{i}}, \hat{\mathbf{j}}, \hat{\mathbf{k}})$, it is convenient to project the components of all the considered unit vectors $\hat{\tau}$, $\hat{\mathbf{b}}$, and $\hat{\mathbf{g}}$ in the *ad hoc* frame $\mathbb{F}_B^{(1)}$ by means of the coordinate transformation matrix

$$\mathbb{T}_{1B} = [\mathbb{T}_{B1}]^T = \left[\hat{\sigma}_B \ : \ \hat{e}_{m_B} \times \hat{\sigma}_B \ : \ \hat{e}_{m_B} \right]^T \quad (3.6)$$

It is then possible to determine the eigenaxis $\hat{\mathbf{g}}$ in $\mathbb{F}_B^{(1)}$ by means of the procedure outlined above, and obtain its body frame components in \mathbb{F}_B through the coordinate transformation matrix $\mathbb{T}_{B1} = \mathbb{T}_{1B}^T$.

3.2.1 Underactuation Direction and Feasible Rotation Axis

In what follows, it will be assumed that the torqueless direction is given by the unit vector parallel to the local geomagnetic field, \mathbf{b} , that is, $\hat{\mathbf{b}} = \mathbf{b} / \|\mathbf{b}\|$. The plane of admissible rotation axes, Γ , is orthogonal to $\hat{\mathbf{b}}$ (Fig. 3.1). Among all the possible combinations described in Eq. (3.2), the need for using a feasible rotation axis restricts the choice to the unit vector $\hat{\mathbf{g}}_\Gamma$ that lies at the intersection of the planes Γ and Σ . This unit vector satisfies the condition

$$\hat{\mathbf{b}} \cdot \hat{\mathbf{g}}_\Gamma = 0 \quad (3.7)$$

3.2 Problem Statement

Assuming $\hat{\mathbf{b}} = b_1\hat{\boldsymbol{\sigma}} + b_2(\hat{\mathbf{e}}_m \times \hat{\boldsymbol{\sigma}}) + b_3\hat{\mathbf{e}}_m$, the value of β to be used in Eqs. (3.3) and (3.5) for the determination of the feasible rotation that takes $\hat{\boldsymbol{\sigma}}$ onto $\hat{\boldsymbol{\tau}}$ is evaluated by solving Eq. (3.7) with respect to β . This is given by

$$\tan \beta = -b_3 / \left(b_1 \cos \frac{\alpha_m}{2} + b_2 \sin \frac{\alpha_m}{2} \right) \quad (3.8)$$

Note that the use of a four quadrant inverse tangent is not necessary, as it is possible to bound the value of β between $-\pi/2$ and $\pi/2$, the same direction being achieved by either adding or subtracting π to β .

During the rotation, the unit vector $\hat{\boldsymbol{\sigma}}$ draws a sector of a cone M around $\hat{\mathbf{g}}_\Gamma$ (Fig. 3.1). Taking into account Eq. (3.3), the semi-aperture μ of the rotation cone M satisfies the condition

$$\cos \mu = \hat{\mathbf{g}}_\Gamma \cdot \hat{\boldsymbol{\tau}} \equiv \hat{\mathbf{g}}_\Gamma \cdot \hat{\boldsymbol{\sigma}} = \sin \beta \cos \frac{\alpha_m}{2} \quad (3.9)$$

where $0 \leq \mu \leq \pi/2$.

3.2.2 Constraint on Bright Light Source Direction

Suppose the unit vector $\hat{\mathbf{l}} = l_1\hat{\boldsymbol{\sigma}} + l_2(\hat{\mathbf{e}}_m \times \hat{\boldsymbol{\sigma}}) + l_3\hat{\mathbf{e}}_m$ identifies the direction that needs to be avoided (*e.g.* a bright light source), surrounded by a clearance cone Λ , characterized by a semi-aperture $0 \leq \lambda \leq \pi/2$. The sensitive axis of the payload, $\hat{\boldsymbol{\sigma}}$, is required to remain out of the prohibited cone Λ during the rotation around $\hat{\mathbf{g}}_\Gamma$. Assuming that $\hat{\boldsymbol{\sigma}}$ initially lies outside Λ , this can happen only if the cones Λ and M intersect along the portion of M spanned by $\hat{\boldsymbol{\sigma}}$ and the angle ξ between $\hat{\mathbf{l}}$ and $\hat{\boldsymbol{\sigma}}$ becomes smaller than the semi-aperture λ of the forbidden cone Λ , for some points in the interval $[0, \hat{\alpha}]$. A parametric formulation of $\hat{\boldsymbol{\sigma}}$ as a function of the rotation angle $\alpha \in [0, \hat{\alpha}]$ is easily obtained considering the first line of the matrix in Eq. (3.4). Then, $\hat{\boldsymbol{\sigma}} = \hat{\boldsymbol{\sigma}}(\alpha)$ enters the forbidden cone if and only if

$$\xi_{\min} = \min_{\alpha \in [0, \hat{\alpha}]} \xi(\alpha) < \lambda. \quad (3.10)$$

Provided that $\cos(\xi) = \hat{\mathbf{l}} \cdot \hat{\boldsymbol{\sigma}}$, the minimum for ξ on the cone M can be found in closed form by maximizing the value of

$$\cos[\xi(\alpha)] = l_1[c\alpha + g_1^2(1 - c\alpha)] + l_2[g_1g_2(1 - c\alpha) + g_3s\alpha] + l_3[g_1g_3(1 - c\alpha) - g_2s\alpha] \quad (3.11)$$

This can be done by solving the equation

$$\frac{d}{d\alpha} [\hat{\mathbf{l}} \cdot \hat{\boldsymbol{\sigma}}(\alpha)] = 0 \quad (3.12)$$

By taking into account Eq. (3.11), this condition can be rearranged in the form

$$\sin(\alpha)(-l_1 + g_1 \cos \gamma) + \cos(\alpha)(l_2g_3 - l_3g_2) = 0 \quad (3.13)$$

that provides the solution

$$\tan(\alpha_{cr}) = \frac{l_2 g_3 - l_3 g_2}{l_1 - g_1 \cos \gamma} \quad (3.14)$$

where $\gamma = \cos^{-1}(\hat{\mathbf{g}}_\Gamma \cdot \hat{\mathbf{l}})$ is the angle between the rotation axis $\hat{\mathbf{g}}_\Gamma$ and the prohibited direction $\hat{\mathbf{l}}$, whereas α_{cr} is such that $\xi_{\min} = \xi(\alpha_{cr})$. The value of α_{cr} obtained from Eq. (3.14) can be finally used into Eq. (3.11) to verify if condition in Eq. (3.10) is satisfied.

Summarizing, if crossing is not expected, then the maneuver described by the rotation around $\hat{\mathbf{g}}_\Gamma$ can take place with $\hat{\alpha}$ angular amplitude (see the Section about the underactuation constraint). If, on the other hand, the condition in Eq. (3.10) is verified, then an alternative maneuver strategy must be adopted.

3.3 Maneuver Planning

3.3.1 Outline of the Maneuver Strategies

If the single-axis pointing maneuver planned by means of the approach discussed in [21] causes the sensor axis $\hat{\boldsymbol{\sigma}}$ to enter the forbidden cone Λ , an alternative angular path needs to be determined. Several options are available in this framework. First of all one can check if a rotation $\hat{\alpha}_{alt} = -(2\pi - \hat{\alpha})$ around $\hat{\mathbf{g}}_\Gamma$ crosses Λ or not. If not, a feasible solution is readily available, without additional computational burden (at the cost of a longer angular travel). If on the converse, the path of $\hat{\boldsymbol{\sigma}}$ along the maneuver cone M determined as in [21] crosses at least one of the obstacles that endanger the sensor, it is necessary to identify a totally different path.

The method proposed here is based on the identification of the minimum angular displacement for $\hat{\boldsymbol{\sigma}}$ around the feasible rotation axis $\hat{\mathbf{b}} \times \hat{\mathbf{g}}_\Gamma$ that then allows for reaching $\hat{\boldsymbol{\tau}}$ by means of a single admissible rotation along a new maneuver cone M^* , such that the forbidden cone remains now outside of the path followed by $\hat{\boldsymbol{\sigma}}$ along M^* . This means that an initial admissible rotation around the axis $\hat{\mathbf{b}} \times \hat{\mathbf{g}}_\Gamma$ (clearly perpendicular to the underactuated direction $\hat{\mathbf{b}}$) is required to move $\hat{\boldsymbol{\sigma}}$ to an intermediate position $\hat{\boldsymbol{\sigma}}^*$, whereas the second step follows the approach discussed in [21]. A numerical procedure is necessary to determine the minimum initial angular displacement that takes $\hat{\boldsymbol{\sigma}}$ onto the nearest admissible rotation cone M^* , tangent to Λ . This method will be referred to as Method 1 in the sequel.

The resulting path for $\hat{\boldsymbol{\sigma}}$ is now based on a sequence of two rotations, but the overall angular path thus determined is not minimum. It is easy to understand that, if $\hat{\boldsymbol{\sigma}}$ is not moved onto M^* rotating it around $\hat{\mathbf{b}} \times \hat{\mathbf{g}}_\Gamma$, but it reaches M^* along another cone M^0 tangent to Λ , than the minimum angular path is obtained. The cone M^0 can be determined by a

3.3 Maneuver Planning

dual application of the same numerical technique, where the minimum displacement of $\hat{\tau}$ around $\hat{\mathbf{b}} \times \hat{\mathbf{g}}_\Gamma$ is sought that takes $\hat{\tau}$ to an intermediate position $\hat{\tau}^*$ that can be reached from the initial position of $\hat{\sigma}$ by means of an angular path running along the cone M^0 , tangent to Λ . At this point, the path of $\hat{\sigma}$ goes along M^0 up to its intersection $\hat{\nu}$ with M^* , and from $\hat{\nu}$ to $\hat{\tau}$ along M^* (see Fig. 3.4). This represents the minimum angular displacement that allows for reaching $\hat{\tau}$ with a two-steps maneuver that remains outside Λ . The computational burden doubles, as the numerical procedure for the identification of the tangent path needs to be run twice. The minimum angular path solution will be referred to as Method 2.

3.3.2 Method 1

In this Section it is shown how to rotate $\hat{\sigma}$ around a feasible rotation axis perpendicular to $\hat{\mathbf{b}}$ to a new position $\hat{\sigma}^*$ from which it is possible to reach the prescribed target direction $\hat{\tau}$ without crossing the clearance cone Λ , thus remaining sufficiently far from the prohibited direction $\hat{\mathbf{l}}$. The two steps are defined as follows:

1. A first admissible rotation $\mathcal{R}_1(\hat{\mathbf{b}} \times \hat{\mathbf{g}}_\Gamma, \delta)$ with angular amplitude δ is performed around the feasible rotation axis $\hat{\mathbf{b}} \times \hat{\mathbf{g}}_\Gamma$, where

$$\begin{aligned} \hat{\mathbf{b}} \times \hat{\mathbf{g}}_\Gamma = & \left[b_2 \cos \beta - b_3 \sin \beta \sin \frac{\alpha_m}{2} \right] \hat{\sigma} + \left[b_3 \sin \beta \cos \frac{\alpha_m}{2} - b_1 \cos \beta \right] (\hat{\mathbf{e}}_m \times \hat{\sigma}) + \\ & + \left[\sin \beta \left(b_1 \sin \frac{\alpha_m}{2} - b_2 \cos \frac{\alpha_m}{2} \right) \right] \hat{\mathbf{e}}_m \end{aligned} \quad (3.15)$$

After the first rotation is performed, a new direction $\hat{\sigma}^*$ is obtained for the sensitive axis.

2. The second rotation of the spacecraft, $\mathcal{R}_2(\hat{\mathbf{g}}_\Gamma^*, \hat{\alpha}^*)$, takes place around a feasible rotation axis $\hat{\mathbf{g}}_\Gamma^*$, with an angular travel $\hat{\alpha}^*$, such that the cone M^* does not intersect the forbidden region identified by the cone Λ along the portion spanned by $\hat{\sigma}$ going from $\hat{\sigma}^*$ to $\hat{\tau}$.

The latter requirement can be fulfilled if the amplitude δ of the first rotation is sufficiently large. The minimum value for δ is found by imposing that M^* is tangent to Λ . Two solutions are found, δ_i and δ_e , such that the two cones are either internally or externally tangent, respectively. A criterion for the choice between the two solutions is later presented, when discussing a practical example.

The first rotation performed around $\hat{\mathbf{b}} \times \hat{\mathbf{g}}_\Gamma$ takes $\mathbb{F}_B^{(1)}$ to an intermediate attitude defined by the frame $\mathbb{F}_B^{(i)} \equiv (O, \hat{\mathbf{i}}_i, \hat{\mathbf{j}}_i, \hat{\mathbf{k}}_i)$, with $\hat{\mathbf{i}}_i \equiv \hat{\sigma}^*$. The rotation matrix \mathbb{T}_{i1} has the same structure introduced in Eq. (3.4), with the difference that $\hat{\mathbf{b}} \times \hat{\mathbf{g}}_\Gamma = (d_1, d_2, d_3)^T$ and δ are

3. Kinematic Planning for Single-Axis Pointing in the Presence of Path Constraints

the Euler axis/angle pair to be used instead of $(g_1, g_2, g_3)^T$ and $\hat{\alpha}$, respectively. The first line of \mathbb{T}_{i_1} thus gives the three components of the intermediate position $\hat{\sigma}^*$ for the sensitive axis in the initial frame $\mathbb{F}_B^{(1)} \equiv (O, \hat{i}_1, \hat{j}_1, \hat{k}_1)$, namely

$$\hat{\sigma}^*(\delta) = [c\delta + d_1^2(1 - c\delta)]\hat{\sigma} + [d_1d_2(1 - c\delta) + d_3s\delta](\hat{e}_m \times \hat{\sigma}) + [d_1d_3(1 - c\delta) - d_2s\delta]\hat{e}_m \quad (3.16)$$

The angular separation, α_m^* , between $\hat{\sigma}^*$ and $\hat{\tau}$ is given by

$$\cos[\alpha_m^*(\delta)] = \hat{\sigma}^*(\delta) \cdot \hat{\tau} = c\alpha_m[c\delta + d_1^2(1 - c\delta)] + s\alpha_m[d_1d_2(1 - c\delta) + d_3s\delta] \quad (3.17)$$

with $0 \leq \alpha_m^* \leq \pi$. From this point onwards the geometry of the problem exactly follows that introduced in [21] and recalled in the Problem Statement section, with the difference that, after the first rotation, the sensitive axis achieves an orientation $\hat{\sigma}^*$ different from the initial one. After updating the vectors $\hat{e}_m^*(\delta) = (\hat{\sigma}^* \times \hat{\tau})/\|\hat{\sigma}^* \times \hat{\tau}\|$, $\hat{e}_M^*(\delta) = (\hat{\sigma}^* + \hat{\tau})/\|\hat{\sigma}^* + \hat{\tau}\|$, and the plane Σ^* that contains both of them, \hat{g}^* is the generic rotation axis that lies on Σ^* and can take $\hat{\sigma}^*$ onto $\hat{\tau}$. Letting β^* be the angle between \hat{e}_m^* and \hat{g}^* , the generic rotation axis that allows for the desired pointing is

$$\hat{g}^*(\delta) = \hat{e}_m^*(\delta) \cos \beta^* + \hat{e}_M^*(\delta) \sin \beta^* \quad (3.18)$$

where $-\pi/2 \leq \beta^* \leq \pi/2$. The rotation axis lies on the plane of feasible rotation axes Γ if the constraint given in Eq. (3.7) is enforced to the unit vector \hat{g}^* in Eq. (3.18). This is obtained by choosing β^* such that

$$\tan[\beta^*(\delta)] = -[\hat{e}_m^*(\delta) \cdot \hat{b}]/[\hat{e}_M^*(\delta) \cdot \hat{b}] \quad (3.19)$$

Finally, the amplitude of the second rotation around \hat{g}_Γ^* , namely $\hat{\alpha}^*(\delta)$, and the semi-aperture, $\mu^*(\delta)$, of the cone M^* can be calculated by means of Eqs. (3.5) and (3.9), respectively, in which the new values, $\hat{\alpha}^*(\delta)$ and $\beta^*(\delta)$, must be used.

The overall angular travel, α_{tot} , spanned by the sensitive axis $\hat{\sigma}^*$ during the two-steps maneuver is given by

$$\alpha_{tot}(\delta) = |\delta| + \hat{\alpha}^*(\delta) \quad (3.20)$$

Generally speaking, the torqueless direction \hat{b} can be prescribed in either the fixed frame $\mathbb{F}_B^{(1)}$ or in the body frame \mathbb{F}_B . This latter aspect was not relevant in previous works on kinematic approach for maneuver planning of underactuated satellites, such as Refs. [21] and [30], where a single non-nominal eigenaxis rotation was taken into account. As a matter of fact, when two rotations are considered, the position of the plane of admissible axes after the first rotation depends on whether \hat{b} is constant in either $\mathbb{F}_B^{(1)}$ or \mathbb{F}_B [31]. In this framework, the torqueless direction is prescribed in the orbit frame, as it is for

3.3 Maneuver Planning

the case of magnetic actuation. A similar planning strategy could be applied in the case when the torqueless direction is prescribed in the body frame. Nonetheless, non-trivial considerations would be required in this case, thus altering the mathematical outline of the present work.

3.3.3 Choice of δ for Method 1

As stated before, the minimum rotation amplitude for δ , required to take the sensitive axis out of the prohibited cone, Λ , can be derived by imposing internal and external tangency conditions between M^* and Λ . After the first rotation, the angular distance between the axes of the two cones is given by $\gamma^* = \cos^{-1} [\hat{\mathbf{g}}_{\Gamma}^*(\delta) \cdot \hat{\mathbf{l}}]$. If the cones Λ and M^* are externally tangent, then $\gamma^* = \mu^* + \lambda$. Conversely, when the cone Λ is tangent on the internal side of the surface of the cone M^* , one gets $\gamma^* = \mu^* - \lambda$. Note that M^* cannot lie inside Λ because $\hat{\boldsymbol{\sigma}}$ is assumed to be initially outside of Λ .

The angles γ^* and μ^* depend on the amplitude of the first rotation, δ , whereas λ is assigned by the geometry of the problem. According to the considered nomenclature, it is $\gamma = \gamma^*(\delta = 0)$ and $\mu = \mu^*(\delta = 0)$. It is possible to provide two equations

$$\varepsilon(\delta) = \gamma^*(\delta) - \mu^*(\delta) - \lambda \quad (3.21)$$

for internal tangency and

$$\varepsilon(\delta) = \gamma^*(\delta) - \mu^*(\delta) + \lambda \quad (3.22)$$

for external tangency, where the condition $\varepsilon(\delta) = 0$ implies that the cones Λ and M^* are tangent.

It is not necessary to solve both the Eqs. (3.21) and (3.22). In this framework, a criterion is provided in order to determine whether the shortest overall angular path, $\alpha_{tot}(\delta)$, can be reached through external or internal tangency. As already stated, if crossing occurs, then $\hat{\boldsymbol{\sigma}}$ spans a sector of the cone M , which intersects the cone Λ . Depending on whether the light source direction, $\hat{\mathbf{l}}$, lies internally or externally with respect to M , a smaller amplitude, $|\delta|$, is requested to reach external or internal tangency conditions, respectively. Define $\zeta(\delta) = \gamma^*(\delta) - \mu^*(\delta)$. In mathematical terms it follows that, if $\zeta(\delta = 0) < 0$ ($\hat{\mathbf{l}}$ lies inside M), then Eq. (3.22) is solved to obtain δ_e and drive $\hat{\boldsymbol{\sigma}}$ to external tangency. If, on the contrary, $\zeta(\delta = 0) > 0$ ($\hat{\mathbf{l}}$ lies outside M), then internal tangency is pursued by means of the Eq. (3.21).

Nonetheless, the trigonometric equations above cannot be solved analytically, and a numerical algorithm, like Newton-Raphson, is suggested [32]. Few iterations are needed for convergence, owing to the smooth shape of the function $\varepsilon = \varepsilon(\delta)$, whose first and second derivatives are continuous and different from zero in the interval $[\min \{\delta_i, \delta_e\}, \max \{\delta_i, \delta_e\}]$.

3. Kinematic Planning for Single-Axis Pointing in the Presence of Path Constraints

Consider the following practical case as an example:

$$\alpha = 55 \text{ deg}, \quad \hat{\mathbf{b}} = (0.6908, 0.4642, -0.5544)^T, \quad (3.23)$$

$$\hat{\mathbf{l}} = (0.9374, 0.3483, 0)^T$$

with a semi-aperture $\lambda = 10$ deg for the prohibited cone. In Tab. 3.1 the main parameters of the starting geometry are calculated, following the definitions given in the Problem Statement section.

Table 3.1: Maneuver case analysis: crossing verification.

Parameters	Test case (angles in [deg])
$\hat{\boldsymbol{\sigma}}$	$(1, 0, 0)^T$
$\hat{\boldsymbol{\tau}}$	$(0.5736, 0.8192, 0)^T$
$\hat{\mathbf{e}}_m$	$(0, 0, 1)^T$
$\hat{\mathbf{e}}_M$	$(0.8870, 0.4617, 0)^T$
β	33.83
$\hat{\mathbf{g}}_\Gamma$	$(0.4939, 0.2571, 0.8307)^T$
$\hat{\alpha}$	64.15
$\hat{\alpha}_{alt}$	-295.85
μ	60.40
γ	56.46
$\zeta(\delta = 0)$	$-\lambda < -3.94 < \lambda$
α_{cr}	23.52
$\xi(\alpha_{cr})$	$3.49 < \lambda$

The condition introduced in Eq. (3.10) is satisfied, so that crossing occurs and the double-step maneuver is required. In Fig. 3.2 the ζ curve is plotted as a function of δ , with lower and upper bounds represented by $-\lambda$ and λ , respectively. The grey sector includes all the values of δ for which $-\lambda < \zeta < \lambda$, i.e. all the amplitudes of the first rotation around $\hat{\mathbf{b}} \times \hat{\mathbf{g}}_\Gamma$ for which the sensitive axis still crosses the prohibited cone during the second rotation about $\hat{\mathbf{g}}_\Gamma^*$. The tangency values result to be $\delta_i = -11.38$ deg and $\delta_e = 42.41$ deg after a Newton-Raphson algorithm is applied to Eqs. (3.21) and (3.22), respectively, with a tolerance $tol = 10^{-3}$ deg. The dash-dot line in Fig. 3.2 instead represents the overall angular travel defined in Eq. (3.20), that results to be monotonically increasing with $|\delta|$.

3.3 Maneuver Planning

The shortest travel is reached by choosing the value of δ such that

$$|\delta| = \min \{|\delta_i|, |\delta_e|\} \quad (3.24)$$

In this case $\delta = \delta_i = -11.38$ deg with internal tangency, as expected from the above considerations on the sign of $\zeta(\delta = 0)$. It is now possible to provide the geometry of the problem after the first rotation, as resumed in Tab. 3.2. It is worth to note that the overall amplitude of the two-steps maneuver, α_{tot} , is still preferable with respect to the alternative one defined above with $\hat{\alpha}_{alt}$.

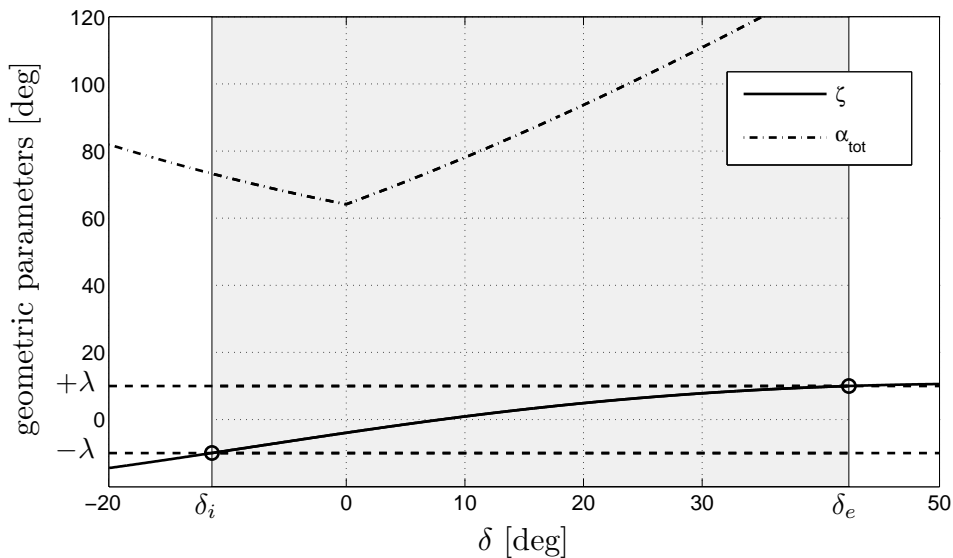


Figure 3.2: Geometric parameters as functions of δ .

In Fig. 3.3 a three-dimensional plot better describes the test case. In particular, it is possible to observe the path that $\hat{\sigma}$ would follow about $\hat{\mathbf{g}}_\Gamma$ (crossing the prohibited cone) and the path actually followed during the two-steps maneuver.

3.3.4 Method 2

The method introduced in the previous Section shows to be efficient both from the computational point of view and the overall angular path. Nonetheless, an application of the given approach is possible in the sense of an optimization of the whole maneuver at the cost of a doubled computational burden. The two-steps maneuver depicted in Fig. 3.3 is characterized by a tangency condition between the second rotation cone, M^* , and the prohibited one, Λ , driving $\hat{\sigma}$ onto $\hat{\tau}$ with the rotations $\mathcal{R}_1^{(a)}(\hat{\mathbf{b}} \times \hat{\mathbf{g}}_\Gamma, \delta^{(a)})$ and $\mathcal{R}_2^*(\hat{\mathbf{g}}_\Gamma^*, \hat{\alpha}^*)$, where the superscript ' \star ' refers to a rotation defining M^* . The same procedure can be

3. Kinematic Planning for Single-Axis Pointing in the Presence of Path Constraints

Table 3.2: Maneuver case analysis: crossing avoidance (Method 1).

Parameters	Test case (angles in [deg])
δ	-11.38
$\hat{\sigma}^*$	$(0.9858, 0.0014, -0.1677)^T$
α^*	55.49
\hat{e}_m^*	$(0.1667, -0.1168, 0.9791)^T$
\hat{e}_M^*	$(0.8810, 0.4636, -0.0948)^T$
β^*	28.80
\hat{g}_Γ^*	$(0.5706, 0.1210, 0.8123)^T$
$\hat{\alpha}^*$	61.95
μ^*	64.76
γ^*	54.76
ε^*	-10.00
α_{tot}	73.32

applied to the theoretical case in which $\hat{\tau}$ is taken onto an intermediate position $\hat{\tau}^*$ by means of a rotation $\mathcal{R}_1^{(b)}(\hat{\mathbf{b}} \times \hat{\mathbf{g}}_\Gamma, \delta^{(b)})$, and $\hat{\sigma}$ is driven to $\hat{\tau}^*$ with $\mathcal{R}_2^0(\hat{\mathbf{g}}_\Gamma^0, \hat{\alpha}^0)$, where the superscript '0' refers to a rotation defining M^0 . The two trajectories actually intersect in a direction defined by the vector $\hat{\mathbf{v}} = (v_1, v_2, v_3)^T$, that belongs to both the tangent cones M^* and M^0 (see Fig. 3.4). In other words, $\hat{\mathbf{v}}$ must satisfy the following conditions:

$$\hat{\mathbf{v}} \cdot \hat{\mathbf{g}}_\Gamma^* = \cos \mu^* \quad (3.25)$$

$$\hat{\mathbf{v}} \cdot \hat{\mathbf{g}}_\Gamma^0 = \cos \mu^0 \quad (3.26)$$

$$\hat{\mathbf{v}} \cdot \hat{\mathbf{v}} = 1 \quad (3.27)$$

where μ^* and μ^0 are, respectively, the semi-apertures of the cones M^* and M^0 . Provided $\hat{\mathbf{g}}_\Gamma^* = (\hat{g}_1^*, \hat{g}_2^*, \hat{g}_3^*)^T$ and $\hat{\mathbf{g}}_\Gamma^0 = (\hat{g}_1^0, \hat{g}_2^0, \hat{g}_3^0)^T$, where the subscript 'Γ' has been neglected, the system in Eqs.(3.25)–(3.27) is solved to obtain the components

$$v_1 = C + D v_3, \quad v_2 = E + F v_3 \quad (3.28)$$

provided

$$v_3 = \frac{-(EF + CD) \pm \sqrt{(EF + CD)^2 - (F^2 + D^2 + 1)(E^2 + C^2 - 1)}}{F^2 + D^2 + 1} \quad (3.29)$$

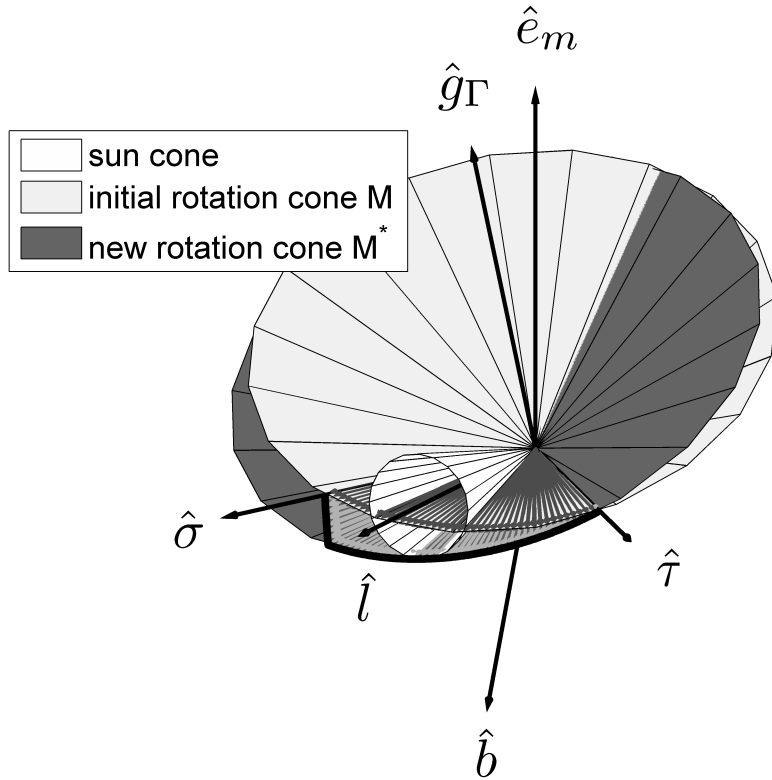


Figure 3.3: The two-steps maneuver (Method 1).

and

$$C \triangleq (\hat{g}_2^0 \cos \mu^* - \hat{g}_2^* \cos \mu^0) / (\hat{g}_1^* \hat{g}_2^0 - \hat{g}_2^* \hat{g}_1^0) \quad (3.30)$$

$$D \triangleq (\hat{g}_2^* \hat{g}_3^0 - \hat{g}_3^* \hat{g}_2^0) / (\hat{g}_1^* \hat{g}_2^0 - \hat{g}_2^* \hat{g}_1^0) \quad (3.31)$$

$$E \triangleq (\hat{g}_1^* \cos \mu^0 - \hat{g}_1^0 \cos \mu^*) / (\hat{g}_1^* \hat{g}_2^0 - \hat{g}_2^* \hat{g}_1^0) \quad (3.32)$$

$$F \triangleq (\hat{g}_3^* \hat{g}_1^0 - \hat{g}_1^* \hat{g}_3^0) / (\hat{g}_1^* \hat{g}_2^0 - \hat{g}_2^* \hat{g}_1^0). \quad (3.33)$$

Between the two solutions related to the sign in Eq. (3.29), the choice falls on the unit vector \hat{v} whose angular distance with respect to \hat{l} is smaller. After defining the angular separations $\nu^0 = \cos^{-1}(\hat{\sigma} \cdot \hat{v})$ between $\hat{\sigma}$ and \hat{v} , and $\nu^* = \cos^{-1}(\hat{\tau} \cdot \hat{v})$ between \hat{v} and $\hat{\tau}$, it is possible to formulate the final maneuver planning method. The two steps are defined as follows:

1. A first admissible rotation $\mathcal{R}_1(\hat{g}_\Gamma^0, \chi^0)$ is performed around the axis \hat{g}_Γ^0 with angular amplitude χ^0 , obtainable on the basis of spheric trigonometry considerations:

$$\chi^0 = 2 \sin^{-1} [\sin(\nu^0/2) / \sin \mu^0] \quad (3.34)$$

3. Kinematic Planning for Single-Axis Pointing in the Presence of Path Constraints

2. A second admissible rotation $\mathcal{R}_2(\hat{\mathbf{g}}_{\Gamma}^*, \chi^*)$ is performed around the axis $\hat{\mathbf{g}}_{\Gamma}^*$ with angular amplitude χ^* , given by

$$\chi^* = 2 \sin^{-1} [\sin(\nu^*/2) / \sin \mu^*] \quad (3.35)$$

With regard to the considered example, the geometry of the problem obtainable with Method 2 is resumed in Tab. 3.3.

Table 3.3: Maneuver case analysis: crossing avoidance (Method 2).

Parameters	Test case (angles in [deg])
$\hat{\mathbf{g}}_{\Gamma}^0$	$(0.2974, 0.5165, 0.8030)^T$
$\hat{\mathbf{g}}_{\Gamma}^*$	$(0.5706, 0.1210, 0.8123)^T$
μ^0	72.70
μ^*	64.76
$\hat{\mathbf{v}}$	$(0.9328, 0.3139, -0.1771)^T$
ν^0	21.13
ν^*	37.61
χ^0	22.14
χ^*	41.75
α_{tot}	63.89

The overall angular path after the two-steps maneuver results to be

$$\alpha_{tot} = \chi^0 + \chi^* = 63.89 \text{ deg} \quad (3.36)$$

that is actually optimized with respect to the value reported in Tab. 3.2 for Method 1.

3.4 Conclusions

In this Chapter a strategy is described that generates attitude profiles in the presence of path constraints, in order to perform single-axis pointing from one observation target to another. The first constraint is represented by the fact that, in underactuated conditions, satellite attitude effectors can deliver a control torque with two independent components only, so that the rotation axes cannot be chosen arbitrarily. The second one is related to the requirement of keeping the pointing axis far from a prohibited direction, as for the case of a

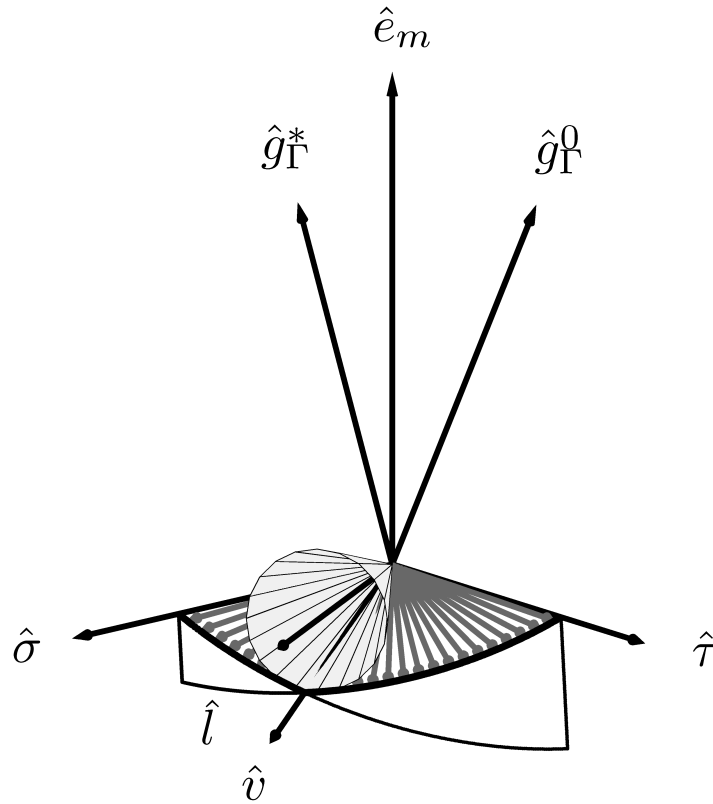


Figure 3.4: The two-steps maneuver (Method 2).

sensor boresight that must avoid bright light sources like Sun, Moon, and Earth albedo to prevent damage. The suggested kinematic solution consists of a two-steps maneuver where both the rotation axes are admissible, being perpendicular to the underactuated direction, which makes them compatible with the first constraint. As a further result, the overall angular path is minimized by means of an efficient numerical scheme and the algorithm is proven to keep the sensitive axis out of a clearance cone around the Sun direction for a case of practical interest, thus satisfying the second constraint with a desired safety margin. A test case is finally discussed in order to show the effectiveness of the approach.

3. Kinematic Planning for Single-Axis Pointing in the Presence of Path Constraints

Acquisition of a Desired Pure Spin Condition

4.1 Introduction

In this Chapter, a proof of global exponential stability is derived for a magnetic control law that drives a rigid satellite toward a pure spin condition around a prescribed principal axis of inertia with a desired angular rate $\bar{\omega}_d$. In a recent paper [14] a proof of global asymptotic stability was proposed for a b-dot-like control law that detumbles a spacecraft by means of magnetic actuators only. In that framework they proved that, in the presence of a time-varying magnetic field, the time derivative of the kinetic energy is strictly decreasing. The physical interpretation of the effects of the b-dot law allowed for the derivation of a criterion for selecting the gain that results into quasi-minimum detumbling time to zero angular speed.

As a matter of fact, in many practical applications, a detumbling maneuver is not designed to drive the spacecraft to zero angular velocity. A spacecraft with almost zero angular rate may be damaged because of thermal loads due to an excessively prolonged exposition of the sun-facing side to solar radiation. In other cases, a residual spinning motion is required to preserve a certain amount of angular momentum necessary to spin-up the momentum-wheel that provides gyroscopic stabilization. In such cases, the detumbling maneuver is required to drive the spacecraft toward a pure spin condition.

The use of magnetic actuators, where full three-axes control is not available, poses

Reference: Avanzini, G., de Angelis, E.L., and Giulietti, F., "Acquisition of a desired pure spin condition for a magnetically actuated spacecraft," *Journal of Guidance, Control, and Dynamics*, in press.

4. Acquisition of a Desired Pure Spin Condition

several challenges, also for the control task here considered. In this respect, a control law similar to that discussed in Ref. [14] works well also for the acquisition of a prescribed pure-spin condition (where the complete detumbling becomes a particular case of a more general command law), but the extension of the proof to the new scenario is not trivial. This extension represents the major contribution of the present work. The whole problem, including the command law, is rephrased in terms of angular momentum vector, rather than angular velocity components, where the acquisition of a pure spin condition is expected to be performed for spacecraft where angular rate measurements are available. In this case, provided there is no momentum/reaction-wheel, Eq. (2.1) is reshaped into

$$\dot{\mathbf{h}} = \mathbf{M} - (\mathbf{J}^{-1} \mathbf{h}) \times \mathbf{h} \quad (4.1)$$

where $\mathbf{h} = \mathbf{J} \boldsymbol{\omega}$ is the angular momentum vector. No external disturbance is considered in the analysis, so that the only external torque acting on the spacecraft is the magnetic control torque, $\mathbf{M} = \mathbf{m} \times \mathbf{b}$.

In what follows, the proof of stability in the case of acquisition of a desired spin rate is derived in terms of robustness of the global exponential stability of a nominal system by means of generalized exponential asymptotic stability in variations (GEASV) tools [16, 17]. To this aim, the error dynamics equation is first derived in the classical form of a nominal system perturbed by a vanishing perturbation term. Then, after proving the generalized exponential stability for the nominal system, such result is extended to the perturbed system [18].

As a further contribution, the approach derived in [14] for the choice of the control law gain is tailored to the present application, thus allowing to perform the acquisition of the desired pure spin condition in quasi-minimum time from arbitrary initial tumbling conditions. Stability and performance of the approach are extensively tested by means of numerical simulation.

4.2 Acquisition of a Desired Pure Spin Condition

Let $\hat{\mathbf{b}} = \mathbf{b}/\|\mathbf{b}\|$ be the body-frame geomagnetic unit vector. The scope of this Section is to prove that the control law

$$\mathbf{M}^{(c)} = k_h \left(\mathbb{I}_3 - \hat{\mathbf{b}} \hat{\mathbf{b}}^T \right) (\mathbf{h}_d - \mathbf{h}) \quad (4.2)$$

with $k_h > 0$, drives the spacecraft toward a desired pure spin condition around one of the principal axes of inertia, in spite of the fact that the resulting control torque is perpendicular to $\hat{\mathbf{b}}$ and does not provide full actuation. In what follows it will be assumed that the

4.2 Acquisition of a Desired Pure Spin Condition

desired spin axis is $\hat{\mathbf{e}}_2$, so that $\mathbf{h}_d = \mathbf{J} \boldsymbol{\omega}_d$, where $\boldsymbol{\omega}_d = (0, \bar{\omega}_d, 0)^T$. Upon substitution of Eq. (4.2) into Eq. (4.1), the latter can be rearranged as follows:

$$\dot{\mathbf{h}} = -k_h \left(\mathbb{I}_3 - \hat{\mathbf{b}} \hat{\mathbf{b}}^T \right) (\mathbf{h}_d - \mathbf{h}) - (\mathbf{J}^{-1} \mathbf{h}) \times \mathbf{h} \quad (4.3)$$

After defining the error between desired and current angular momentum vectors as $\boldsymbol{\varepsilon} = \mathbf{h}_d - \mathbf{h}$, the error dynamics is given by

$$\dot{\boldsymbol{\varepsilon}} = -k_h \left(\mathbb{I}_3 - \hat{\mathbf{b}} \hat{\mathbf{b}}^T \right) \boldsymbol{\varepsilon} + [\mathbf{J}^{-1} (\mathbf{h}_d - \boldsymbol{\varepsilon})] \times (\mathbf{h}_d - \boldsymbol{\varepsilon}). \quad (4.4)$$

The formulation of the spin stabilization problem, when external disturbances are not accounted for, becomes analytically treatable with GEASV tools if attitude dynamics in Eq. (4.4) is represented in terms of vector components expressed in the inertial frame, \mathbb{F}_I , rather than in the body frame, \mathbb{F}_B . With this choice, the dynamics of the angular momentum error for a magnetically controlled spacecraft can be written as

$$\dot{\mathbf{E}} = -k_h \mathbb{T}_{BI}^T \left(\mathbb{I}_3 - \hat{\mathbf{b}} \hat{\mathbf{b}}^T \right) \mathbb{T}_{BI} \mathbf{E} - \mathbb{T}_{BI}^T (\mathbf{J}^{-1} \mathbb{T}_{BI} \mathbf{E} \times \mathbf{h}_d) \quad (4.5)$$

where \mathbb{T}_{BI} is the coordinate transformation matrix between \mathbb{F}_I and \mathbb{F}_B and $\mathbf{E} = \mathbb{T}_{BI}^T \boldsymbol{\varepsilon}$.

The system in the form of Eq. (4.5) matches the classical linear time-varying perturbed system structure $\dot{\mathbf{E}} = \mathbf{A}(t) \mathbf{E} + \mathbf{g}(t, \mathbf{E})$, where $\mathbf{A}(t) = -k_h \mathbb{T}_{BI}^T \left(\mathbb{I}_3 - \hat{\mathbf{b}} \hat{\mathbf{b}}^T \right) \mathbb{T}_{BI}$ governs the nominal system and $\mathbf{g}(t, \mathbf{E}) = -\mathbb{T}_{BI}^T (\mathbf{J}^{-1} \mathbb{T}_{BI} \mathbf{E} \times \mathbf{h}_d)$ is a vanishing perturbation term.

Definition 1 *The solution $\mathbf{x} = \mathbf{0}$ of the system $\dot{\mathbf{x}} = \mathbf{f}(t, \mathbf{x})$ is said to be generalized exponentially asymptotically stable in variation (GEASV) if*

$$\|\Phi(t, t_0, \mathbf{x}_0)\| \leq K(t) e^{p(t_0) - p(t)} \quad (4.6)$$

for $t \geq t_0 \geq 0$, where $\Phi(t, t_0, \mathbf{x}_0) = \partial \mathbf{x}(t, t_0, \mathbf{x}_0) / \partial \mathbf{x}_0$ is the fundamental matrix, $\mathbf{x}_0 = \mathbf{x}(t_0)$, $K > 0$ is continuous on \mathbb{R}^+ , and $p \in C(\mathbb{R}^+)$, $p(0) = 0$, is strictly increasing in $t \in \mathbb{R}^+$.

In the following Theorem conditions are given such that GEASV of a linear time-varying perturbed system is obtained if the origin of the nominal system is globally exponentially stable.

Theorem 1 *Given the linear time-varying perturbed system $\dot{\mathbf{x}} = \mathbf{A}(t) \mathbf{x} + \mathbf{g}(t, \mathbf{x})$, let the origin $\mathbf{x} = \mathbf{0}$ be an exponentially stable solution of the nominal system $\dot{\mathbf{x}} = \mathbf{A}(t) \mathbf{x}$, and the perturbed term satisfy $\|\mathbf{g}(t, \mathbf{x})\| \leq \bar{\varphi} \|\mathbf{x}\|$, $\bar{\varphi} > 0$, $t \geq t_0 \geq 0$, $\|\mathbf{x}\| < \infty$. Then every solution of the perturbed system is GEASV.*

4. Acquisition of a Desired Pure Spin Condition

Proof: The nominal system is linear time-varying, and its solution takes the form $\mathbf{x}(t, t_0) = \Phi(t, t_0) \mathbf{x}_0$, where $\Phi(t, t_0)$ is independent of the initial state \mathbf{x}_0 . If the origin $\mathbf{x} = \mathbf{0}$ is a globally exponentially stable equilibrium point of the nominal system, then there exist constants $K_1 > 0$ and $\lambda_1 > 0$ such that

$$\|\Phi(t, t_0)\| \leq K_1 e^{-\lambda_1 (t-t_0)} \quad (4.7)$$

The definition in Eq. (4.6) can be tailored to the present case with the function $p(t) = \bar{\varphi}t + t^c$,

$$\|\Phi(t, t_0)\| \leq K_2 e^{[(\bar{\varphi}t_0 + t_0^c) - (\bar{\varphi}t + t^c)]} \quad (4.8)$$

for some $0 < c < 1$, $K(t) = K_2 \geq K_1$, and a proper choice of K_1 and a sufficiently large $\lambda_1 > \bar{\varphi}$ such that Eq. (4.7) holds. In Ref. [18] (see Theorem 3.8) it is proven that, if the maximal solution of the scalar differential equation

$$\dot{u}(t) = [-\dot{p}(t) + \bar{\varphi}] K(t) u(t), \quad u_0 = u(t_0) \geq 0, \quad (4.9)$$

is GEASV with the given choice of $p(t)$ and $K(t)$, then every solution of the perturbed system is GEASV. Note that GEASV implies exponential stability [33]. In this case, the differential problem in Eq. (4.9) becomes

$$\dot{u}(t) = -cK_2 t^{c-1} u(t) \quad (4.10)$$

It is easy to prove that the maximal solution of Eq. (4.10) is

$$u(t) = u_0 e^{K_2 (t_0^c - t^c)}, \quad u_0 \geq 0, \quad (4.11)$$

governed by the fundamental function

$$\Phi(t, t_0) = e^{K_2 (t_0^c - t^c)} \quad (4.12)$$

Provided $K_3 \leq K_2$, it follows that

$$\Phi(t, t_0) \leq K_4 e^{K_3 (t_0^c - t^c)} \quad (4.13)$$

where the definition of GEASV in Eq. (4.8) is applied to the present case with a function $p(t) = K_3 t^c$ and a constant $K_4 = 1$.

Remark For spin stabilization about the y -axis, hypotheses of Theorem 1 are satisfied. In particular, the origin $\mathbf{E} = \mathbf{0}$ is a globally exponentially stable equilibrium point of the nominal system $\dot{\mathbf{E}} = -k_h \mathbb{T}_{BI}^T (\mathbb{I}_3 - \hat{\mathbf{b}} \hat{\mathbf{b}}^T) \mathbb{T}_{BI} \mathbf{E}$ (see Appendix), and the perturbation term satisfies $\|\mathbf{g}(t, \mathbf{E})\| \leq \bar{\varphi} \|\mathbf{E}\|$, $t \geq t_0 \geq 0$, $\|\mathbf{E}\| < \infty$, provided $\bar{\varphi} = (J_2/J_{min}) |\bar{\omega}_d|$, where J_{min} is the minimum moment of inertia of the spacecraft.

4.2 Acquisition of a Desired Pure Spin Condition

4.2.1 Choice of the Control Gain

A reasonable choice for the control gain, k_h , that allows for reaching the desired spin condition in quasi-minimum time, can be derived by following an approach similar to that derived in Ref. [14] for the detumbling maneuver. A few difference need to be taken into account: 1) the whole system is now represented in terms of angular momentum dynamics; 2) a value of the desired final angular rate $\bar{\omega}_d \neq 0$ is expected at the end of the maneuver, which in turn requires that 3) the whole procedure is rephrased in terms of closed loop dynamics of the component of the error $\boldsymbol{\varepsilon}$ perpendicular to the Earth magnetic field, defined as $\boldsymbol{\varepsilon}_\perp = (\mathbb{I}_3 - \hat{\mathbf{b}}\hat{\mathbf{b}}^T)\boldsymbol{\varepsilon}$. The gain is then sized assuming that the error signal is a first order perturbation of the desired final spin condition.

The time derivative of $\boldsymbol{\varepsilon}_\perp$ is given by

$$\begin{aligned} \frac{d\boldsymbol{\varepsilon}_\perp}{dt} &= (\mathbb{I}_3 - \hat{\mathbf{b}}\hat{\mathbf{b}}^T) \left\{ -k_h (\mathbb{I}_3 - \hat{\mathbf{b}}\hat{\mathbf{b}}^T) \boldsymbol{\varepsilon} + [\mathbf{J}^{-1}(\mathbf{h}_d - \boldsymbol{\varepsilon})] \times (\mathbf{h}_d - \boldsymbol{\varepsilon}) \right\} + \\ &\quad - \left[\frac{d\hat{\mathbf{b}}}{dt} \hat{\mathbf{b}}^T + \hat{\mathbf{b}} \left(\frac{d\hat{\mathbf{b}}}{dt} \right)^T \right] \boldsymbol{\varepsilon} \end{aligned} \quad (4.14)$$

The gyroscopic term can no longer be neglected, as it was done in Ref. [14], but provided that $\mathbf{h}_d = (0, J_2\bar{\omega}_d, 0)^T$, it is

$$[\mathbf{J}^{-1}(\mathbf{h}_d - \boldsymbol{\varepsilon})] \times (\mathbf{h}_d - \boldsymbol{\varepsilon}) \approx - [(\mathbf{J}^{-1}\boldsymbol{\varepsilon}) \times \mathbf{h}_d + (\mathbf{J}^{-1}\mathbf{h}_d) \times \boldsymbol{\varepsilon}]$$

where $(\mathbf{J}^{-1}\mathbf{h}_d) \times \mathbf{h}_d = \mathbf{0}$ and higher order terms proportional to ε^2 were dropped.

Equation (4.14) can thus be recast in the form

$$\frac{d\boldsymbol{\varepsilon}_\perp}{dt} \cong -k_h \mathcal{A}\boldsymbol{\varepsilon} - \mathcal{A}\mathcal{G}\boldsymbol{\varepsilon} - \mathbb{T}_{BO} \mathcal{B} \mathbb{T}_{BO}^T \boldsymbol{\varepsilon} + \mathcal{C}\boldsymbol{\varepsilon} \quad (4.15)$$

where $\mathcal{A} = (\mathbb{I}_3 - \hat{\mathbf{b}}\hat{\mathbf{b}}^T)$ is the projection operator,

$$\mathcal{G}\boldsymbol{\varepsilon} = \bar{\omega}_d [(J_3 - J_2)\varepsilon_3/J_3, 0, (J_2 - J_1)\varepsilon_1/J_1]^T \quad (4.16)$$

is the gyroscopic term, and the last two terms, namely

$$\mathcal{B} = (1/\|\mathbf{b}_O\|^2) [\dot{\mathbf{b}}_O \mathbf{b}_O^T + \mathbf{b}_O \dot{\mathbf{b}}_O^T - (2/\|\mathbf{b}_O\|^2)(\dot{\mathbf{b}}_O^T \mathbf{b}_O) \mathbf{b}_O \mathbf{b}_O^T]$$

and

$$\mathcal{C} = \tilde{\boldsymbol{\Omega}}^r (\hat{\mathbf{b}}\hat{\mathbf{b}}^T) - (\hat{\mathbf{b}}\hat{\mathbf{b}}^T) \tilde{\boldsymbol{\Omega}}^r$$

are related to the rotation rate of the Earth magnetic field vector with respect to \mathbb{F}_B . Only the first term in Eq. (4.15) (named the active term) is directly related to the control torque

4. Acquisition of a Desired Pure Spin Condition

and it affects the magnitude of $\boldsymbol{\varepsilon}_\perp$, whereas the other three terms, the gyroscopic and the rotational terms, only affect the direction of $\boldsymbol{\varepsilon}_\perp$ in the body frame.

As explained in more detail in Ref. [14], high values of k_h cause the magnitude of the transverse component $\boldsymbol{\varepsilon}_\perp$ to rapidly vanish and, as a consequence, also the available control moment becomes small. The only possibility to further decrease $\|\boldsymbol{\varepsilon}\|$ relies on the residual angle between \mathbf{b} and $\boldsymbol{\varepsilon}$ induced by the (slow) rotation of \mathbf{b} with respect to the orbit frame, \mathbb{F}_O , which allows for a residual controllability. On the other hand, a small value of the gain causes a slow closed-loop dynamics, with long convergence time before the desired spinning condition is reached. The correct sizing of the gain is critical especially during the final phase of the maneuver, when the error is small, provided that magnetic coils saturate during the initial phase of the maneuver, when the error is large, unless the gain is vanishingly small.

A compromise can be obtained by imposing that the order of magnitude of the active term is equivalent to that of the rotational and gyroscopic ones in Eq. (4.15):

$$\mathcal{O}(\|k_h \mathcal{A} \boldsymbol{\varepsilon}\|) = \mathcal{O}(\|\mathcal{A} \mathcal{G} \boldsymbol{\varepsilon} + \mathbb{T}_{BO} \mathcal{B} \mathbb{T}_{BO}^T \boldsymbol{\varepsilon} - \mathcal{C} \boldsymbol{\varepsilon}\|) \leq \mathcal{O}(\|\mathcal{G} \boldsymbol{\varepsilon}\|) + \mathcal{O}(\|\mathcal{B} \boldsymbol{\varepsilon}\|) + \mathcal{O}(\|\mathcal{C} \boldsymbol{\varepsilon}\|) \quad (4.17)$$

The order of the active term, $\mathcal{A} \boldsymbol{\varepsilon}$, and of the first rotational term, $\mathcal{B} \boldsymbol{\varepsilon}$, can be derived from the discussion presented in Ref. [14]. Given the definition of norm for a linear operator, $\|\mathbf{M}\| = \max_{\mathbf{v} \in \mathbb{R}^n} (\|\mathbf{M} \mathbf{v}\| / \|\mathbf{v}\|) = \max_{1 \leq i \leq n} (|\lambda_i^{\mathbf{M}}|)$, where $\lambda_i^{\mathbf{M}}$, $i = 1, 2, \dots, n$ are the eigenvalues of \mathbf{M} , one gets that $\|\mathcal{A} \boldsymbol{\varepsilon}\| = \mathcal{O}(\boldsymbol{\varepsilon})$ and $\|\mathcal{B} \boldsymbol{\varepsilon}\| = \mathcal{O}(2n \sin \xi_m)$.

Unfortunately, the procedure described in [14] for the determination of $\mathcal{O}(\|\mathcal{C} \boldsymbol{\varepsilon}\|)$ cannot be adopted here, as long as the second rotational term must now take into account that the spacecraft is approaching a spin condition around one of the principal axes of inertia, $\hat{\mathbf{e}}_i$. Assuming that $\boldsymbol{\varepsilon}$ is a first order perturbation of \mathbf{h}_d and that $\bar{\omega}_d \gg \Omega$, one can assume that $\boldsymbol{\omega}^r \approx \boldsymbol{\omega}$ is approximately parallel to the desired spin axis, $\hat{\mathbf{e}}_i$. This means that

$$[\tilde{\boldsymbol{\Omega}}^r (\hat{\mathbf{b}} \hat{\mathbf{b}}^T) - (\hat{\mathbf{b}} \hat{\mathbf{b}}^T) \tilde{\boldsymbol{\Omega}}^r] \boldsymbol{\varepsilon} = (\hat{\mathbf{b}}^T \boldsymbol{\varepsilon})(\boldsymbol{\omega}^r \times \hat{\mathbf{b}}) - [\hat{\mathbf{b}}^T (\boldsymbol{\omega}^r \times \boldsymbol{\varepsilon})] \hat{\mathbf{b}} \approx \bar{\omega}_d \{ (\hat{\mathbf{b}}^T \boldsymbol{\varepsilon})(\hat{\mathbf{e}}_i \times \hat{\mathbf{b}}) - [\hat{\mathbf{b}}^T (\hat{\mathbf{e}}_i \times \boldsymbol{\varepsilon})] \hat{\mathbf{b}} \}$$

Let α be the angle between $\hat{\mathbf{e}}_i$ and $\hat{\mathbf{b}}$ and Γ the plane identified by them (Fig. 4.1). The direction of $\boldsymbol{\varepsilon}$ with respect to $\hat{\mathbf{e}}_i$ is determined by two angles, namely χ (the angular distance between the projection of $\boldsymbol{\varepsilon}$ on Γ and $\hat{\mathbf{e}}_i$) and δ (the elevation of $\boldsymbol{\varepsilon}$ with respect to Γ). On the basis of simple goniometric considerations it is possible to show that

$$\|\bar{\omega}_d \{ (\hat{\mathbf{b}}^T \boldsymbol{\varepsilon)(\hat{\mathbf{e}}_i \times \hat{\mathbf{b}}) - [\hat{\mathbf{b}}^T (\hat{\mathbf{e}}_i \times \boldsymbol{\varepsilon})] \hat{\mathbf{b}} \}\| = \|\boldsymbol{\varepsilon}\| \bar{\omega}_d \sin \alpha [\cos^2(\alpha - \chi) \cos^2 \delta + \sin^2 \delta]^{1/2} \leq \|\boldsymbol{\varepsilon}\| \bar{\omega}_d$$

This means that $\|\mathcal{C} \boldsymbol{\varepsilon}\| = \mathcal{O}(\bar{\omega}_d \boldsymbol{\varepsilon})$. The discussion is simpler for the gyroscopic term, where it is possible to see directly from its definition in Eq. (4.16) that 1) the linear form

4.2 Acquisition of a Desired Pure Spin Condition

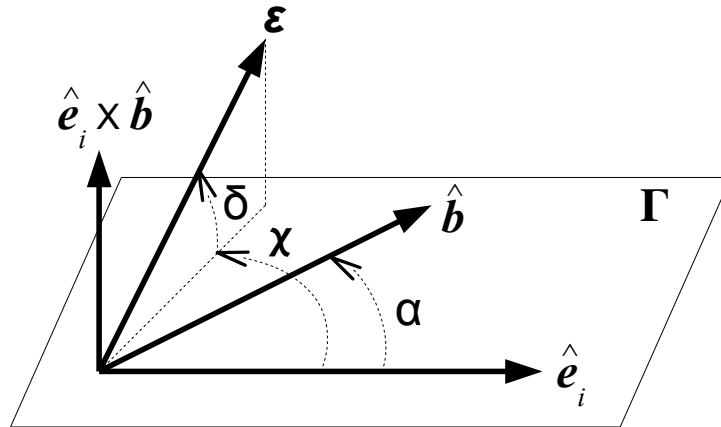


Figure 4.1: Position of \hat{e}_i , \hat{b} and $\boldsymbol{\varepsilon}$.

for the gyroscopic term does not feature any component along the spin axis and 2) the following inequality holds:

$$\|\mathcal{G}\boldsymbol{\varepsilon}\| \leq \mathcal{O}(\sigma_{\max} \bar{\omega}_d \|\boldsymbol{\varepsilon}\|) \quad \text{where } \sigma_{\max} = \max_{k \neq i} \left[\frac{|J_i - J_k|}{J_k} \right]$$

Provided that $n \ll \bar{\omega}_d$, the third term in Eq. (4.14) is negligible and it can be dropped. This in turn means that in this scenario the characteristics of the orbit flown by the spacecraft do not affect the gain selection logic. The remaining ones are required to satisfy the inequality

$$k_h \max_{\boldsymbol{\varepsilon}} \left(\frac{\|\mathcal{A}\boldsymbol{\varepsilon}\|}{\|\boldsymbol{\varepsilon}\|} \right) \leq \max_{\boldsymbol{\varepsilon}} \left(\frac{\|\mathcal{G}\boldsymbol{\varepsilon}\|}{\|\boldsymbol{\varepsilon}\|} \right) + \max_{\boldsymbol{\varepsilon}} \left(\frac{\|\mathcal{C}\boldsymbol{\varepsilon}\|}{\|\boldsymbol{\varepsilon}\|} \right) \approx |\bar{\omega}_d| (1 + \sigma_{\max}) \quad (4.18)$$

For an almost-spherical satellite the values of $|J_i - J_k|/J_k \ll 1$ and also the gyroscopic coupling term can be neglected, so that $k_h \leq |\bar{\omega}_d|$. If this is not the case, one gets

$$\begin{aligned} k_{h,i} &\leq |\bar{\omega}_d| && \text{for the spin axis} \\ k_{h,k} &\leq |\bar{\omega}_d| (1 + \sigma_{\max}) && \text{for } k \neq i \end{aligned} \quad (4.19)$$

This criterion provides an upper bound for the control gain, where higher values are expected to cancel the component of $\boldsymbol{\varepsilon}$ perpendicular to \hat{b} too soon. The actual optimal value that drives the spacecraft to the desired spin condition in minimum time is expected to be smaller than that indicated in Eq. (4.19). Also note that the criterion does not hold for vanishingly small values of the desired angular speed, $\bar{\omega}_d$, as long as in this case the assumption that $n \ll \bar{\omega}_d$ would be violated. In this latter case, the gain selection logic derived for the detumbling maneuver [14] can be shown to provide better results in terms of convergence time.

4.3 Results and Discussion

The control law discussed in the previous sections for the acquisition of a desired pure spin condition is applied to a low Earth orbit micro-satellite equipped with three mutually orthogonal magnetic coils. Relevant spacecraft data and orbit parameters are reported in Table 4.1, together with randomly generated initial conditions for a sample maneuver, that requires the spacecraft to converge toward a spin condition around the y body axis.

Table 4.1: Spacecraft and orbit data, with initial conditions for a sample maneuver (pure spin stabilization).

Parameter	Symbol	Value	Units
<i>Spacecraft data</i>			
Principal moments of inertia	J_1, J_2, J_3	0.33, 0.37, 0.35	kg m ²
Maximum magnetic dipole	m_{\max}	3.0	A m ²
<i>Orbit data</i>			
Radius	r_c	7 021	km
Period	T_{orb}	5855	s
Inclination	i	65	deg
<i>Sample maneuver</i>			
Initial Conditions	$\boldsymbol{\omega}_0$	$(1.2206, -0.1011, 0.5364)^T$	rad/s
	\mathbf{Q}_0	$(-0.822, 0.057, 0.515, 0.236)^T$	

Time histories of angular velocity magnitude, $\|\boldsymbol{\omega}\|$, angular rate component around the y -axis, ω_2 , and the norm of the error on angular momentum $\varepsilon = \|\boldsymbol{\varepsilon}\| = \|\mathbf{h} - \mathbf{h}_d\|$ are reported in Fig. 4.2 for this test case, where the nominal value of the gain $k_h = \bar{\omega}_d = 0.09$ is used, as suggested by Eq. (4.19).

Note that the magnitude of the error on \mathbf{h} is almost monotonically decreasing, where only minor fluctuations are present, induced by the precession motion during the tumbling phase, that starts from a spin condition where the maximum angular velocity component is around the x -axis. For $t/T_{orb} > 1$ the convergence of ε toward 0 becomes monotonous, as soon as $\boldsymbol{\omega}$ crosses the separatrix between spin conditions around the axes of minimum and maximum inertia. From this point onwards, $\|\boldsymbol{\omega}\|$ and ω_2 rapidly converge toward $\bar{\omega}_d = 0.09$. Similar results, not reported in the figures, are obtained for any possible choice of the desired spin axis and different values of $\bar{\omega}_d$.

The value of the gain k_h plays a crucial role on the duration of the spinning maneuver, and it is important to prove that the choice derived from Eq. (4.19) is reasonable in every

4.3 Results and Discussion

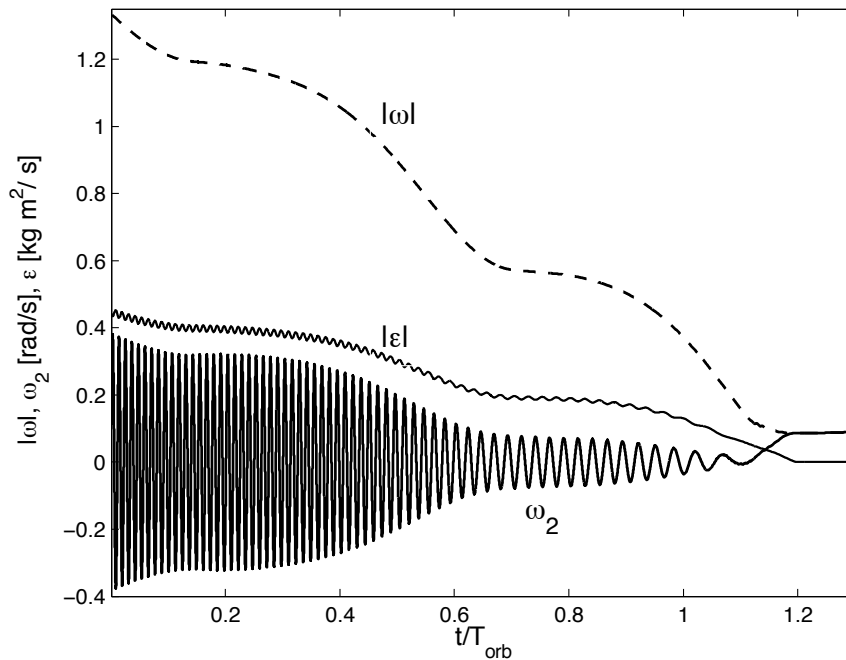


Figure 4.2: Time histories of relevant variables for a sample maneuver

operating condition, remembering that the tumbling motion after the satellite is ejected from the payload bay of the rocket launcher is (at least partially) random. Acceptable performance in terms of convergence time and energy consumption are needed, whichever the tumbling condition experienced by the spacecraft and the random attitude at which the detumbling maneuver is started. With this in mind, a Monte Carlo approach is used as in Ref. [14] to demonstrate the capability of the controller to spin the spacecraft to the desired angular rate starting from arbitrary initial conditions and to analyze the performance of the system for different values of k_h , proving that Eq. (4.19) provides a suitable estimate for the value for the control gain.

Spacecraft initial attitude and angular rates are randomly chosen by means of the psuedo-random number generator, $\text{rand}()$, implemented in MatlabTM environment, so that the same amount of angular momentum, $\|\Delta\mathbf{h}\| = \epsilon_0 = 0.45 \text{ kg m}^2/\text{s}$, is dissipated during each Monte Carlo run. The initial phase along the orbit, t_0 , is also randomly assigned, but the same final spin condition around the y -axis with $\bar{\omega}_d = \omega_2 = 0.09 \text{ rad/s}$ is tracked.

Figure 4.3 shows the results obtained from the Monte Carlo analysis, where t_F indicates the number of orbits necessary for reaching the desired spinning motion. Given the asymptotic nature of the convergence, a threshold on the residual error, $\|\epsilon\| < 10^{-4} \text{ kg m}^2/\text{s}$, is used for stopping the simulation. A population of 1000 test cases was generated and performance in terms of time is reported for different values of the gain k_h , that is varied between $k_h^*/16$ and $2k_h^*$, where $k_h^* = \bar{\omega}_d$ represents the nominal value.

4. Acquisition of a Desired Pure Spin Condition

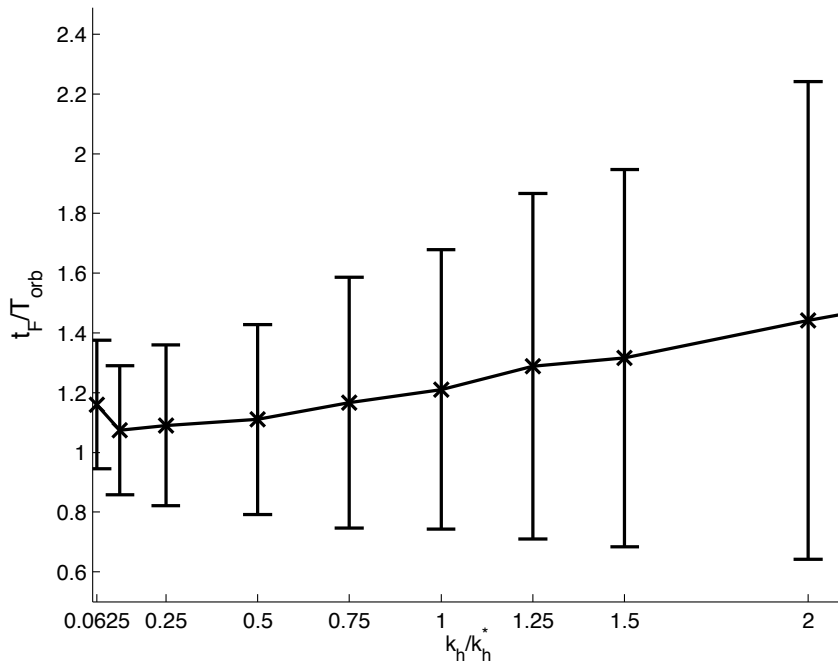


Figure 4.3: Performance analysis in terms of spin acquisition average time

The average value of t_F and its standard deviation obtained for the considered set of test-cases are reported in Fig. 4.3. Note that, by increasing the value of the gain, a longer average convergence time is obtained, as expected, but also an excessively small value of the gain makes convergence times longer on average. Two major differences are evident with respect to the detumbling maneuver considered in [14] (which represents a particular case of the present problem, for $\bar{\omega}_d = 0$). First of all, the sensitivity of the average value of t_F to variations of k_h is significantly weaker, being limited to approximately 10% of the minimum value achieved by t_F over the interval $k_h^*/16 \leq k_h < k_h^*$. Conversely, the standard deviation is larger and it grows with higher values of k_h . Such a growth is related to a stronger sensitivity of the maneuver to the initial attitude variables, that may result into considerably different values of t_F for the same k_h .

The best average performance in terms of t_F is obtained for $k_h = k_h^*/8$, where a minimum for the standard deviation of t_F is also achieved, which means that the dispersion of the results is smaller. It is noteworthy to observe how, in spite of the considerable simplifications at the basis of its derivation, Eq. (4.19) provides a reliable indication for the order of magnitude of the control law gain by means of a simple expression based on a few relevant system parameters that results into quasi-optimal performance ($\bar{t}_F = 1.21$ for $k_h = k_h^*$, to be compared with a minimum value of $\bar{t}_F = 1.08$ for $k_h = k_h^*/8$). The fact that the actual optimal gain is obtained for a smaller value with respect to that provided

4.4 Conclusions

by Eq. (4.19) is reasonable, provided that Eq. (4.19) is derived by means of a sequence of inequalities, aimed at the determination of an upper bound for the norm of the terms in Eq. (4.17).

This situation also holds for different mass distributions. For the considered spacecraft, convergence to desired spin conditions around either the intermediate or minimum inertia axes requires approximately the same amount of time on average. When larger difference between principal moments of inertia are dealt with, convergence to the unstable spin condition around the intermediate axes may require longer settling times.

More serious problems arise only when major differences between principal moments of inertia are present (e.g. the maximum moment of inertia is two or three times larger than the minimum one) and dipole moments generated by the coils are not correctly sized with respect to spacecraft inertia. In the presence of large gyroscopic terms, one or two coils can remain saturated at the same time for long intervals. Convergence is still achieved, but a large amount of time (up to several orbits) is spent tumbling after most of the excess angular momentum is dissipated, with only a minor residual reduction of angular momentum error per orbit. When the error is reduced below saturation level, convergence to the desired spin state is rapidly achieved.

Note that this scenario is unlikely for most practical applications of magnetic control to small-scale spacecraft, where almost cubic or cylindrical oblate configurations are usually employed. Anyway, if dipole moments are correctly sized with respect to spacecraft inertias, the problem is never encountered.

4.4 Conclusions

A proof for the global exponential stability of a magnetic controller that stabilizes a satellite with a spin rate around one of the principal axes of inertia is derived. The physical interpretation of the control law allows for a preliminary design of the control law gain k_h , with the aim of minimizing (on average) the required maneuver time for the acquisition of the desired spin condition. Numerical simulations confirm closed-loop stability and a reasonable response of spacecraft attitude parameters to the considered control action. A Monte Carlo approach allows for the study of the behavior of the system for a large number of randomly generated test cases, demonstrating that, on average, gain values smaller than the nominal one may improve performance. A large dispersion in the results is evident, which indicates how the acquisition of a desired spin condition is sensitive to the initial random tumbling motion, thus making the gain selection issue less critical than for the detumbling case.

4. Acquisition of a Desired Pure Spin Condition

5.1 Introduction

The objective of this study is the determination of a control law that allows for the acquisition of a desired pure spin condition of a rigid spacecraft around one of its principal axes of inertia by means of magnetic actuators only, while aiming the spin axis in a prescribed direction in the inertial frame.

In Cheon et al. [34], the problem of target pointing is tackled in the case where only magnetic devices are used, more specifically magnetometers and magnetic torquers, with the function, respectively, of attitude sensors and actuators. As a major limitation, the approach, derived after a linearization of the governing equations of motion, provides local asymptotic stability only for the resulting controller. In Ref. [35] a pointing control law is proven to asymptotically stabilize an axisymmetric spacecraft under controller saturation and multiple failures of up to two magnetic torque-rods, with good numerical results also extended to satellites with triaxial inertia properties.

In this work, a continuous control law based on angular momentum shaping successfully achieves the mission task. The analysis partially follows the philosophy introduced in Ch. 4, where convergence toward a desired spin rate is obtained by proving robustness of generalized exponential asymptotic stability in variation (GEASV) of a linear time-varying nominal system with respect to a vanishing perturbation. In this framework, the

Reference: Avanzini, G., de Angelis, E.L., and Giulietti, F., “Spin-Axis Pointing of a Magnetically Actuated Spacecraft,” *Acta Astronautica*, in press.

error dynamics equation is conversely derived for two error signals, namely the angular momentum error in the body frame and the angular momentum error with respect to the desired direction of the spin axis in the inertial frame. The error dynamics is thus cast in the form of a nonlinear time-varying nominal system perturbed by a vanishing term. After proving the global exponential stability for the nominal system, such result is extended to the perturbed one.

The control law is then tested by means of numerical simulations, in order to demonstrate the performance and stability properties of the method. In particular, a Monte Carlo approach is used to empirically evaluate the convergence capability of the controller to obtain single-axis pointing from arbitrary initial conditions and determine average convergence time as a function of control gains.

5.2 Acquisition of a Pure Spin Condition in the Inertial Frame

Let $\hat{\boldsymbol{\tau}}$ be the unit vector that identifies the target direction, which is fixed in the inertial frame, and $\boldsymbol{\omega}_d$ is the desired pure spin condition about one of the principal axes of inertia, *e.g.* $\boldsymbol{\omega}_d = (0, \bar{\omega}_d, 0)^T$. The components of the desired angular momentum vector, expressed in a set of principal axes and in the inertial frame, are given by $\mathbf{h}_d = \mathbf{J} \boldsymbol{\omega}_d$ and $\mathbf{H}_d = \|\mathbf{h}_d\| \hat{\boldsymbol{\tau}}$, respectively. Two different angular momentum error variables can thus be introduced, namely

$$\boldsymbol{\zeta} = \mathbf{H}_d - \mathbf{h} \quad (5.1)$$

and

$$\boldsymbol{\varepsilon} = \mathbf{h}_d - \mathbf{h} \quad (5.2)$$

where all the vector quantities, including \mathbf{H}_d , are represented in terms of body-frame components.

The scope of this Section is to prove that, on inclined LEOs, the magnetic control law

$$\mathbf{M}^{(c)} = (\mathbb{I}_3 - \hat{\mathbf{b}} \hat{\mathbf{b}}^T) (k_\zeta \boldsymbol{\zeta} + k_\varepsilon \boldsymbol{\varepsilon}) \quad (5.3)$$

with $k_\zeta > 0$ and $k_\varepsilon > 0$, drives the spacecraft toward a pure spin condition about one of the principal axes of inertia (*i.e.* $\boldsymbol{\varepsilon} \rightarrow \mathbf{0}$), while pointing the spin axis along the target direction $\hat{\boldsymbol{\tau}}$ (*i.e.* $\boldsymbol{\zeta} \rightarrow \mathbf{0}$), despite the fact that the resulting control torque, perpendicular to the direction $\hat{\mathbf{b}}$ of the geomagnetic field, does not provide full actuation. No momentum/reaction-wheel is considered in the present analysis.

5.2 Acquisition of a Pure Spin Condition in the Inertial Frame

Since \mathbf{H}_d is fixed in the inertial frame, its dynamics is given in body coordinates by

$$\dot{\mathbf{H}}_d = -\boldsymbol{\omega} \times \mathbf{H}_d \quad (5.4)$$

By recalling the definition of the error one has

$$\dot{\boldsymbol{\zeta}} = -\mathbf{M}^{(c)} - \boldsymbol{\omega} \times \boldsymbol{\zeta} \quad (5.5)$$

From Eq. (5.2) it immediately follows that

$$\boldsymbol{\omega} = \mathbf{J}^{-1}(\mathbf{h}_d - \boldsymbol{\varepsilon}) \quad (5.6)$$

that can be substituted in Eq. (5.5). By taking into account Eq. (5.3), it is

$$\dot{\boldsymbol{\zeta}} = -(\mathbb{I}_3 - \hat{\mathbf{b}}\hat{\mathbf{b}}^T)(k_\zeta \boldsymbol{\zeta} + k_\varepsilon \boldsymbol{\varepsilon}) - \mathbf{J}^{-1}(\mathbf{h}_d - \boldsymbol{\varepsilon}) \times \boldsymbol{\zeta} \quad (5.7)$$

Since \mathbf{h}_d is a constant vector in body axes and taking into account Eq. (5.6), the body frame angular momentum error dynamics achieves the form

$$\dot{\boldsymbol{\varepsilon}} = -(\mathbb{I}_3 - \hat{\mathbf{b}}\hat{\mathbf{b}}^T)(k_\zeta \boldsymbol{\zeta} + k_\varepsilon \boldsymbol{\varepsilon}) + \mathbf{J}^{-1}(\mathbf{h}_d - \boldsymbol{\varepsilon}) \times (\mathbf{h}_d - \boldsymbol{\varepsilon}) \quad (5.8)$$

As already pointed out, the formulation of the momentum management problem in Eqs. (5.7) and (5.8), when external disturbances are not accounted for, can be conveniently represented in terms of vector components in the inertial frame, \mathbb{F}_I , rather than in the body frame, \mathbb{F}_B . In addition, let the inverse of the inertia matrix, \mathbf{J}^{-1} , be written as the sum of two terms: 1) the first one is related to an axisymmetric configuration, namely $\mathbf{J}_a^{-1} = \text{diag}(1/\bar{J}, 1/J^*, 1/\bar{J})$, where $\bar{J}, J^* \in \mathbb{R}^+$ and $\bar{J} \neq J^*$; 2) the second one, $\boldsymbol{\Delta} = \text{diag}(\delta_1, \delta_2, \delta_3)$, is a perturbation term such that $\mathbf{J}^{-1} = \mathbf{J}_a^{-1} + \boldsymbol{\Delta}$, provided that $\delta_1, \delta_2, \delta_3 \in \mathbb{R}$. Without loss of generality, one can pose $J^* = J_2$ and $\bar{J} = (J_1 + J_3)/2$, so that one gets $\delta_2 = 0$, $\delta_1 = \sigma/J_1$ and $\delta_3 = -\sigma/J_3$, where $\sigma = (J_3 - J_1)/(J_1 + J_3)$.

With this choice, the error dynamics for the magnetically controlled spacecraft formulated in Eqs. (5.7) and (5.8) can be rewritten in terms of inertial components,

$$\dot{\mathbf{Z}} = -\left[\mathbb{T}_{BI}^T \left(\mathbb{I}_3 - \hat{\mathbf{b}}\hat{\mathbf{b}}^T\right) \mathbb{T}_{BI}\right] (k_\zeta \mathbf{Z} + k_\varepsilon \mathbf{E}) \quad (5.9)$$

$$\dot{\mathbf{E}} = -\left[\mathbb{T}_{BI}^T \left(\mathbb{I}_3 - \hat{\mathbf{b}}\hat{\mathbf{b}}^T\right) \mathbb{T}_{BI}\right] (k_\zeta \mathbf{Z} + k_\varepsilon \mathbf{E}) - \mathbb{T}_{BI}^T \left\{[(\mathbf{J}_a^{-1} + \boldsymbol{\Delta}) \mathbb{T}_{BI} \mathbf{E}] \times \mathbf{h}_d\right\} \quad (5.10)$$

where $\mathbf{Z} = \mathbb{T}_{BI}^T \boldsymbol{\zeta}$ and $\mathbf{E} = \mathbb{T}_{BI}^T \boldsymbol{\varepsilon}$. Defined $\mathbf{Y} = (\mathbf{Z}^T, \mathbf{E}^T)^T$, $\mathbf{Y} \in \mathbb{R}^6$, the system in Eqs. (5.9) and (5.10) is reshaped into

$$\dot{\mathbf{Y}} = -\mathbf{A}(t)\mathbf{K}\mathbf{Y} - \mathbf{B}(t, \mathbf{Y}) - \mathbf{C}(t, \mathbf{Y}) \quad (5.11)$$

where

$$\mathbf{A}(t) = \begin{pmatrix} \mathbb{T}_{BI}^T \left(\mathbb{I}_3 - \hat{\mathbf{b}} \hat{\mathbf{b}}^T \right) \mathbb{T}_{BI} & \mathbb{T}_{BI}^T \left(\mathbb{I}_3 - \hat{\mathbf{b}} \hat{\mathbf{b}}^T \right) \mathbb{T}_{BI} \\ \mathbb{T}_{BI}^T \left(\mathbb{I}_3 - \hat{\mathbf{b}} \hat{\mathbf{b}}^T \right) \mathbb{T}_{BI} & \mathbb{T}_{BI}^T \left(\mathbb{I}_3 - \hat{\mathbf{b}} \hat{\mathbf{b}}^T \right) \mathbb{T}_{BI} \end{pmatrix} \in \mathbb{R}^{6 \times 6} \quad (5.12)$$

is a time-dependent matrix,

$$\mathbf{K} = \begin{pmatrix} k_\zeta \mathbb{I}_3 & \mathbf{0}_{3 \times 3} \\ \mathbf{0}_{3 \times 3} & k_\varepsilon \mathbb{I}_3 \end{pmatrix} \in \mathbb{R}^{6 \times 6} \quad (5.13)$$

is a gain matrix, and

$$\mathbf{B}(t, \mathbf{Y}) = \begin{pmatrix} \mathbf{0}_{3 \times 1} \\ \mathbb{T}_{BI}^T [(\mathbf{J}_a^{-1} \mathbb{T}_{BI} \mathbf{E}) \times \mathbf{h}_d] \end{pmatrix}, \quad \mathbf{C}(t, \mathbf{Y}) = \begin{pmatrix} \mathbf{0}_{3 \times 1} \\ \mathbb{T}_{BI}^T [(\Delta \mathbb{T}_{BI} \mathbf{E}) \times \mathbf{h}_d] \end{pmatrix} \quad (5.14)$$

are gyroscopic coupling terms.

Equation (5.11) matches the formulation of a perturbed system $\dot{\mathbf{Y}} = \mathbf{f}(t, \mathbf{Y}) + \mathbf{g}(t, \mathbf{Y})$ where $\mathbf{f}(t, \mathbf{Y}) = -\mathbf{A}(t)\mathbf{K}\mathbf{Y} - \mathbf{B}(t, \mathbf{Y})$ governs the nominal system, while $\mathbf{g}(t, \mathbf{Y}) = -\mathbf{C}(t, \mathbf{Y})$ is a vanishing perturbation term, that is $\mathbf{g}(t, \mathbf{0}) = \mathbf{0}$. The following lemma gives stability conditions of a system in the perturbed form from stability properties of the nominal system [36].

Lemma 1 *Consider the system*

$$\dot{\mathbf{x}} = \mathbf{f}(t, \mathbf{x}) + \mathbf{g}(t, \mathbf{x}) \quad (5.15)$$

where $\mathbf{f} : [0, \infty) \times \mathcal{D} \rightarrow \mathbb{R}^n$ and $\mathbf{g} : [0, \infty) \times \mathcal{D} \rightarrow \mathbb{R}^n$ are piecewise continuous in t and locally Lipschitz in \mathbf{x} on $[0, \infty) \times \mathcal{D}$, and $\mathcal{D} \subset \mathbb{R}^n$ is a domain that contains the origin $\mathbf{x} = \mathbf{0}$. Let $\mathbf{x} = \mathbf{0}$ be an exponentially stable equilibrium point of the nominal system $\dot{\mathbf{x}} = \mathbf{f}(t, \mathbf{x})$. Let $V(t, \mathbf{x})$ be a Lyapunov function of the nominal system that satisfies the inequalities

$$c_1 \|\mathbf{x}\|^2 \leq V(t, \mathbf{x}) \leq c_2 \|\mathbf{x}\|^2 \quad (5.16)$$

$$\frac{\partial V}{\partial t} + \frac{\partial V}{\partial \mathbf{x}} \mathbf{f}(t, \mathbf{x}) \leq -c_3 \|\mathbf{x}\|^2 \quad (5.17)$$

$$\left\| \frac{\partial V}{\partial \mathbf{x}} \right\| \leq c_4 \|\mathbf{x}\| \quad (5.18)$$

for all $(t, \mathbf{x}) \in [0, \infty) \times \mathcal{D}$ for some positive constants c_1 , c_2 , c_3 , and c_4 . Suppose the perturbation term $\mathbf{g}(t, \mathbf{x})$ satisfies the linear growth bound

$$\|\mathbf{g}(t, \mathbf{x})\| \leq \gamma \|\mathbf{x}\|, \quad \forall t \geq 0, \forall \mathbf{x} \in \mathcal{D} \quad (5.19)$$

5.2 Acquisition of a Pure Spin Condition in the Inertial Frame

where γ is a nonnegative constant such that

$$\gamma < \frac{c_3}{c_4} \quad (5.20)$$

Then, the origin is an exponentially stable equilibrium point of the perturbed system in Eq. (5.15). Moreover, if all the assumptions hold globally, then the origin is globally exponentially stable.

Remark For spin stabilization about the y -axis, hypotheses of Lemma 1 are satisfied. In particular, the origin $\mathbf{Y} = \mathbf{0}$ is a globally exponentially stable equilibrium point of the nominal system $\dot{\mathbf{Y}} = -\mathbf{A}(t)\mathbf{K}\mathbf{Y} - \mathbf{B}(t, \mathbf{Y})$ (see Appendix), and the perturbation term satisfies $\|\mathbf{g}(t, \mathbf{Y})\| \leq \bar{\gamma} \|\mathbf{Y}\|$ for all $(t, \mathbf{Y}) \in [0, \infty) \times \mathbb{R}^6$, provided $\bar{\gamma} = J_2 |\bar{\omega}_d| \delta_{\max}$, where $\delta_{\max} = \max\{|\delta_1|, |\delta_2|, |\delta_3|\}$. According to the factorization chosen for the gyroscopic coupling terms in Eq. (5.14), it is

$$\delta_{\max} = \frac{|J_1 - J_3|}{\min\{J_1, J_3\} (J_1 + J_3)}. \quad (5.21)$$

Lemma 1 is conceptually important because it shows that exponential stability of the origin is robust with respect to a class of perturbations that satisfy Eqs. (5.19) and (5.20). To assert this robustness property, it is not necessary to know $V(t, \mathbf{x})$ explicitly. It is just enough to know that the origin is an exponentially stable equilibrium of the nominal system. Sometimes, it is possible to show that the origin is exponentially stable without actually finding a Lyapunov function that satisfies Eqs. (5.16)–(5.18). This is the case, for example, when exponential stability of the origin is shown using Corollary 1 in the Appendix. Irrespective of the method used to show exponential stability of the origin, the existence of $V(t, \mathbf{x})$ satisfying Eqs. (5.16)–(5.18) can be asserted by application of Theorem 4.14 in Ref. [36] (provided the Jacobian matrix $[\partial V/\partial \mathbf{x}]$ is bounded). However, if the Lyapunov function $V(t, \mathbf{x})$ is unknown, the bound of Eq. (5.20) cannot be calculated. Consequently, the robustness conclusion becomes a qualitative one where it is proven that the origin is exponentially stable for all perturbations satisfying Eq. (5.20) with sufficiently small γ . On the other hand, if $V(t, \mathbf{x})$ is known, the bound of Eq. (5.20) is explicitly calculated, which is an additional piece of information. Be careful not to overemphasize the usefulness of such bounds because they could be conservative for a given perturbation $\mathbf{g}(t, \mathbf{x})$. The conservatism is a consequence of the worst case analysis philosophy.

In this framework, the bound on $\bar{\gamma}$ translates into a requirement on the maximum magnitude of the desired spin rate, actually relaxed when the moments of inertia of the spacecraft other than the one of the spinning axis are sufficiently close (thus approaching the case when the satellite has axisymmetric inertia properties). This scenario is likely for many practical applications regarding small-scale spacecraft, where almost cubic or cylindrical

oblate configurations are usually employed. As an example, when spin stabilization is adopted as a simple and cost-effective method of keeping a spacecraft pointed in a certain direction, configurations are generally designed with axisymmetric properties and spin is provided about the axis of symmetry. In any case, regardless of the explicit knowledge of the bound, simulations have been performed for various magnitudes of the desired spin rate (see the Results and Discussion section). The results have been omitted, not adding further information to the test case, but they have proven that exponential stability is not at stake for a wide range desired spin rates of practical interest.

5.2.1 Effects Due to Uncertainties on the Geomagnetic Field

As a final issue, it is important to discuss the effects of uncertainties on the magnetic field on expected performance of the control law, where the actual geomagnetic vector, $\tilde{\mathbf{b}} = \mathbf{b} + \Delta\mathbf{b}$, can be written as the sum of its ideal (or estimated) value \mathbf{b} plus an uncertainty, $\Delta\mathbf{b}$. The commanded dipole moment $\mathbf{m} = \mathbf{b} \times \mathbf{M} / \|\mathbf{b}\|^2$ is evaluated as in [14], for the nominal values of geomagnetic field vector, \mathbf{b} , and control torque, $\mathbf{M} = (\mathbb{I}_3 - \hat{\mathbf{b}}\hat{\mathbf{b}}^T)(k_\zeta\boldsymbol{\zeta} + k_\varepsilon\boldsymbol{\varepsilon})$. The actual control torque, $\tilde{\mathbf{M}} = \mathbf{m} \times \tilde{\mathbf{b}}$, thus achieves the form

$$\tilde{\mathbf{M}} = [(\mathbf{b}^T\tilde{\mathbf{b}})\mathbf{M} - (\mathbf{M}^T\tilde{\mathbf{b}})\mathbf{b}] / \|\mathbf{b}\|^2$$

A condition on the maximum acceptable deviation for the magnetic field with respect to its nominal value assumed in the derivation of the control law can be found, such that asymptotic convergence to the desired spin condition can be obtained also in the presence of an uncertain geomagnetic field. Noting that \mathbf{m} , \mathbf{b} , and \mathbf{M} are mutually perpendicular, the uncertainty on the geomagnetic field can be represented in terms of components parallel to \mathbf{m} , \mathbf{b} , and \mathbf{M} , respectively, that is, $\Delta\mathbf{b} = (\Delta b_m, \Delta b_b, \Delta b_M)^T$. The first component of the uncertainty does not affect the actual torque at all, whereas the second one, which varies the magnitude of \mathbf{b} , affects the magnitude of the resulting torque only, but it does not change its direction, and it is thus equivalent to a variation of the gains, k_ε and k_ζ . Both these perturbations of \mathbf{b} can thus be rather large, without consequences on the stability of the control law, and Δb_M is the only uncertainty component that needs to be bounded.

When only Δb_M is considered, $\tilde{\mathbf{b}}$ is rotated by an angle δ with respect to its nominal direction \mathbf{b} in the plane identified by \mathbf{b} and \mathbf{M} , such that $(\mathbf{b}^T\tilde{\mathbf{b}}) / \|\mathbf{b}\|^2 \approx \cos \delta$, with $\tan \delta = \Delta b_M / \|\mathbf{b}\|$. The direction of the error signal, $\mathbf{e} = k_\zeta\boldsymbol{\zeta} + k_\varepsilon\boldsymbol{\varepsilon}$ also lies on the plane identified by \mathbf{M} and \mathbf{b} , forming an angle β with \mathbf{b} . Assuming for the sake of simplicity that the gains k_ε and k_ζ are equal ($k_\varepsilon = k_\zeta = k$), the nominal control torque is given by $\|\mathbf{M}\| = k\|\boldsymbol{\varepsilon} + \boldsymbol{\zeta}\| \sin \beta$. At this point it is possible to show that the dot product represented by $\mathbf{e}^T\tilde{\mathbf{M}}$ remains positive if $\delta < \beta$, that is, the magnitude of the error signal decreases thanks

5.3 Results and Discussion

to the considered control law in spite of the uncertainty on \mathbf{b} . This translates into a requirement on the maximum admissible value for Δb_M , that is required to satisfy the inequality $\Delta b_M / \|\mathbf{b}\| = \tan \delta < \tan \beta$.

The sum of the error signals $\boldsymbol{\varepsilon}$ and $\boldsymbol{\zeta}$ can, in general, achieve any value, and β can thus become arbitrarily small. In this condition, the robustness requirement on the exact estimate of \mathbf{b} appears as a severe one. But when the error signal is close to the nominal direction of \mathbf{b} , the corresponding nominal torque, proportional to $\sin \beta$, is also small. In such a case, errors on the control action do not affect significantly convergence performance, which becomes only marginally slower. Moreover, the choice of the control gains requires that the error signal is maintained as much as possible far from the direction of the magnetic field, as suggested in [14] and [37]. In any case, provided that it is not possible to activate magnetic coils during the measurement of \mathbf{b} with magnetometers, it is possible to exploit intervals during which the angle β becomes small in order to switch the control law off and activate magnetometers to update the estimate of \mathbf{b} .

5.3 Results and Discussion

The control law proposed in the previous Section for the acquisition of the desired pure spin condition and the desired orientation of the spin axis is now applied to a low Earth orbit micro-satellite, equipped with three mutually orthogonal magnetic coils. Table 5.1 shows spacecraft data and orbit parameters. The angle α , defined as

$$\alpha = \cos^{-1}(\hat{\boldsymbol{\tau}} \cdot \hat{\mathbf{e}}_2), \quad (5.22)$$

that represents the angular distance between the desired spin axis $\hat{\mathbf{e}}_2$ and the target direction $\hat{\boldsymbol{\tau}}$, will be used as a measure of the misalignment.

A set of Monte Carlo simulations is performed in order to investigate merit functions, such as convergence time and electrical power consumption, as a function of control law gains k_ζ and k_ε for randomly chosen initial conditions representative of the (at least partially) unknown tumbling motion of the payload after its ejection from the upper stage of the rocket launcher and the attitude and phase along the orbit at which the spin maneuver is started.

Initial conditions are determined by means of the pseudo-random number generator, `rand()`, implemented in MatlabTM environment. In particular, initial angular rates are generated so that the same amount of angular momentum $\|\Delta \mathbf{h}_0\|$ is dissipated for each test case of the Monte Carlo simulation, where

$$\|\Delta \mathbf{h}_0\| = \max_{i \in \{1,2,3\}} (J_i) \omega_{ref} \quad (5.23)$$

Table 5.1: Spacecraft and orbit data, with initial conditions for a sample maneuver (spin-axis stabilization).

Parameter	Symbol	Value	Units
<i>Spacecraft data</i>			
Principal moments of inertia	J_1, J_2, J_3	0.951, 0.970, 0.946	kg m ²
Maximum magnetic dipole	m_{\max}	3	A m ²
<i>Orbit data</i>			
Radius	r_c	7064	km
Period	T_{orb}	5909	s
Inclination	i	98	deg
<i>Sample maneuver</i>			
Initial Conditions	$\boldsymbol{\omega}_0$	$(0.3678, 0.8732, 0.5498)^T$	rad/s
	\boldsymbol{Q}_0	$(-0.3009, 0.2263, 0.2813, 0.8827)^T$	

with $\omega_{ref} = 1$ rad/s, and $\Delta\mathbf{h}_0 = \mathbf{h}_d - \mathbf{h}_0$, $\mathbf{h}_0 = \mathbf{h}(t_0)$ being the angular momentum vector at the initial time, t_0 . The desired spin condition is represented by a desired angular rate $\bar{\omega}_d = 0.110$ rad/s about $\hat{\mathbf{e}}_2$, aligned with the orbit normal $\hat{\boldsymbol{\tau}}$.

As a last issue of practical relevance, an estimate of the maneuver cost is provided in terms of electrical power consumption. A maximum magnetic dipole $m_{\max} = 3$ A m² is assumed for each of the torque-rods, its actual value being proportional to the current absorbed. The total electrical energy, \mathcal{E} , necessary for completing the maneuver is thus proportional to

$$\mathcal{E} \propto E = \int_0^{t_F} \left(\sum_{i=1}^3 |m_i| \right) dt \quad (5.24)$$

Figure 5.1 shows the results obtained from the first set of Monte Carlo simulations, performed over a population of 1000 test cases, where performance in terms of time and energy consumption are reported for different values of k , when $k_\varepsilon = k_\zeta = k$. The value t_F indicates the number of orbits necessary to dissipate the angular momentum in excess of the commanded value and reach the desired spin condition. A value of 99.99% of the initial error on angular momentum, assumed equal for all the test cases, was chosen as the threshold for a sufficiently small residual error, with $\|\boldsymbol{\zeta}\| < 10^{-4} \cdot \|\Delta\mathbf{h}_0\|$. For each performance parameter, average value and standard deviation are reported, the latter providing an indication of the dispersion of the results.

In the first set of Monte Carlo simulations, the best performance in terms of average convergence time is obtained for $k = k_{t_{min}} = 0.004$, that represents a minimum for t_F in

5.3 Results and Discussion

Figure 5.1. This behavior can be explained as in [14]. On the one hand, when the gain is too small, the maneuver becomes slower, because one does not fully exploit the available control power for a long portion of the final convergence. On the other hand, when the gain is too large, the error component in the direction normal to the geomagnetic field would be rapidly canceled, thus leaving the angular momentum error vector parallel to $\hat{\mathbf{b}}$, that is, parallel to the underactuated direction along which no control action is available. This makes the convergence very slow, inasmuch as it relies on the (indeed) slow motion of the geomagnetic field in the orbital frame.

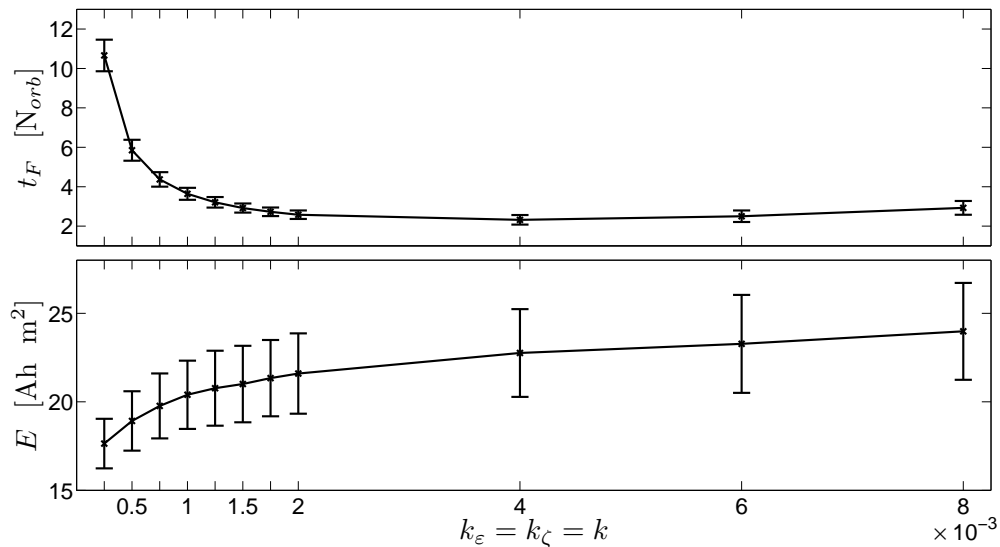


Figure 5.1: Convergence time and electrical energy consumption of the test cases, as functions of $k_\varepsilon = k_\zeta = k$.

In Ch. 4 it is shown that, when the spacecraft is required to achieve a desired pure spin condition with no constraints on the direction of the spin axis, it is possible to estimate a reasonable order of magnitude for the gain k_ε on the basis of a sequence of inequalities that provide an upper bound to k_ε . The actual optimal value is thus expected to be smaller than its bound, $k_\varepsilon = \bar{\omega}_d$. In the present case, the optimal gain appears to be one order of magnitude smaller than the suggested value obtained from the rule of thumb discussed in Ch. 4 for the simple pure spin acquisition case (without pointing).

As for the energy necessary to achieve the desired spin condition, note that it monotonically increases with k . This makes that sub-optimal performance in terms of convergence time to be considered as acceptable in all those cases when significant savings in terms of electrical energy consumption result into smaller and lighter systems of batteries.

A typical example of the behavior of the pointing error α is reported in Fig. 5.2, together with the variation of three components of the angular rate vector $\boldsymbol{\omega}$ (Fig. 5.3) for $k_\varepsilon =$

$k_\zeta = 0.004$, starting from the randomly chosen initial angular rate $\boldsymbol{\omega}_0$ and attitude \boldsymbol{Q}_0 reported in Table 5.1, that correspond to a pointing error of about 50 deg between $\hat{\boldsymbol{e}}_2$ and the orbit normal.

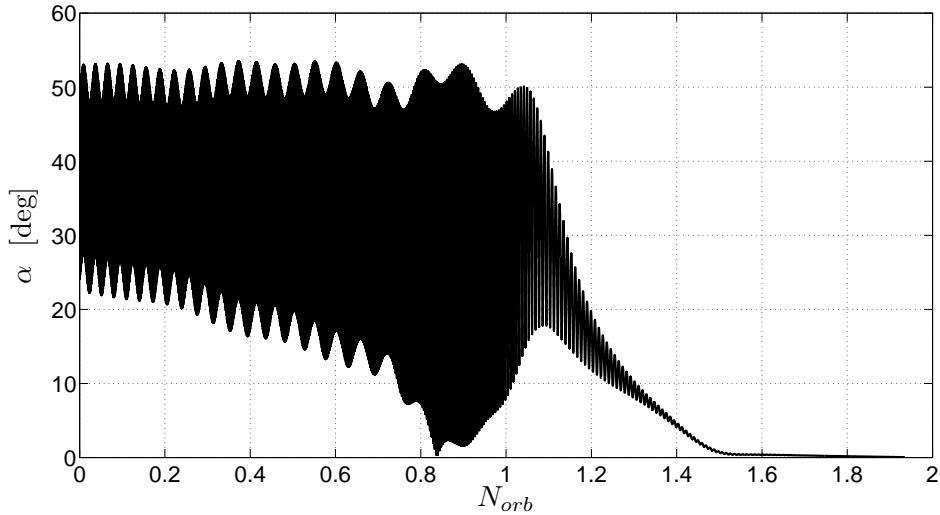


Figure 5.2: Pointing error time history.

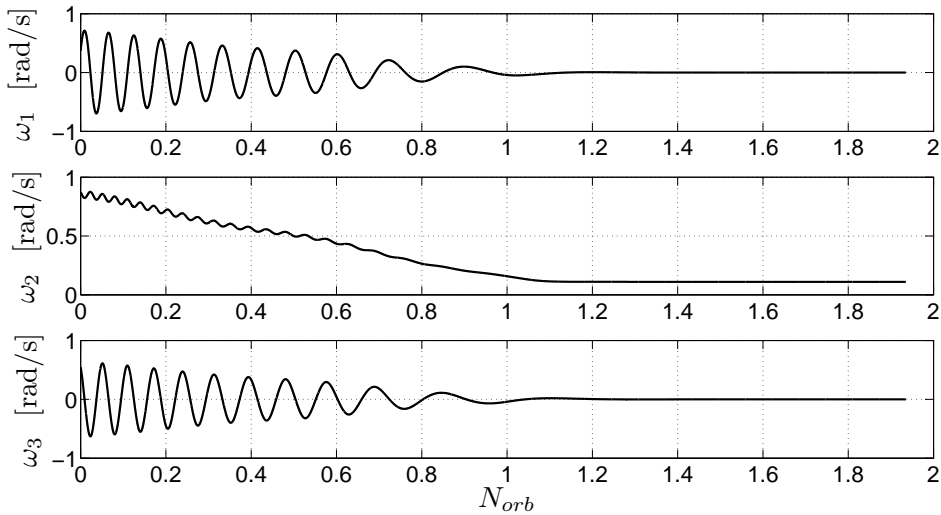


Figure 5.3: Angular rates time history ($\boldsymbol{\omega}_d = (0, 0.110, 0)^T$ rad/s).

During the initial phase of the detumbling, when the angular rate is high, the pointing error of the desired spin axis with respect to the prescribed inertial direction (that is, $\hat{\boldsymbol{e}}_2$ and the normal to the orbit plane, respectively, in the considered example) exhibits a high frequency oscillation, where the frequency is related to the angular speed. For

5.3 Results and Discussion

$0 < t/T_{orb} < 1$, the coils work at saturation and the control law is, in practice, similar to a switching control logic, simply aimed at reducing the angular rate. Once the tumbling motion is slowed, the oscillation of the pointing error is rapidly reduced ($t/T_{orb} > 1.1$) and its behavior transformed into an almost monotonous convergence toward zero for $t/T_{orb} > 1.4$.

A second set of Monte Carlo simulations is performed in order to analyze the effects of variations of the ratio k_ε/k_ζ , i.e. different weightings between the control actions that lead the satellite to the desired spin, respectively, in the body-frame and in the inertial-frame. Figure 5.4 gives a graphical representation of the results in terms of average convergence time and electrical energy consumption parameter when the ratio k_ε/k_ζ is varied between 0.1 and 10. The ratio is varied while keeping the sum of the gains constant, that is, $k_\varepsilon + k_\zeta = 2k_{t_{min}}$, so that when $k_\varepsilon/k_\zeta = 1$ the best case of the previous set of Monte Carlo runs is recovered.

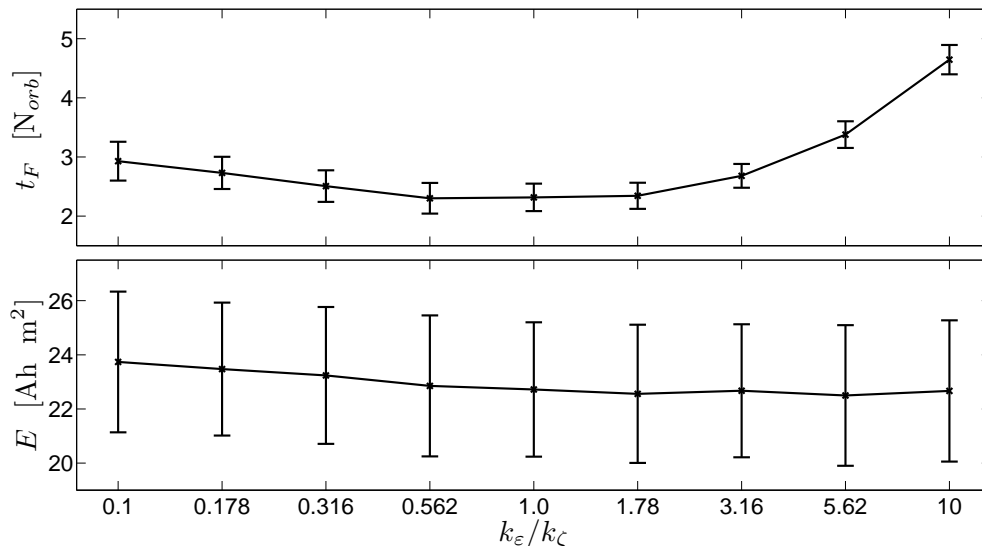


Figure 5.4: Convergence time and electrical energy consumption of the test cases, as functions of $\log_{10}(k_\varepsilon/k_\zeta)$.

Figure 5.4 shows that when the ratio k_ε/k_ζ is increased, the convergence time also increases significantly, becoming almost twice as much for $k_\varepsilon/k_\zeta = 10$. This behavior is due to the fact that the desired spin condition is rapidly reached and, at this point, gyroscopic stability makes it harder for the control system to stir the angular momentum vector toward the desired direction. Conversely, when k_ε becomes smaller and the term proportional to k_ζ becomes dominant, the angular momentum vector is aligned with the desired fixed direction $\hat{\tau}$ first, whereas the body-fixed spin-axis \hat{e}_2 moves toward the same direction at a slower pace. Convergence time again increases, but less significantly, becoming only

40% higher than the minimum value for $k_\varepsilon/k_\zeta = 0.1$. This behavior is essentially due to gyroscopic cross-coupling terms in Euler equation, Eq. (2.1), which result into oscillations in the attitude variables that, in turn, maintain a higher average control power for reducing the remaining error signal around the three body axes. It is quite clear that best average convergence time are obtained around 1, for $0.562 < k_\varepsilon/k_\zeta < 1.78$.

As a final observation, the ratio k_ε/k_ζ apparently has a negligible effect on power expenditure, evaluated through the energy consumption parameter, E . This appears reasonable, provided that the sum of the gains is constant and higher gains are associated with higher levels of required power. The increment for $k_\varepsilon/k_\zeta < 1$ is limited to approximately 4% of the average energy required for the reference case, $k_\varepsilon = k_\zeta = k_{t_{min}}$, and it is well within the dispersion interval defined by the standard deviation of E . In general, variations of k_ε/k_ζ do not represent an issue in the selection of control gains, as far as energy consumption is concerned, and $k_\varepsilon = k_\zeta = k$ thus results into a reasonable choice for the convergence characteristics demonstrated.

5.4 Conclusions

In this Chapter a control law based on the use of purely magnetic actuation for spin-axis stabilization is presented and discussed. It is shown that, under certain conditions and adequate orbit inclination, the control law globally exponentially stabilizes a three-inertial spacecraft, driving it toward a desired spin condition around a prescribed, yet arbitrary, axis fixed in the inertial frame. The proof of stability partially follows the philosophy adopted for the acquisition of a pure spin around a principal axis of inertia, where the additional feature of aiming the spin axis in a desired direction is particularly relevant for practical applications.

The variability of the magnetic field along the orbit plays an important role in the proof of asymptotic stability of the system toward an equilibrium point (see Appendix). Monte Carlo simulation is used in order to confirm closed-loop stability and evaluate performance of the controller, showing a robust behavior with respect to the choice of the control gains and the uncertainty on the geomagnetic field and initial tumbling conditions.

Attitude Control Using Magnetic and Mechanical Actuation

6.1 Introduction

In this Chapter, the control of a spacecraft using both magnetic and mechanical actuation is considered. A proof of global asymptotic stability is derived for control laws that drive a rigid satellite toward attitude stabilization in the orbit frame. Modern small-scale spacecraft are often provided with magnetic torquers and some kind of mechanical actuators (e.g. reaction and/or momentum-wheels). The former are generally used for detumbling purpose after the release of the spacecraft from the launch vehicle [14], and for momentum dumping of the wheels during desaturation maneuvers [38]. The latter are used for fine pointing control and attitude stabilization in the presence of external disturbance torques. It is the case of ALMASat-1, a micro-satellite developed by the Università di Bologna for demonstrative purposes, where a set of magnetic coils is supported by a momentum-wheel along the pitch axis. In this framework, attitude control is performed according to six different states, all managed by a finite-state machine, each one endowed with specific control laws, allowing angular rates damping and/or attitude tracking. The transition through the states occurs when certain variables (e.g. angular rates and misalignment errors) measured by the sensors satisfy conditions defined during the design phase [39].

As a matter of fact, magnetic and mechanical devices are seldom used simultaneously. The combined use of the two actuation systems would actually lead to power savings and less stringent requirements on wheel control torques. In Refs. [6] and [7], inertial

pointing of a spacecraft by means of magnetic actuators only was considered, with stabilization results based on general averaging theory. It was shown how, in the presence of a time-varying magnetic field along the orbit, the system possesses certain dynamic properties on average, with closed-loop performance limitations due to a limited choice of the proportional-derivative gains. Attitude control of spacecraft using two actuation systems was then considered in [40], where the same magnetic control law was assisted by a set of reaction-wheels, thus relaxing the above limitations, while in [41] attitude control was performed with a hybrid controller based on magnetorquers and thrusters, with a linear time-periodic approach and the analysis of actuator saturation. A geometric scheme was finally proposed in [42], where the desired control vector was decomposed along orthogonal and parallel directions with respect to the orientation of the local geomagnetic field vector. The orthogonal component was actuated by magnetic torquers, while the parallel component was generated by a set of one, two, or three wheels.

In Ch. 5 a proof of global exponential stability is proposed for a control law that leads a spacecraft to acquire a desired spin condition around one of the principal axes of inertia by means of magnetic actuators only, while aiming the spin axis in a prescribed direction in the inertial frame [43]. Convergence toward the desired condition is proven by demonstrating robustness of global exponential stability of a nominal system with respect to a vanishing perturbation term, which represents a measure of the distance between the actual spacecraft inertia properties and an axisymmetric configuration. The same considerations are taken into account in this framework, where momentum management is obtained by means of the same magnetic controller, while three-axes attitude stabilization is completed with a proper choice of the wheel control law governing the pitch angle dynamics.

The combined use of a mechanical device with the suggested magnetic control law represents the major contribution of the present work, where attitude stabilization is obtained in the case when angular rate and attitude measurements are available.

6.2 Attitude Stabilization in the Orbit Frame

6.2.1 Control Laws

Let $\hat{\boldsymbol{\tau}}$ be the unit vector aiming in the direction of the y_O -axis, which is fixed both in the orbit and in the inertial frame, and Ω_d be the desired spin rate condition of the wheel with respect to the spacecraft. The components of the desired angular momentum vector, expressed in a set of principal axes and in the orbit frame, are given by $\mathbf{h}_d = (0, h_d, 0)^T$, where $h_d = J_w \Omega_d - J_2 n$ with $\Omega_d \neq n J_2 / J_w$, and $\mathbf{H}_d = h_d \hat{\boldsymbol{\tau}}$, respectively. Similarly to what was done in Ch. 5, two different angular momentum error variables are introduced,

6.2 Attitude Stabilization in the Orbit Frame

namely

$$\boldsymbol{\zeta} = \mathbf{H}_d - \mathbf{h}_w - \mathbf{J} \boldsymbol{\omega} \quad (6.1)$$

and

$$\boldsymbol{\varepsilon} = \mathbf{h}_d - \mathbf{h}_w - \mathbf{J} \boldsymbol{\omega} \quad (6.2)$$

where all the vector quantities, including \mathbf{H}_d , are represented in terms of body frame components.

The aim of this Section is to prove that, on an inclined LEO, the magnetic control law

$$\mathbf{M}^{(c)} = \left(\mathbb{I}_3 - \hat{\mathbf{b}} \hat{\mathbf{b}}^T \right) (k_\zeta \boldsymbol{\zeta} + k_\varepsilon \boldsymbol{\varepsilon}) \quad (6.3)$$

with $k_\zeta > 0$ and $k_\varepsilon > 0$, and the control law for the momentum wheel

$$\dot{h}_w = J_2 \left[\lambda \dot{\theta} + k (\lambda \theta + n + \omega_2) \right] \quad (6.4)$$

with $\lambda > 0$ and $k > 0$, stabilize spacecraft attitude in the orbit frame, while driving the wheel spin rate to the desired value, Ω_d .

The desired angular momentum vector, \mathbf{H}_d , is fixed in the inertial frame. Its dynamics is thus given in body coordinates by Eq. (5.4). From the definition of the error in Eq. (6.1) and taking into account the control law in Eq. (6.3), one has

$$\dot{\boldsymbol{\zeta}} = - \left(\mathbb{I}_3 - \hat{\mathbf{b}} \hat{\mathbf{b}}^T \right) (k_\zeta \boldsymbol{\zeta} + k_\varepsilon \boldsymbol{\varepsilon}) - \boldsymbol{\omega} \times \boldsymbol{\zeta} \quad (6.5)$$

At the same time, \mathbf{h}_d is a constant vector in body axes and the body frame angular momentum error dynamics achieves the form

$$\dot{\boldsymbol{\varepsilon}} = - \left(\mathbb{I}_3 - \hat{\mathbf{b}} \hat{\mathbf{b}}^T \right) (k_\zeta \boldsymbol{\zeta} + k_\varepsilon \boldsymbol{\varepsilon}) + \boldsymbol{\omega} \times (\mathbf{h}_d - \boldsymbol{\varepsilon}) \quad (6.6)$$

The pitch equation is derived from Eq. (2.1),

$$J_2 \dot{\omega}_2 + (J_1 - J_3) \omega_1 \omega_3 = -\dot{h}_w + M_2^{(c)} \quad (6.7)$$

Taking \dot{h}_w as the control input defined in Eq. (6.4) and introducing the error on the body frame pitch angular rate, $\xi = -n - \omega_2$, then Eq. (6.7) becomes

$$\dot{\tilde{\xi}} + k \tilde{\xi} = d, \quad (6.8)$$

where $d = \left[-(J_1 - J_3) \omega_1 \omega_3 + M_2^{(c)} \right] / J_2$ can be considered as a disturbance term and $\tilde{\xi} = \lambda \theta - \xi$ is a filtered pitch error.

6.2.2 Momentum Management

The system represented by Eqs. (6.5) and (6.6) possesses the same structure of Eqs. (5.7) and (5.8) obtained in Ch. 5. The only difference consists in the fact that the total momentum of the spacecraft, including the contribution of the wheel, is now managed. With identical considerations, one can thus reformulate the attitude stabilization problem in terms of vector components expressed in the inertial frame, \mathbb{F}_I , rather than in the body frame, \mathbb{F}_B . Then, given $\mathbf{Y} = (\mathbf{Z}^T, \mathbf{E}^T)^T$, $\mathbf{Y} \in \mathbb{R}^6$, the system in Eqs. (6.5) and (6.6), finally achieves the form

$$\dot{\mathbf{Y}} = -\mathbf{A}(t)\mathbf{K}\mathbf{Y} - \mathbf{B}(t, \mathbf{Y}) - \mathbf{C}(t, \mathbf{Y}), \quad (6.9)$$

already introduced in Eq. (5.11), with the same definitions of the three terms on the right-hand side.

Proposition 1 *The origin $\mathbf{Y} = \mathbf{0}$ is a globally exponentially stable equilibrium point of the perturbed system in Eq. (6.9).*

Proof: See Lemma 1 in Ch. 5 for the proof of convergence. In this framework, for a given choice of the wheel inertia J_w , the bound introduced in Eq. (5.20) translates into a maximum desired value of the wheel spin rate, Ω_d . In fact, the linear-growth bound on the perturbation term, namely $\|\mathbf{C}(t, \mathbf{Y})\| \leq \bar{\gamma} \|\mathbf{Y}\|$, holds if $\bar{\gamma} = |J_w \Omega_d - J_2 n| \delta_{\max}$, where δ_{\max} is defined in Eq. (5.21).

The analysis proposed above demonstrates that error dynamics introduced in Eqs. (5.9) and (5.10) drives the error variables \mathbf{E} and \mathbf{Z} asymptotically to zero. This feature is independent of the frame in which vectors are represented. As a consequence, one gets that also $\boldsymbol{\zeta}$ and $\boldsymbol{\varepsilon}$ approach null vectors asymptotically. Note that the system in Eq. (6.9) cannot be analyzed without taking into account the information about the attitude of the spacecraft, affecting the terms $\mathbf{B}(t, \mathbf{Y})$ and $\mathbf{C}(t, \mathbf{Y})$. In other words, it is not possible to decouple the momentum management equation, namely Eq. (6.9), from the attitude kinematics in Eqs. (2.10)–(2.12) and the pitch control law proposed in Eq. (6.4). On the other hand, the same consideration does not hold for the proof of stability discussed in this Section. In fact, the presence of the attitude matrix, that also depends on the pitch angle and thus introduces a time-variability in the terms $\mathbf{B}(t, \mathbf{Y})$ and $\mathbf{C}(t, \mathbf{Y})$, actually influences only the rate of convergence toward the equilibrium, without flawing the asymptotic nature of the problem. This justifies a proof of stability that is independent of the pitch angle behavior and allows for a decoupled stability analysis.

6.2 Attitude Stabilization in the Orbit Frame

From Eq. (6.5), the components of $\boldsymbol{\varepsilon}$ are given by

$$\boldsymbol{\varepsilon} = \begin{pmatrix} 0 \\ h_d \\ 0 \end{pmatrix} - \begin{pmatrix} 0 \\ h_w \\ 0 \end{pmatrix} - \begin{pmatrix} J_1\omega_1 \\ J_2\omega_2 \\ J_3\omega_3 \end{pmatrix} \quad (6.10)$$

When $\boldsymbol{\varepsilon} \rightarrow \mathbf{0}$, one gets that

$$\omega_1, \omega_3 \rightarrow 0 ; \quad h_w + J_2\omega_2 \rightarrow h_d \quad (6.11)$$

Provided that $\mathbf{H}_d = h_d \hat{\boldsymbol{\tau}}$, where $\hat{\boldsymbol{\tau}} = \mathbb{T}_{BO}(0, 1, 0)^T$ is the normal to the orbit plane, the components of the desired angular momentum vector in the inertial frame, projected in the body frame for the current attitude represented by means of a 3-1-2 sequence of Euler angles, are given by

$$\mathbf{H}_d = h_d \begin{pmatrix} \cos \theta \sin \psi + \sin \phi \sin \theta \cos \psi \\ \cos \phi \cos \psi \\ \sin \theta \sin \psi - \sin \phi \cos \theta \cos \psi \end{pmatrix} \quad (6.12)$$

Since also $\boldsymbol{\zeta} \rightarrow \mathbf{0}$, it is possible to state that

$$h_d (\cos \theta \sin \psi + \sin \phi \sin \theta \cos \psi) - J_1\omega_1 \rightarrow 0 \quad (6.13)$$

$$h_d \cos \phi \cos \psi - (h_w + J_2\omega_2) \rightarrow 0 \quad (6.14)$$

$$h_d (\sin \theta \sin \psi - \sin \phi \cos \theta \cos \psi) - J_3\omega_3 \rightarrow 0 \quad (6.15)$$

Taking into account the limits in Eq. (6.11), one obtains

$$\cos \theta \sin \psi + \sin \phi \sin \theta \cos \psi \rightarrow 0 \quad (6.16)$$

$$\cos \phi \cos \psi \rightarrow 1 \quad (6.17)$$

$$\sin \theta \sin \psi - \sin \phi \cos \theta \cos \psi \rightarrow 0 \quad (6.18)$$

From Eq. (6.17), it follows that $\cos \phi \rightarrow \pm 1$ and $\cos \psi \rightarrow \pm 1$. This implies that $\lim_{t \rightarrow +\infty} \cos \phi = \lim_{t \rightarrow +\infty} \cos \psi$, with the limits having the same sign. Consequently also $\sin \phi, \sin \psi \rightarrow 0$. This is possible only if the pitch axis becomes aligned, as required, with the direction $\hat{\boldsymbol{\tau}}$, normal to the orbit plane.

6.2.3 Control of the Pitch Angle

Consider the kinematics of the Euler angles in Eqs. (2.10) and (2.11). It can be rearranged as follows:

$$\dot{\phi} = \omega_1 \cos \theta + \omega_3 \sin \theta + n \sin \psi \quad (6.19)$$

$$\dot{\theta} = \omega_2 + (\omega_1 \sin \phi \sin \theta - \omega_3 \sin \phi \cos \theta + n \cos \psi) / \cos \phi \quad (6.20)$$

$$\dot{\psi} = (-\omega_1 \sin \theta + \omega_3 \cos \theta - n \sin \phi \cos \psi) / \cos \phi \quad (6.21)$$

6. Attitude Control Using Magnetic and Mechanical Actuation

As mentioned in Ch. 2, the 3-1-2 Euler sequence has a singularity at $\phi = \pm\pi/2$. For practical control implementation purposes, it is not possible to determine θ when the attitude is at the singularity. However, due to the fact that $\sin\phi \rightarrow 0$, there will be a finite time after which it can be guaranteed that the singularity will not be crossed. Therefore, the stability analysis will be now focused on the pitch dynamics.

It was established that $\omega_1, \omega_3 \rightarrow 0$ and $\sin\phi, \sin\psi \rightarrow 0$. As a consequence, Eqs. (6.19)–(6.21) show that $\dot{\phi}, \dot{\psi} \rightarrow 0$. Since Eq. (6.8) is an exponentially stable system in $\tilde{\xi}$ with asymptotically vanishing disturbance d , it is possible to conclude that $\tilde{\xi} \rightarrow 0$ as $t \rightarrow +\infty$. From the definition of the filtered error, $\tilde{\xi}$, and the Eq. (2.11), this becomes:

$$\tilde{\xi} = \lambda\theta + n + \dot{\theta} + \dot{\psi} \sin\phi - n \cos\phi \cos\psi \rightarrow 0 \quad (6.22)$$

Since $\dot{\psi}, \sin\phi \rightarrow 0$ and $\cos\phi \cos\psi \rightarrow 1$, it follows that

$$\dot{\theta} + \lambda\theta \rightarrow 0 \quad (6.23)$$

Let

$$\dot{\theta} + \lambda\theta = \bar{r}. \quad (6.24)$$

Then, by Eq. (6.23), $\bar{r} \rightarrow 0$. Since Eq. (6.24) is exponentially stable in θ with disturbance $\bar{r} \rightarrow 0$, it can be finally concluded that $\dot{\theta}, \theta \rightarrow 0$.

6.3 Results and Discussion

The control laws proposed in the previous Section for the attitude stabilization of the spacecraft and the acquisition of a desired spin rate for the momentum-wheel are now applied to a low Earth orbit micro-satellite, equipped with three mutually orthogonal magnetic coils. Table 6.1 shows relevant spacecraft data and orbit parameters, together with initial conditions for a sample maneuver.

A nonlinear model for spacecraft attitude dynamics is used in the simulations. The initial phase during which the satellite is magnetically detumbled after injection into its orbit is not analysed in this framework. It is assumed that, after the initial detumbling phase (see Ch. 4), the spacecraft is spinning about its pitch axis with a total angular momentum $J_2\omega_2 = 1.2h_d$, 20% bigger than the desired one, h_d , and the wheel is at rest relative to the satellite. The direction of the initial angular momentum is 20 deg distant from the orbit normal. During the maneuver, the excess of angular momentum is thus dissipated by magneto-torquers and, at the same time, the residual angular momentum is transferred to the wheel, which accelerates from rest to a desired spin rate of 5000 rpm.

6.3 Results and Discussion

Table 6.1: Spacecraft and orbit data, with initial conditions for a sample maneuver (attitude stabilization).

Parameter	Symbol	Value	Units
<i>Spacecraft data</i>			
Principal moments of inertia	J_1, J_2, J_3	0.951, 0.970, 0.946	kg m ²
Wheel moment of inertia	J_w	4.58×10^{-5}	kg m ²
Maximum magnetic dipole	m_{\max}	3	A m ²
Dimensions	$\bar{l}_1, \bar{l}_2, \bar{l}_3$	0.3, 0.6, 0.3	m
Drag coefficient	C_D	2.2	
<i>Orbit data</i>			
Radius	r_c	7064	km
Period	T_{orb}	5909	s
Inclination	i	98	deg
<i>Sample maneuver</i>			
Initial Conditions	$\boldsymbol{\omega}_0$ \boldsymbol{Q}_0	$(0, 0.0297, 0)^T$ $(0.0543, 0.9050, -0.1650, 0.3884)^T$	rad/s

In the first simulation (Case 1), no external disturbance is applied to the spacecraft, in order to demonstrate convergence of the control law. In the second test case (Case 2), starting from the same initial conditions, gravity gradient, aerodynamic, and residual magnetic torques are applied in order to test the robustness of the closed-loop system with respect to external disturbances. The gains for the roll/yaw magnetic control law are selected as $k_\zeta = k_\varepsilon = 0.004$ (see Ch. 5), whereas the gains for the wheel control law are $k = 0.05$ and $\lambda = 0.001$.

Figures 6.1 and 6.2 show the results without disturbances (Case 1). Let α be the overall misalignment error between \mathbb{F}_B and \mathbb{F}_O , represented by the magnitude of the single rotation that takes \mathbb{F}_B onto \mathbb{F}_O according to Euler’s rotation theorem, namely

$$\alpha = \frac{1}{2} [\text{tr}(\mathbb{T}_{BO}) - 1], \quad (6.25)$$

where $\text{tr}(\mathbb{T}_{BO})$ is the trace of \mathbb{T}_{BO} [13]. Given the asymptotic nature of the convergence, the simulation is stopped when a threshold on the residual error, $\alpha < 0.01$ deg, is reached. Time histories of angular momenta are reported in Fig. 6.1, where $\mathbf{h}_{tot} = \mathbf{J}\boldsymbol{\omega} + \mathbf{h}_w$ is the total angular momentum of the spacecraft, including the contribution of the momentum-wheel. As predicted by GEASV stability tools, the magnitude of the total momentum converges to the desired value, $\|\mathbf{h}_{tot}\| \rightarrow \|\mathbf{h}_d\| = |J_w \Omega_d - J_2 n|$, while pitch-axis pointing is performed along the orbit normal, with the “yaw” and “roll” angles, ψ and ϕ , respectively,

6. Attitude Control Using Magnetic and Mechanical Actuation

approaching zero (see Fig. 6.1). At the same time, the pitch control torque provides the desired distribution of \mathbf{h}_{tot} between the spacecraft and the momentum-wheel, finally reaching three-axes stabilization in about 7.5 orbits. In particular, the pitch angle θ converges with almost-exponential decay as predicted by Eq. (6.24), where the disturbance \bar{r} vanishes as $t \rightarrow +\infty$. In this condition, the residual motion of the rigid body about the orbit normal equals the orbital speed, $\boldsymbol{\omega} \rightarrow \boldsymbol{\omega}^{orb}$, while the momentum wheel is driven to the desired spin rate with respect to the spacecraft, $\Omega \rightarrow \Omega_d$.

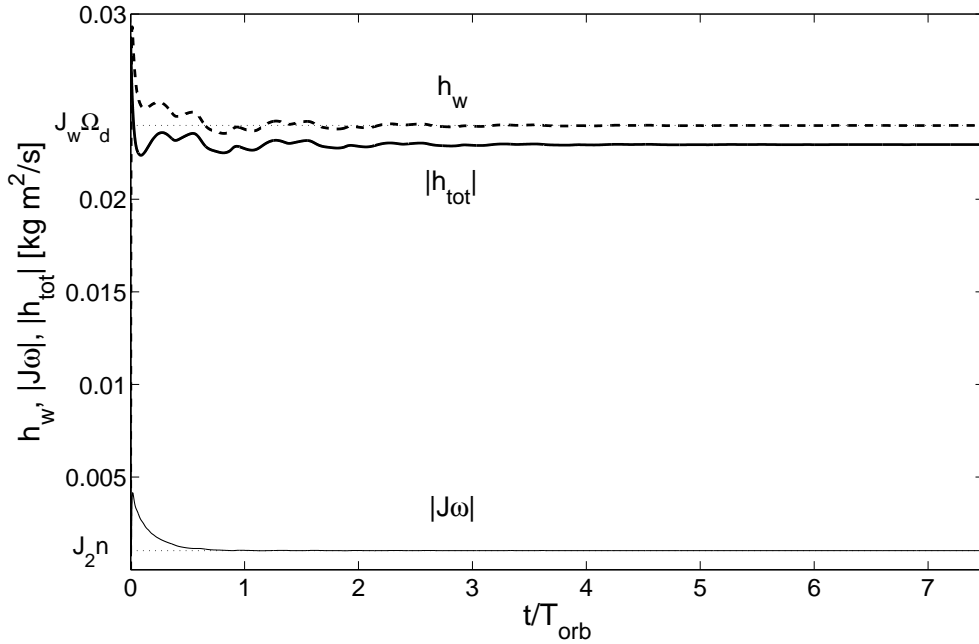


Figure 6.1: Spacecraft and wheel angular momenta.

Figures 6.3 and 6.4 show the results of the second simulation (Case 2), where all the considered disturbances are applied and a residual magnetic dipole $\mathbf{m}_r = (0.01, -0.01, 0.015)^T$ affects the spacecraft actuation performance. The time histories of both the angular momenta of the spacecraft and the attitude variables are quite similar to Case 1 in the first phase of the maneuver, where momentum management takes place. As a matter of fact, it is possible to realize how, for about $t/T_{orb} > 2$, the same error variables show a residual oscillation about the desired values with period equal to T_{orb} , thus remaining bounded in the presence of unmodeled disturbances. The wheel accelerates between about 4980 to 5020 rpm, thus providing torque, while the overall misalignment error α consequently oscillates, with a maximum of 0.38 deg. In particular, the pitch angle θ shows a residual fluctuation with amplitude 0.08 deg, not perceived in Fig. 6.4. This behavior is due to the fact that the disturbance term in Eq. (6.24), that is function of ϕ , ψ , and $\dot{\psi}$, does not

6.4 Conclusions

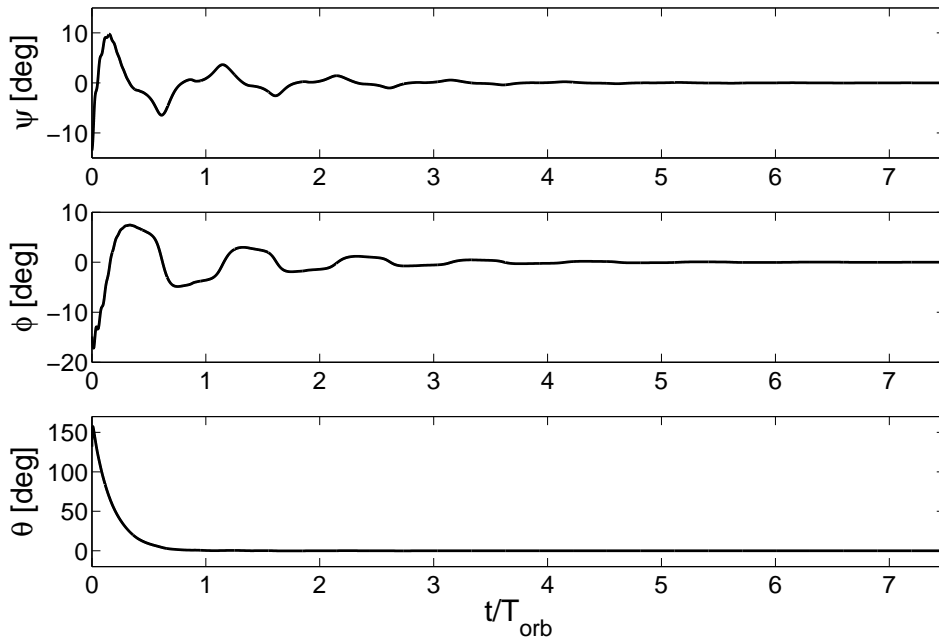


Figure 6.2: Spacecraft attitude error.

vanish asymptotically, thus preventing θ to converge toward the equilibrium.

The simulation results demonstrate the feasibility of the proposed approach and, in particular, illustrate the ability of the controllers to drive the spacecraft to attitude stabilization as derived from the stability analysis. The closed loop system is also shown to be robust with respect to unmodeled disturbances.

6.4 Conclusions

A proof of convergence is derived for magnetic and mechanical control laws that drive a rigid spacecraft to attitude stabilization in the orbit frame by means of magnetic torquers and a momentum-wheel along the pitch axis. It is assumed in the theoretical analysis that the spacecraft principal and body axes coincide. The proof extends a method developed for angular momentum management by means of magnetic actuators which was already discussed for the case represented by spin-axis pointing in the inertial frame (see Ch. 5). The pitch angle stabilization proof, which represents the additional contribution of the present paper, then immediately follows after a proper choice of the wheel control law.

Some numerical examples have been presented in order to demonstrate the effectiveness of the control laws and validate the theoretical results. Additionally, the control laws are shown to perform well even in the presence of external disturbances, such as gravity

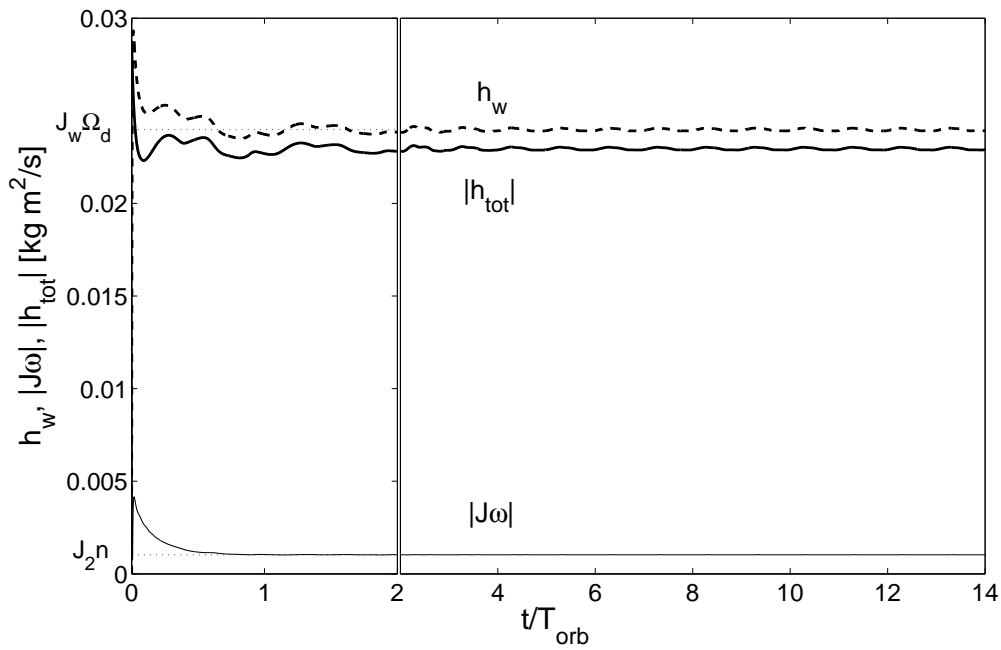


Figure 6.3: Spacecraft and wheel angular momenta (external disturbances).

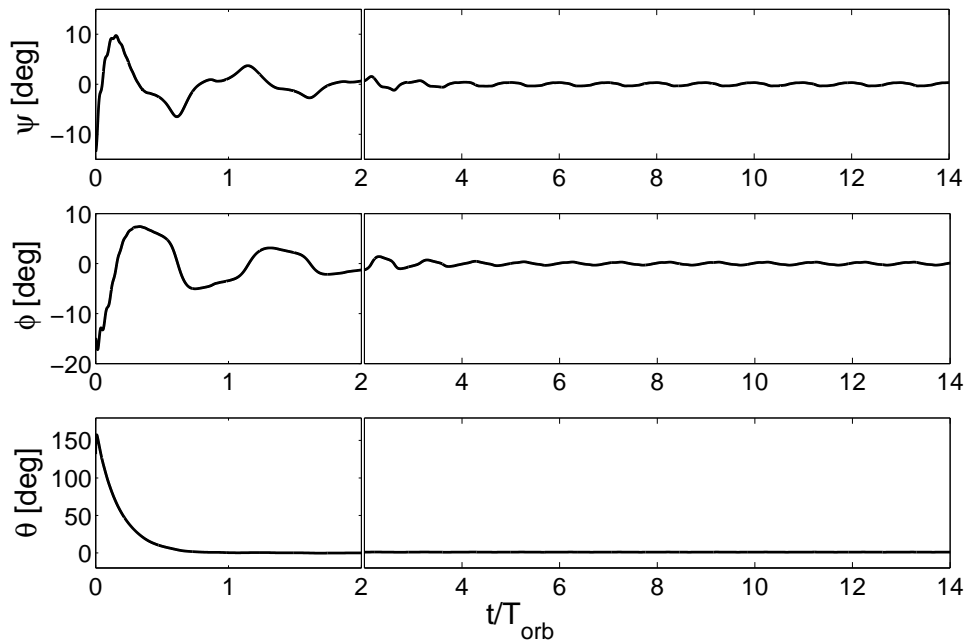


Figure 6.4: Spacecraft attitude error (external disturbances).

6.4 Conclusions

gradient, aerodynamic, and residual magnetic torques.

6. Attitude Control Using Magnetic and Mechanical Actuation

CHAPTER 7

Conclusions

In this thesis the attitude stabilization of a magnetically actuated spacecraft has been studied. The model of a rigid satellite has been presented, with the description of the main disturbance torques acting in low Earth orbits. The use of magnetic coils is shown to make the considered system inherently underactuated, because control torques can be delivered only in a plane that is orthogonal to the local direction of the geomagnetic field vector. Several properties of the underactuated spacecraft have been presented, most important being the fact that it cannot be stabilized using time-invariant continuous control laws.

In the present work continuous time-varying state feedbacks have been presented based on projection method, where the nominal control torque is projected on a plane that is perpendicular to the geomagnetic field vector. Three different controllers have been proven to drive a three-inertial spacecraft to 1) a pure spin condition about a principal axis of inertia, 2) spin-axis pointing in a prescribed direction that is fixed in the inertial frame, 3) attitude stabilization in the orbit frame with the support of a momentum-wheel spinning about one of the principal axes. Global exponential stability has been obtained for the first two cases, while global asymptotic convergence characterizes the third one. As a further contribution, exponential stability has been proven for a detumbling maneuver presented in a recent paper, that, in this framework, represents a particular case of the pure spin acquisition maneuver. A kinematic result has been also suggested in a single-axis pointing scenario, where a sensor boresight is required to stay out of a cone defined about the direction of bright sources of light, while the rotation eigenaxis is constrained on a plane perpendicular to the torqueless direction.

The variability of the magnetic field along the orbit has played an important role in the proofs of asymptotic stability of the closed-loop systems toward an equilibrium point. Closed-loop stability and performance of the approaches have been then extensively tested by means of numerical simulations.

Proofs of Global Exponential Stability

Global exponential stability of the origin $\mathbf{E} = \mathbf{0}$ for the nominal system (see Ch. 4)

$$\dot{\mathbf{E}} = -k_h \mathbb{T}_{BI}^T \left(\mathbb{I}_3 - \hat{\mathbf{b}} \hat{\mathbf{b}}^T \right) \mathbb{T}_{BI} \mathbf{E} \quad (\text{A.1})$$

and of the origin $\mathbf{Y} = \mathbf{0}$ for the nominal system (see Chs. 5 and 6)

$$\dot{\mathbf{Y}} = -\mathbf{A}(t) \mathbf{K} \mathbf{Y} - \mathbf{B}(t, \mathbf{Y}) \quad (\text{A.2})$$

is provided by the following corollary.

Corollary 1 *Consider a non-linear non-autonomous dynamic system $\dot{\mathbf{x}} = \mathbf{f}(t, \mathbf{x})$, where $\mathbf{f} : \mathbb{R}^n \times \mathbb{R} \rightarrow \mathbb{R}^n$ is piecewise continuous in t and Lipschitz in \mathbf{x} . Let $\mathbf{x} = \mathbf{0}$ be an equilibrium point for the system at $t = 0$. Also assume that a strictly positive definite Lyapunov-like function $V(\mathbf{x}) > 0$ exists, where (i) $V : \mathbb{R}^n \rightarrow \mathbb{R}$ is a smooth scalar function of the state \mathbf{x} only and (ii) its gradient vanishes at the origin only, that is, $\nabla_{\mathbf{x}} V = \mathbf{0}$ at $\mathbf{x} = \mathbf{0}$ and $\nabla_{\mathbf{x}} V \neq \mathbf{0}$ elsewhere. If the Lyapunov-like function $V(\mathbf{x})$ and its time derivative $\dot{V}(t, \mathbf{x})$ satisfy the conditions:*

1. $k_1 \|\mathbf{x}\|^c \leq V(\mathbf{x}) \leq k_2 \|\mathbf{x}\|^c \quad k_1 > 0, k_2 > 0, c > 0;$
2. \dot{V} is negative semi-definite, that is, $\dot{V}(t, \mathbf{x}) \leq 0;$
3. \dot{V} is uniformly continuous;
4. the iso-surfaces S of $V(\mathbf{x})$ in the state space \mathbb{R}^n do not contain any integral curves $\mathbf{x}(t)$ of the vector field \mathbf{f} other than the constant ones ($\mathbf{x}(t) = \mathbf{x}_e, \forall t$);

then the state converges to one of the (at least locally) stable equilibria. If the origin is the only equilibrium, it is globally exponentially stable.

Proof: Since the Lyapunov candidate function V only depends on the state \mathbf{x} one has:

$$\dot{V}(t, \mathbf{x}) = \lim_{\delta t \rightarrow 0} \frac{V(\mathbf{x}(t + \delta t)) - V(\mathbf{x}(t))}{\delta t} = \nabla_x V \mathbf{f}(t, \mathbf{x}) \quad (\text{A.3})$$

Since the iso-surfaces S of $V(\mathbf{x}(t))$ do not contain any integral curves of \mathbf{f} , the right-hand term cannot be zero if an equilibrium point is not reached. Thus, for all $t > 0$ the quantity

$$V(\mathbf{x}(t + \delta t)) - V(\mathbf{x}(t)) = \int_t^{t+\delta t} \nabla_x V \mathbf{f}(\tau, \mathbf{x}(\tau, \mathbf{x})) d\tau < 0 \quad (\text{A.4})$$

is a finite negative term, and there exists a $0 < \lambda < 1$ such that

$$V(\mathbf{x}(t + \delta t)) - V(\mathbf{x}(t)) < -\lambda V(\mathbf{x}(t)). \quad (\text{A.5})$$

From this point onwards the proof follows that of Theorem 8.5 in Ref. [36].

System A.1

For the case represented by Eq. (A.1), the Lyapunov candidate

$$V(\mathbf{E}) = 1/2 \mathbf{E}^T \mathbf{E} \quad (\text{A.6})$$

satisfies Conditions 1, 2, and 3, with

$$\dot{V}(t, \mathbf{E}) = -k_h \mathbf{E}^T \left[\mathbb{T}_{BI}^T \left(\mathbb{I}_3 - \hat{\mathbf{b}} \hat{\mathbf{b}}^T \right) \mathbb{T}_{BI} \right] \mathbf{E}. \quad (\text{A.7})$$

In case of torque-free motion, the nominal system (A.1) reduces to $\dot{\mathbf{E}} = \mathbf{0}$, with the result that \mathbf{E} remains fixed in the inertial frame. Conversely, the Earth magnetic field is time-varying, so that the trajectory $\mathbf{E}(t) = \|\mathbf{E}\| \hat{\mathbf{b}}(t)$ cannot be a solution for the nominal system (A.1). Thus, also Condition 4 is satisfied and the origin $\mathbf{E} = \mathbf{0}$ is globally exponentially stable.

System A.2

For the case represented by Eq. (A.2), the Lyapunov candidate is

$$V(\mathbf{Y}) = 1/2 \mathbf{Y}^T \mathbf{K} \mathbf{Y} \quad (\text{A.8})$$

and Conditions 1, 2, and 3 are satisfied with

$$\dot{V}(t, \mathbf{Y}) = -(\mathbf{K} \mathbf{Y})^T \mathbf{A}(t) (\mathbf{K} \mathbf{Y}) \quad (\text{A.9})$$

where $\mathbf{A}(t)$ is positive semi-definite. The Corollary can thus be applied if one demonstrates that Condition 4 also holds. From Eq. (A.9), the time derivative of $V(t, \mathbf{Y})$ can vanish if one of the following conditions holds:

-
- a) The equilibrium point at the origin is reached, $(\mathbf{Z}^T, \mathbf{E}^T)^T = \mathbf{0}$ or
 - b) The angular momentum error variables are such that the error signal, $\mathbf{e} = k_\zeta \mathbf{Z} + k_\varepsilon \mathbf{E}$, becomes parallel to the Earth magnetic field (and the nominal torque $\mathbf{M}^{(c)}$ thus vanishes) or
 - c) The linearly independent angular momentum error variables are such that the error signal, $\mathbf{e} = k_\zeta \mathbf{Z} + k_\varepsilon \mathbf{E}$, becomes null with $\mathbf{Z} \neq \mathbf{0}$, $\mathbf{E} \neq \mathbf{0}$, and the nominal torque $\mathbf{M}^{(c)}$ again vanishes.

In case of torque-free motion (Conditions b and c), the nominal system (A.2) reduces to $\dot{\mathbf{Y}} = -\mathbf{B}(t, \mathbf{Y})$. Taking into account the definition of the term $\mathbf{B}(t, \mathbf{Y})$ in Eq. (5.14), this means that \mathbf{Z} remains fixed in the inertial frame.

Suppose Condition b holds. This situation can be maintained over time if and only if the vector $(k_\zeta \mathbf{Z}^T, k_\varepsilon \mathbf{E}^T)^T$ remains in the null-space of the time varying matrix, $\mathbf{A}(t)$, $\mathcal{N}_A = \ker(\mathbf{A})$. Letting $\mathbf{0} = (0, 0, 0)^T$, a basis for the null-space of \mathbf{A} is given by the vectors $\mathbf{n}_1 = (\mathbf{b}^T, \mathbf{0}^T)^T$, $\mathbf{n}_2 = (\mathbf{0}^T, \mathbf{b}^T)^T$, $\mathbf{n}_3 = (\mathbf{u}^T, -\mathbf{u}^T)^T$, and $\mathbf{n}_4 = (\mathbf{v}^T, -\mathbf{v}^T)^T$, where \mathbf{u} and \mathbf{v} are vectors perpendicular to \mathbf{b} . The vector $(k_\zeta \mathbf{Z}^T, k_\varepsilon \mathbf{E}^T)^T \in \mathcal{N}_A$ if $k_\zeta \mathbf{Z}$ and $k_\varepsilon \mathbf{E}$ have the same component along \mathbf{b} and components opposite in sign on the plane perpendicular to \mathbf{b} , which means that the three vectors $k_\zeta \mathbf{Z}$, $k_\varepsilon \mathbf{E}$, and \mathbf{b} must belong to the same plane. Such a condition can be reached, but it cannot be maintained over a finite time-interval during a torque-free phase, since the error signal \mathbf{e} should rotate about the inertially fixed direction of \mathbf{Z} . But this is in contrast with the motion of \mathbf{b} in the inertial frame, as described by the tilted dipole or IGRF model.

Now suppose Condition c holds. The error signals, \mathbf{Z} and \mathbf{E} , are such that $k_\zeta \mathbf{Z} = -k_\varepsilon \mathbf{E}$, with the result that, during the torque-free motion, both \mathbf{Z} and \mathbf{E} remain fixed in the inertial frame. Considering the definition of the momentum error vector \mathbf{E} from Eq. (5.2) or Eq. (6.2), this means that \mathbf{h}_d does not move in the inertial frame too, being the (total) momentum vector fixed during a torqueless condition. This situation may occur in two cases: 1) the spacecraft spins about the prescribed principal axis of inertia, namely $(\mathbb{T}_{BI} \mathbf{E}) \times \mathbf{h}_d = \mathbf{0}$, while the spin axis aims in the direction of the orbit normal; as a matter of fact, this situation is in contrast, when $\mathbf{E} \neq \mathbf{0}$, with the condition $\dot{\mathbf{Y}} = \mathbf{B}(t, \mathbf{Y}) = \mathbf{0}$, that implies $(\mathbf{J}_a^{-1} \mathbb{T}_{BI} \mathbf{E}) \times \mathbf{h}_d = \mathbf{0}$; 2) in case the satellite is in a rest condition, then $\|\mathbf{Z}\| = \|\mathbf{E}\| = |h_d|$; the situation $k_\zeta \mathbf{Z} = -k_\varepsilon \mathbf{E}$ can thus be avoided by choosing $k_\zeta \neq k_\varepsilon$.

Given the above considerations, also Condition 4 is satisfied and the origin $\mathbf{Y} = \mathbf{0}$ is globally exponentially stable.

Bibliography

- [1] Stickler, A.C. and Alfriend, K., “Elementary Magnetic Attitude Control System,” *Journal of Spacecraft and Rockets*, Vol. 13, No. 5, 1976, pp. 282–287.
doi: 10.2514/3.57089.
- [2] Sidi, M.J., *Spacecraft Dynamics and Control: a Practical Engineering Approach*, Cambridge University Press, Cambridge, 1997.
- [3] White, J.S., Shigemoto, F.H., and Bourquin, K., “Satellite Attitude Control Utilizing the Earth’s Magnetic Field,” NASA TN D-1068, Ames Research Center, Moffett Field, CA, 1961.
- [4] Grassi, M. and Pastena, M., “Minimum Power Optimum Control of Microsatellite Attitude Dynamics,” *Journal of Guidance, Control, and Dynamics*, Vol. 23, No. 5, 2000, pp. 798–804.
- [5] Giulietti, F., Quarta, A.A., and Tortora, P., “Optimal Control Laws for Momentum Wheel Desaturation Using Magnetorquers,” *Journal of Guidance, Control, and Dynamics*, Vol. 29, No. 6, 2006, pp. 1464–1468.
doi: 10.2514/1.23396.
- [6] Lovera, M., and Astolfi, A., “Spacecraft Attitude Control Using Magnetic Actuators,” *Automatica*, Vol. 40, 2004, pp. 1405–1414.
doi: 10.1016/j.automatica.2004.02.022.
- [7] Lovera, M., and Astolfi, A., “Global Magnetic Attitude Control of Inertially Pointing Spacecraft,” *Journal of Guidance, Control, and Dynamics*, Vol. 28, No. 5, Sept.-Oct.

- 2005, pp. 1065–1067.
doi: 10.2514/1.11844.
- [8] Coverstone-Carroll, V., “Detumbling and Reorienting Underactuated Rigid Spacecraft,” *Journal of Guidance, Control, and Dynamics*, Vol. 19, No. 3, 1996, pp. 708–710.
doi: 10.2514/3.21680.
- [9] Silani, E. and Lovera, M., “Magnetic Spacecraft Attitude Control: a Survey and Some New Results,” *Control Engineering Practice*, 13 (2005), pp. 357–371.
doi: 10.1016/j.conengprac.2003.12.017.
- [10] Tsiotras, P. and Longuski, J.M., “Spin-Axis Stabilization of Symmetric Spacecraft with Two Control Torques,” *Systems and Control Letters*, Vol. 23, No. 6, 1994, pp. 395–402.
- [11] Krishnan, H., McClamroch, N.H., and Reyhanoglu, M., “Attitude Stabilization of a Rigid Spacecraft Using Two Momentum Wheel Actuators,” *Journal of Guidance, Control, and Dynamics*, Vol. 18, No. 2, 1995, pp. 256–263.
- [12] Kim, S. and Kim, Y., “Spin-Axis Stabilization of a Rigid Spacecraft Using Two Reaction Wheels,” *Journal of Guidance, Control, and Dynamics*, Vol. 24, No. 5, 2001, pp. 1046–1049.
- [13] Wertz, J., *Spacecraft Attitude Determination and Control*, Kluwer, Dordrecht, The Netherlands, 1978, Chs. 5 and 17.
- [14] Avanzini, G. and Giulietti, F., “Magnetic Detumbling of a Rigid Spacecraft,” *Journal of Guidance, Control, and Dynamics*, Vol. 35, No. 4, Jul.-Aug. 2012, pp. 1326–1334.
doi: 10.2514/1.53074.
- [15] Slotine, J.J.E., and Li, W., *Applied Nonlinear Control*, Prentice-Hall, Upper Saddle River, NJ, 1991, Ch. 4.
- [16] Athanassov, Zh.S., “Perturbation Theorems for Nonlinear Systems of Ordinary Differential Equations,” *Journal of Mathematical Analysis and Applications*, Vol. 86, 1982, pp. 194–207.
- [17] Elaydi, S. and Farran, H.R., “Exponentially Asymptotically Stable Dynamical Systems,” *Applicable Analysis: an International Journal*, Vol. 25, 1987, pp. 243–252.
-

BIBLIOGRAPHY

- [18] Choi, S.K, Koo, K.S., and Lee, K., “Lipschitz Stability and Exponential Asymptotic Stability in Perturbed Systems,” *Journal of the Korean Mathematical Society*, Vol. 29, No. 1, 1992, pp. 175–190.
- [19] Hablani, H., “Comparative Stability Analysis and Performance of Magnetic Controllers for Bias Momentum Satellites,” *Journal of Guidance, Control, and Dynamics*, Vol. 18, No. 6, Nov.–Dec. 1995, pp. 1313–1320.
doi: 10.2514/3.21547.
- [20] Wie, B., *Space Vehicle Dynamics and Control*, American Institute of Aeronautics and Astronautics, Inc., Reston, VA, 1998, Ch. 7.
- [21] Avanzini, G., and Giulietti, F., “Constrained Slews for Single-Axis Pointing,” *Journal of Guidance, Control, and Dynamics*, Vol. 31, No. 6, pp. 1813–1816.
doi: 10.2514/1.38291.
- [22] Sorensen, A.M., “ISO Attitude Maneuver Strategies,” *American Astronautical Society*, Paper AAS 93-317, 1993, pp. 975–987.
- [23] Singh, G., Macala, G., Wong, E., and Rasmussen, R., “A Constraint Monitor Algorithm for the Cassini Spacecraft,” *AIAA Guidance, Navigation, and Control Conference*, Paper AIAA-97-3526, 1997, pp. 272–282.
- [24] Hablani, H.B., “Attitude Commands Avoiding Bright Objects and Maintaining Communication with Ground Station,” *Journal of Guidance, Control, and Dynamics*, Vol. 22, No. 6, 1999, pp. 759–767.
- [25] Wisnewski, R., and Kulczycki, P., “Slew Maneuver Control for Spacecraft Equipped with Star Camera and Reaction Wheels,” *Control Engineering Practice*, Vol. 13, No. 3, 2005, pp. 349–356.
doi: 10.1016/j.conengprac.2003.12.006.
- [26] Avanzini, G., and Giulietti, F., “Kinematic Planning of Slew Maneuvers After Actuator Failure for Low-Cost Satellites,” *Journal of Loss Prevention in the Process Industries*, Vol. 22, 2009, pp. 649–656.
doi: 10.1016/j.jlp.2009.04.008.
- [27] McInnes, C.R., “Large Angle Slew Maneuvers with Autonomous Sun Vector Avoidance,” *Journal of Guidance, Control, and Dynamics*, Vol. 17, No. 4, 1994, pp. 875–877.
doi: 10.2514/3.21283.

- [28] Bosco, M., Fabbri, V., and Tortora, P., “ALMASat-EO Attitude Determination Algorithms: Evaluation, Implementation and Numerical Simulation,” *Proceedings of the 8th International ESA Conference on Guidance, Navigation, and Control Systems*, Carlsbad, Czech Republic, 5-10 June 2011.
- [29] Pandiyan, R., Ramesh, A.S., and Sharanappa, S., “Kinematic Attitude Maneuvers with Path Constraints for Astrosat - An Indian Astronomy Satellite,” *DyCoSS' 2012, 1st IAA Conference on Dynamics and Control of Spacecraft Systems*, Paper IAA-AAS-DyCoSS1-05-07, 2012.
- [30] Giulietti, F., and Tortora, P., “Optimal Rotation Angle About a Nonnominal Euler Axis,” *Journal of Guidance, Control, and Dynamics*, Vol. 30, No. 5, 2007, pp. 1561–1563.
doi: 10.2514/1.31547.
- [31] Avanzini, G., Berardo, L., Giulietti, F., and Minisci, E.A., “Optimal Rotation Sequences in Presence of Constraints on Admissible Rotation Axes,” *Journal of Guidance, Control, and Dynamics*, Vol. 34, No. 2, 2011, pp. 554–563.
doi: 10.2514/1.49805.
- [32] Press, W.H., Teukolsky, S.A., Vetterling W.T., and Flannery B.P., *Numerical Recipes - The Art of Scientific Computing*, Third Edition, Cambridge University Press, NY, 2007, Chap. 9, pp. 456–461.
- [33] Dannan, F.M. and Elaydi, S., “Lipschitz Stability of Nonlinear Systems of Differential Equations,” *Journal of Mathematical Analysis and Applications*, Vol. 113, 1986, pp. 562–577.
- [34] Cheon, Y.J., Lee, S.H. and Kim, J.H., “Fully Magnetic Devices-Based Control for Gyroless Target Pointing of a Spinning Spacecraft”, *IEEE Transactions on Aerospace and Electronic Systems*, Vol. 46, No. 3, July 2010, pp. 1484–1491.
doi: 10.1109/TAES.2010.5545203.
- [35] de Ruiter, A., “A fault-tolerant magnetic spin stabilizing controller for the JC2Sat-FF mission,” *Acta Astronautica*, Vol. 68, No. 1-2, Jan.-Feb. 2011, pp. 160–171.
doi: 10.1016/j.actaastro.2010.07.012.
- [36] Khalil, H.K., *Nonlinear Systems*, Third Edition, Prentice-Hall, Upper Saddle River, NJ, 2001, Chs. 4, 8, and 9.
-

BIBLIOGRAPHY

- [37] Avanzini, G., de Angelis, E.L., and Giulietti, F., “Acquisition of a desired pure spin condition for a magnetically actuated spacecraft,” *Journal of Guidance, Control, and Dynamics*, in press.
- [38] Giulietti, F., Quarta, A.A., and Tortora, P., “Optimal Control Laws for Momentum-Wheel Desaturation Using Magnetorquers,” *Journal of Guidance, Control, and Dynamics*, Vol. 29, No. 6, Nov.-Dec. 2006, pp. 1464–1468.
doi: 10.2514/1.23396.
- [39] Tortora, P., Giulietti, F., Corbelli, A., and Fabbri, V., “ALMASat Attitude Control Hardware-In-the-Loop Simulation,” *Proceedings of the International Astronautical Congress (IAC 2006)*, IAC-06-C1.P.2.03, Valencia, Spain, Oct. 2006.
- [40] Damaren, C.J., “Hybrid Magnetic Attitude Control Gain Selection,” *Proceedings of the Institution of Mechanical Engineers, Part G, Journal of Aerospace Engineering*, Vol. 223, No. 8, 2009, pp. 1041–1047.
doi: 10.1243/09544100JAERO641.
- [41] Pulecchi, T., and Lovera, M., “Attitude Control of Spacecraft with Partially Magnetic Actuation,” *Proceedings of the 17th IFAC Symposium on Automatic Control in Aerospace*, Vol. 17, No. 1, International Federation of Automatic Control, Laxenburg, Austria, June 2007.
doi: 10.3182/20070625-5-FR-2916.00104.
- [42] Forbes, J.R., and Damaren, C.J., “Geometric Approach to Spacecraft Attitude Control Using Magnetic and Mechanical Actuation,” *Journal of Guidance, Control, and Dynamics*, Vol. 33, No. 2, Mar.-Apr. 2010, pp. 590–595.
doi: 10.2514/1.46441.
- [43] Avanzini, G., de Angelis, E.L., and Giulietti, F., “Spin-Axis Pointing of a Magnetically Actuated Spacecraft,” *Acta Astronautica*, in press.